General Disclaimer

One or more of the Following Statements may affect this Document

- This document has been reproduced from the best copy furnished by the organizational source. It is being released in the interest of making available as much information as possible.

- This document may contain data, which exceeds the sheet parameters. It was furnished in this condition by the organizational source and is the best copy available.

- This document may contain tone-on-tone or color graphs, charts and/or pictures, which have been reproduced in black and white.

- This document is paginated as submitted by the original source.

- Portions of this document are not fully legible due to the historical nature of some of the material. However, it is the best reproduction available from the original submission.

NASA CR 135315
ASRL TR 154-12

EXPERIMENTAL TRANSIENT AND PERMANENT DEFORMATION STUDIES OF STEEL-SPHERE-IMPACTED OR EXPLOSIVELY-IMPULSED ALUMINUM PANELS

Emmett A. Witmer
Fred Merlis
José J.A. Rodal
Thomas R. Stagliano

May 1977

Aeroelastic and Structures Research Laboratory
Department of Aeronautics and Astronautics
Massachusetts Institute of Technology
Cambridge, Massachusetts 02139

Prepared for
AEROSPACE SAFETY RESEARCH AND DATA INSTITUTE
LEWIS RESEARCH CENTER
NATIONAL AERONAUTICS AND SPACE ADMINISTRATION
CLEVELAND, OHIO 44135

NASA Grant NGR 22-009-339

NASA CR 135315
ASRL TR 154-12

EXPERIMENTAL TRANSIENT AND PERMANENT DEFORMATION STUDIES OF STEEL-SPHERE-IMPACTED OR EXPLOSIVELY-IMPULSED ALUMINUM PANELS

Emmett A. Witmer
Fred Merlis
José J.A. Rodal
Thomas R. Stagliano

Aeroelastic and Structures Research Laboratory
Department of Aeronautics and Astronautics
Massachusetts Institute of Technology
Cambridge, Massachusetts 02139

May 1977

Prepared for

AEROSPACE SAFETY RESEARCH AND DATA INSTITUTE
LEWIS RESEARCH CENTER
NATIONAL AERONAUTICS AND SPACE ADMINISTRATION
CLEVELAND, OHIO 44135

NASA Grant NGR 22-009-339

1. Report No.	2. Government Accession No.	3. Recipient's Catalog No.
NASA CR-135315		

4. Title and Subtitle	5. Report Date
Experimental Transient and Permanent Deformation Studies of Steel-Sphere-Impacted or Explosively-Impulsed Aluminum Panels	May 1977
	6. Performing Organization Code

7. Author(s)	8. Performing Organization Report No.
Emmett A. Witmer, Fred Merlis, José J.A. Rodal, and Thomas R. Stagliano	ASRL TR 154-12
	10. Work Unit No.

9. Performing Organization Name and Address	11. Contract or Grant No.
Aeroelastic and Structures Research Laboratory Department of Aeronautics and Astronautics Massachusetts Institute of Technology Cambridge, Massachusetts 02139	NGR 22-009-339
	13. Type of Report and Period Covered
12. Sponsoring Agency Name and Address	Contractor Report
National Aeronautics and Space Administration Washington, D.C. 20546	14. Sponsoring Agency Code

15. Supplementary Notes

Technical Monitors: Solomon Weiss and Arthur G. Holms
Aerospace Safety Research and Data Institute
NASA Lewis Research Center

16. Abstract

The sheet explosive loading technique (SELT) has been employed to obtain elastic-plastic, large-deflection 3-d transient and/or permanent strain data on simple well-defined structural specimens and materials: initially-flat 6061-T651 aluminum panels with all four sides ideally clamped via integral construction. The SELT loading technique was chosen since it is both convenient and provides "forcing function information" of small uncertainty. These data will be useful for evaluating pertinent 3-d structural response prediction methods.

A second objective of the present study was to obtain high-quality transient-strain data for a well-defined structural/material model subjected to impact by a "rigid body" of known mass, impact velocity, and geometry; large-deflection, elastic-plastic transient 3-d response conditions are of primary interest. Accordingly, (a) uniform-thickness and integrally-stiffened panels with all four sides clamped and (b) a steel sphere as the impacting body were chosen. The steel sphere was launched vertically by explosive propulsion to achieve various desired impact velocities. The sphere/panel impact tests conducted resulted in producing a wide range of structural responses and permanent deformations, including rupture of the panel from excessive structural response in several cases. The transient and permanent strain data as well as the permanent deflection data obtained are of high quality and should be quite useful for checking and evaluating methods for predicting the 3-d structural responses of panels subjected to fragment (sphere) impact. Unfortunately, however, transient strain data very close to the point of impact were not obtained over as long a time as desirable because the gage(s) in that region became detached during the transient response. Nevertheless, a considerable amount of useful transient strain data was obtained.

Both of these types of experimental structural response data will be valuable for checking structural response prediction methods. In particular, the present impact-induced structural response data will be employed to evaluate the adequacy and accuracy of methods developed to predict the responses of protective structures subjected to impact by aircraft engine rotor fragments.

17. Key Words (Suggested by Author(s))		18. Distribution Statement
Air Transportation and Safety Impact Loading Impulse Loading Elastic-Plastic Behavior Large Deflections Permanent Deformations	Transient Strain Data Large Strains Structural Failure	Unclassified, Unlimited

19. Security Classif. (of this report)	20. Security Classif. (of this page)	21. No. of Pages	22. Price*
Unclassified	Unclassified	142	

*For sale by the National Technical Information Service, Springfield, Virginia 22151

FOREWORD

This research was carried out by the Aeroelastic and Structures Research Laboratory, Department of Aeronautics and Astronautics, Massachusetts Institute of Technology, Cambridge, Massachusetts under NASA Grant No. NGR 22-009-339 from the Lewis Research Center, National Aeronautics and Space Administration, Cleveland, Ohio 44135, as part of the NASA Rotor Burst Protection Program. Mr. Solomon Weiss, Mr. Robert D. Siewert, and Mr. Arthur G. Holms of NASA-LeRC served as technical monitors. The valuable advice and cooperation from these individuals is acknowledged gratefully.

The authors are indebted to Earle Wassmouth of the MIT-ASRL for much assistance in model and test-fixture preparation and to Dr. R.L. Spilker for advice and assistance. The test specimens were machined by the Whitman Tool and Die Co., Whitman, Massachusetts. Photo-etched grids were provided on some of the test specimens by Tech-Etch Inc. of Plymouth, Mass.

The use of SI units (NASA Policy Directive NPD 2220.4, September 14, 1970) was waived for the present document in accordance with provisions of paragraph 5d of that Directive by the authority of the Director of the Lewis Research Center.

CONTENTS

CONTENTS (Concluded)

LIST OF ILLUSTRATIONS

LIST OF ILLUSTRATIONS (Continued)

LIST OF ILLUSTRATIONS (Continued)

LIST OF ILLUSTRATIONS (Concluded)

LIST OF TABLES

LIST OF TABLES (Concluded)

SUMMARY

The sheet explosive loading technique (SELT) has been employed to obtain elastic-plastic, large-deflection 3-d transient and/or permanent strain data on simple well-defined structural specimens and materials: initially-flat 6061-T651 aluminum panels with all four sides ideally clamped via integral construction. The SELT loading technique was chosen since it is both convenient and provides "forcing function information" of small uncertainty. These data will be useful for evaluating pertinent 3-d structural response prediction methods.

A second objective of the present study was to obtain high-quality transient-strain data for a well-defined structural/material model subjected to impact by a "rigid body" of known mass, impact velocity, and geometry; large-deflection, elastic-plastic transient 3-d response conditions are of primary interest. Accordingly, (a) uniform-thickness and integrally-stiffened panels with all four sides clamped and (b) a steel sphere as the impacting body were chosen. The steel sphere was launched vertically by explosive propulsion to achieve various desired impact velocities. The sphere/panel impact tests conducted resulted in producing a wide range of structural responses and permanent deformations, including rupture of the panel from excessive structural response in several cases. The transient and permanent strain data as well as the permanent deflection data obtained are of high quality and should be quite useful for checking and evaluating methods for predicting the 3-d structural responses of panels subjected to fragment (sphere) impact. Unfortunately, however, transient strain data very close to the point of impact were not obtained over as long a time as desirable because the gage(s) in that region became detached during the transient response. Nevertheless, a considerable amount of useful transient strain data was obtained.

Both of these types of experimental structural response data will be valuable for checking structural response prediction methods. In particular, the present impact-induced structural response data will be employed to evaluate the adequacy and accuracy of methods developed to predict the responses of protective structures subjected to impact by aircraft engine rotor fragments.

SECTION 1

INTRODUCTION

In order to determine whether or not methods for predicting the large-deflection elastic-plastic transient responses of structures provide reliable and accurate predictions, it is essential that they be evaluated by carrying out detailed comparisons of predictions against pertinent well-defined experimental data. It is for this purpose that the present experiments have been performed.

In particular experimental data are sought to provide detailed transient strain data on simple structures which undergo three-dimensional structural deformations when subjected to low-velocity impact of a well-defined fragment; previous experiments [1]* have provided similar data on simple structures exhibiting principally planar deformations. Accordingly, 6061-T651 aluminum square panel models with all four sides "ideally clamped" were prepared and were subjected to steel-sphere impact near the midpanel location on the lower surface of the panel. Nominally on each specimen, from 9 to 17 high-elongation strain gages were affixed at various stations on the upper (non-impacted) surface of each specimen; usually transient strain records were recorded for 8 of these gages, and permanent strain was recorded for all surviving gages. Since measurements were made also to define the location and the instant of initial impact of the steel sphere against the panel specimen, the resulting transient strain data have high resolution in both space and common time. It is intended, therefore, that these data will be used to make a critical evaluation of computer codes which are designed to predict the large-deflection elastic-plastic transient responses of simple structures subjected to aircraft engine rotor fragment impact; the development and verification of prediction methods of this type constitute an important part of the NASA Rotor Burst Protection Program. Typically these codes (see, for example, Refs. 2 and 3 for 2-d structural response and Ref. 4 for 3-d structural response) include an approximate impact-interaction model whose adequacy has not been definitively evaluated. By employing the present transient strain data to compare with predictions, it is intended to assess whether or not the approximate impact-

*Numbers in square brackets [ ] indicate references given in the reference list.

interaction model being used is adequate and, if not, to gain indications of aspects requiring improvement so that appropriate modifications and improvements can be carried out.

A second theoretical-analysis aspect requiring further study and appropriate evaluative experimental data, is the adequacy, accuracy, and efficiency of the finite-element structural-response analysis itself -- quite apart from the impact-interaction model questions noted previously. Assumed-displacement finite-element models for straight beams and curved rings have been developed [5, for example] and are utilized in the computer codes described in Refs. 2, 3, and 6. These elements employ 4 degrees of freedom (DOF) per node and have been shown [5,7] to provide reasonably accurate predictions of transient deflections and strains. Assumed-displacement finite elements have been developed to analyze the large-deflection elastic-plastic transient structural responses of uniform-thickness and longeron-stiffened flat plates and cylindrical shells [7]; appropriate experimental data [8] are available for assessing the cylindrical shell analysis, but further data are desired to assess the flat-panel predictions [4]. Some well-defined transient-strain data for large-deflection elastic-plastic planar structural response conditions [1] will be valuable for assessing these elements. Accordingly, 6061-T651 panel specimens were prepared, instrumented with strain gages, and subjected to impulsive loading over a small square region centered at the midpanel location by the sheet-explosive loading technique (SELT). This technique provides an accurately-known impulse applied to the structure and hence a well-defined initial-condition problem is established; this type of problem is very convenient for use in testing finite-element analysis adequacy and accuracy for application to large-deflection, elastic-plastic transient response problems.

Section 2 is devoted to describing the test specimens, instrumentation, test procedure, and results for the impulsively-loaded uniform-thickness panels. Section 3 contains a similar description for the uniform-thickness and longeron-stiffened panels subjected to steel sphere impact. Section 4 documents uniaxial stress-strain data for the material from which the panel specimens were made. Summary observations are given in Section 5.

SECTION 2

SHEET HE LOADING AND RESPONSE TESTS OF 6061-T651 ALUMINUM PANELS WITH CLAMPED EDGES

2.1 Objectives

Sought were both transient response and permanent deformation experimental data of high quality for use in evaluating the reliability and accuracy of methods for predicting the large-deflection elastic-plastic transient and permanent deformations of a well-defined structure, including the following desired structural, material property, forcing function, and deformation features:

(1) Structural Features: The structure shall be an initially-flat panel with ideally-clamped sides.

(2) Material Properties: The material shall exhibit well-defined mechanical properties -- initially-isotropic, very little strain hardening, and with little to moderate strain rate sensitivity.

(3) Forcing Function: The externally-applied forces which produce the structural response shall be well-defined and repeatable with minimum uncertainty.

(4) Deformation Features: Large structural deformations with strains ranging to moderate levels shall be included.

To meet these objectives, an initially-flat square panel model of 6061-T651 aluminum with clamped sides and impulse loading provided by the sheet explosive loading technique were chosen. In view of the instrumentation available at the MIT Aeroelastic and Structures Research Laboratory, it was decided to attempt to make measurements of transient strains, permanent strains, and permanent deformations.

In the following subsections of Section 2, discussed are: (a) the panel models and mounts, (b) the experimental arrangement and procedure, and (c) the experimental results obtained.

2.2 Panel Models and Mounts

To circumvent the difficulties that experimenters have had repeatedly in trying to achieve an ideally-clamped edge of a structure by utilizing a variety of clamping arrangements (massive serrated clamps, hardened faces, massive bolts, etc.) most of which unfortunately revealed post-test evidence of slippage, an "integral-edge arrangement" was tried in the present test program. This consisted, as shown in Fig. 1, of integrally machining the panel specimen (of nominal 8-in by 8-in span and 0.060 thickness) from a solid block (1.55 by 12 by 12 in) of 6061-T651 aluminum. Although the "integral support collar" provided a reasonably rigid restraint to simulate ideally-clamped edges, this collar was securely bolted to a heavy flat-ground 1 by 12 by 12 in steel plate and a steel channel support structure with eight 1/2"-13 Holo-Krome socket head shoulder screws with nuts torqued to a uniform 651 inch-pounds, producing an axial load of about 38,000 pounds per bolt. Note in Fig. 1 that to reduce the hazard of undesired or "premature" cracking at the boundary because of stress concentrations at a sharp re-entrant corner, all "inside corners" were machined to a radius of about 0.125 in, which is somewhat larger than the nominal panel thickness.

Two specimens ("clamped panel models" CP-1 and CP-2) were prepared and subjected to impulse loading. The dimensions of these specimens are given in Table 1. Post-fabrication measurements of panel thickness h and panel spans L_x and L_y were made at 0.5-in intervals along both the x and the y direction (see Figs. 1 and 2). It was found that these dimensions were uniform: at the values shown with a standard deviation within 0.5 per cent for thickness, and within about 0.03 per cent for span. The top and bottom faces of the "support collar" portion of the specimens were flat and parallel to within a standard deviation of 0.3 per cent; the support collar dimensions are also listed in Table 1.

2.3 Experimental Arrangement and Procedure

2.3.1 Test Procedure

Shown in Fig. 3 is a schematic of the test arrangement. The panel specimen bolted to the heavy steel support plate and channel has a square portion of its lower surface midspan region covered with a 0.25-in thick by

2.5-in by 2.5-in spanwise layer of polyester-type polyurethane foam[+] weighing 2 lb/ft^3; this "buffer" material (provided to prevent stress-wave-induced spall fracture of the panel by sheet HE detonation) is overlaid by a uniform-thickness layer of du Pont Detasheet D (sometimes called EL 506D) covering a square 2-in by 2-in region centered at the midpanel point, and weighing 1.45 gm/cc. The Detasheet leader, nominally 40-in long, 0.25-in wide, and 0.015-in thick is attached to the main HE panel-patch by a 0.25-in by 0.25-in by 0.015-in thick "end region" centered at the midwidth-midspan point; the Detasheet leader is detonated by firing a Hercules No. 6 detonator. The detonation then proceeds along the leader and initiates the detonation of the HE patch on the panel specimen. A detonation wave then proceeds radially from this "initiation point", resulting in progressive detonation of the HE panel-patch; since according to the manufacturer [9] the detonation front travels at 7200 meters/sec (283,464 in/sec), the entire HE-covered region becomes loaded almost simultaneously (within about 3.5 microseconds of simultaneity).

Panel specimens CP-1 and CP-2 were loaded impulsively by the detonation of HE layers of nominal 0.025 thickness composed of the superposition of 0.015 and 0.010-in thick layers obtained from large sheets of Detasheet D from the same HE batch but with nominal thicknesses of 0.010 and 0.015 in. To improve the intimacy of contact between layers, these two-layer HE sheets were placed on "separator paper" and upon firm cardboard, and a pattern of thin-needle punctures was applied to effect some "mechanical knitting". Since the Detasheet is supplied in sizes 10-in wide by a 20-in long in various "uniform" thicknesses, sheets of nominal 0.010 and 0.015-in thickness were measured to determine the thickness distribution over the entire sheet. Only uniform-thickness regions were employed in constructing each loading patch for each panel specimen.

The resulting HE weight per square inch for each panel specimen is given in Table 2. Shown also in Table 2 is the "initial velocity" imparted impulsively to the HE-covered portion of each panel specimen, where the

---

[+]Attached with du Pont 4684 cement; the HE sheet was similarly attached to the buffer.

specific impulse from calibration tests [8] is taken to be 18.1×10^4 dyne-sec/gm of HE or 0.407 lb-sec/gm of HE, and a panel material weight density of 0.098 lb/in^3 is used.

2.3.2 Strain Measurements

In an effort to measure transient strains, type EP-08-125AD-120 high elongation annealed constantan foil-type polyimide-backed strain gages* were oriented and attached at various locations on the upper surface, as listed in Table 3. These gages were attached with Armstrong A-12 cement and cured at 200°F for 60 minutes as advised by the manufacturer; according to the manufacturer, this system should permit one to measure strains (relative elongations) reliably up to about 20 per cent. One-foot long varnish-covered copper leads, type AWG 36, were attached to each transient-strain gage, fed via a shielded cable+ to a standard Wheatstone bridge, and the strain signal was recorded on a dual-beam Tektronix oscilloscope. As indicated in Fig. 3, the scope sweeps were triggered by passage of the detonation front at a station along the HE leader 25 inches from the HE panel-load patch; hence, impulse loading to the beam is initiated about 88 microseconds after this instant (also the instant of scope sweep initiation). Each scope trace was set to sweep at a known rate; thus, all transient strains are correlatable to a common time. These strain traces were recorded on Polaroid type 47 film with a Tektronix 196A scope camera.

In addition to measuring transient strain (on nominally, 8 gages on each panel specimen), 9 additional gages were used to obtain only permanent strain. Permanent strain data were obtained on all surviving gages. Summarized in Table 3 are the strain gage locations, the gages used for transient strain measurements, and the permanent strain indicated on all surviving strain gages.

2.3.3 Deflection Measurements

Since appropriate photographic or other equipment for measuring or recording transient deformations of structures is not available at the

---

*Manufactured by Micro-Measurements Corp., 38905 Chase Road, Romulus, Michigan 48174.

+Four conductor type with 2 leads in parallel to reduce resistance; capacitance of 25 pF/ft.

MIT-ASRL, only pre-test and post-test configuration measurements have been obtained for these specimens. Since each panel model had its upper and lower "collar support" surfaces machined flat and parallel, each specimen was clamped securely to the moveable carriage of a Model H Milwaukee universal milling machine. The vertical location of the "lower surface" of each panel specimen both pre-test and post-test was determined at 0.5-in intervals along x and y (and more finely also in certain regions) as the specimen was traversed by a station monitored by an Ames dial-gage indicator with 0.001-inch divisions readable to the nearest 0.0002 inch. The changes z_ℓ between pre-test and post-test vertical locations of the lower surface are listed in Table 4 for model CP-1 and in Table 5 for model CP-2. Note in Tables 4 and 5 that the center of the panel is located at (x,y)=(0,0).

2.4 Test Results

The panel specimens identified in Table 1 as CP-1 and CP-2 were tested by impulsive loading in this sequence. The test arrangement used is indicated schematically in Fig. 3. The weight per unit area of explosive (HE) covering each specimen and the attendant impulsively-imparted (initial) velocity in the 2 in by 2 in HE-covered region are shown in Table 2; essentially identical buffers were used in both cases. The "initial velocity" values are based upon a specific impulse for this Detasheet D batch and HE/buffer system of 0.407 lb-sec/gm (=18.1×10^4 dyne-sec/gm of HE); this impulse calibration procedure and information are given in Ref. 8.

Specimens CP-1 and CP-2 were loaded such that their initial velocities were of the order of 15,200 and 16,300 in/sec, respectively. This resulted in a moderate degree of permanent deflection for model CP-1 but no evidence of cracking; the midspan permanent deflection being about 1.02 in (compared with an initial panel thickness of 0.064 in). Specimen CP-2 exhibited somewhat more severe deformation as well as essentially incipient-level cracking; a "circumferential type" crack located about 0.7 in from the panel center and having a length of about 1.4 in was produced. It appears that where the crack initiated, the normal to the crack surface points in the transverse direction of the panel material; this is consistent with the smaller "fracture strain data" discussed in Section 4 for a transverse specimen compared

with a longitudinal specimen. Also model CP-2 had a midpanel permanent deflection of about 1.10 in (compared with an initial panel thickness of 0.062 in).

Post-test photographs of these two models are shown in Fig. 4.

2.4.1 Deformed Panel Data

Tables 4 and 5 list the post-test lower-surface vertical location change z_ℓ data measured along both x and y for specimens CP-1 and CP-2, respectively. Note that the pre-test dimensions of these specimens are given in Table 1; the nominal panel dimensions are: span = 8 in by 8 in, and thickness 0.064 and 0.062 in, respectively. Since model CP-2 is the thinner of these two models and was subjected to more severe impulse loading, its exhibiting greater deformation (and incipient structural-response-induced cracking) is consistent compared with the model CP-1 results.

Note in Tables 4 and 5 that the permanent deflections of these panel specimens are not perfectly symmetric along x=0 and y=0 about the panel-center location (x,y)=(0,0). This may be the result of several factors, including (a) a slightly off-center and/or non-uniform HE patch, (b) panel thickness variations, (c) panel material anisotropy, etc. It is believed, however, that the specimen geometry and material properties, the loading conditions, and the permanent deformation data are sufficiently well defined to provide reliable data for evaluating appropriate prediction methods involving very large elastic-plastic deformations.

2.4.2 Transient and Permanent Strain Data

The locations of each of the strain gages for which transient strain measurements were attempted are denoted by an asterisk (*) in Table 3. Transient strain traces (some very good throughout, some good for a part of the time span, and others of questionable value) were obtained for the following models and gages, and are shown in the indicated figures:

Model	Gages	Figure
CP-1	1 2 3 5 7 8 10 15	5
CP-2	2 3 4 5 6 7 8 18	6

For each of these strain traces, the sweep speed (time scale) and the as-read or nominal relative elongation E_r in per cent are given on each figure. For

sufficiently large "strain" values, a nonlinear correction must be applied to obtain the "corrected relative elongation" E_{rc} as given by the following relation [10]; tension is + and compression is -:

$$E_{rc} = \frac{\Delta R}{R(GF + E_r)} \equiv \frac{(GF)\ (E_r)}{GF + E_r} \tag{2.1}$$

where

ΔR = change of resistance of the strain gage because of its elongating

R = original strain gage resistance (nominally 120 ohms $\pm$ 0.15%)

GF = gage factor of the strain gage (2.075 $\pm$ 0.5%)

E_r = strain reading on the oscilloscope based on a linear scale used for calibration convenience during a test; units of in/in

Note that, in general, two strain traces appear on each photograph. Identified for each trace are the strain gage number, the pre-test zero strain position, and the "instant" of HE panel-patch detonation (which may be interpreted as zero time at which the specimen is subjected to a uniform initial velocity over the HE-covered region). Unless noted explicitly to the contrary, both traces have the same sweep speed (in microseconds per division).

Certain strain traces appear to be valid throughout the recorded time history, while others vanish after a short time (probably because of broken lead wires), and still others drop rapidly to essentially zero strain after apparently behaving in a plausible fashion for an initial period. In this latter case, it is likely that the strain gage became detached from the specimen (hence a drop in indicated strain) after a short time; in all cases, post-test observations confirmed that such a gage had become detached from the panel specimen.

As can be seen from Figs. 5 and 6 and Table 3, strain gages located closer than about 1 inch from the panel center became detached from the panel early in the response period. The permanent strains indicated by all surviving strain gages are given in Table 3 where such strains range up to about 5.4 per cent. Closer to the panel center, however, much larger permanent strains must have occurred as a visual inspection of each specimen makes evident.

In an attempt to obtain a rough estimate of the permanent strain in this central region, a pattern of closely-spaced (ℓ_o apart) lightly-scribed lines was made on the upper surface of model CP-2 over a centered 3-in by 3-in region; on a centered 1-in by 3-in region in each direction the "grid spacing" was 0.025-in, and was 0.050-in over the remainder of this 3-in by 3-in region. Post-test measurements of the spacing (now denoted by ℓ_f) of the readable* grids (which were those along y=0) with a cross-hair equipped microscope viewing the grid lines as the specimen is translated past on a milling machine carriage resulted in the "upper surface" permanent relative elongation values plotted in Fig. 7; these relative elongation values ($\equiv(\ell_f-\ell_o)/\ell_o$) are averages over each ℓ_o region. Included also in Fig. 7 are relative elongations determined from the available final strain gage readings. These two determinations of the upper surface permanent relative elongation are plausible but do not form a cross check of each other since none of these two determinations occurs in a common region; see Table 3 for the strain gage locations to which the Fig. 7 data apply. Finally, the seemingly erratic behavior of the permanent relative elongations determined from the "grid spacings" appears to be consistent with the observed pronounced "orange peel" state of the upper surface of those regions.

*As can be seen from Fig. 4 and Table 3, some strain gages were placed in this gridded region; at those gage locations, surface preparation for gaging obliterated the grids. Hence, at such locations where strain gages became detached, post-test grid spacing measurements could not be made.

SECTION 3

PANELS SUBJECTED TO STEEL-SPHERE IMPACT

3.1 Objectives

In this part of the investigation, high-quality transient-strain data are sought for well-defined structural specimens which undergo large three-dimensional (3-d) elastic-plastic structural deformations when impacted by an essentially non-deformable body of well-defined geometry, known mass, and known impact velocity. These data are intended to be used to evaluate prediction methods such as that in Ref. 4, for example, especially the adequacy of the approximate impact-interaction portion of the analysis. Accordingly, simple initially-flat panels of 6061-T651 aluminum with all four sides ideally clamped were chosen, each to be impacted by a steel sphere of one-inch diameter. Two types of panel models were selected: (1) uniform-thickness square panels and (2) similar panels but with integral orthogonal stiffeners to provide impact/response data on geometrically-stiffened structures since this type of structure is both common and such data will permit evaluating the capability of the Ref. 4 prediction method for analyzing this type of impacted stiffened structure.

In the following subsections of Section 3, discussed are: (a) the panel models and mounts, (b) the experimental arrangement and procedure, and (c) the experimental results obtained.

3.2 Panel Models and Mounts

The uniform-thickness 6061-T651 aluminum panel models employed were essentially the same as those described in Subsection 2.2. The specimens subjected to steel-sphere impact are identified as clamped panel specimens CP-7, CP-8, CP-9, and CP-12 in Table 1; the dimensions of these models are given in Table 1 and were determined as described in Subsection 2.2. These values show a standard deviation of about 0.5 per cent in thickness for panels CP-7 and CP-8, and below 2.6 per cent for panels CP-9 and CP-12. The span and "support collar" measurements were found to be uniform within the same standard deviations as the models described in Subsection 2.2.

The geometry and dimensions of the integrally-stiffened panel models are shown in Fig. 8. Post-fabrication measurements of these stiffened clamped panel models, SCP-1 and SCP-2, revealed the "average" panel, stiffener, and collar dimensions listed in Table 6. More detailed measurements are shown for models SCP-1 and SCP-2 in Figs. 9 and 10, respectively; here the x,y origin is defined to be at the center of the nominal 4-in by 4-in central panel. Shown for each model are (a) the average thickness of each subpanel, (b) the width and total depth of each stiffener, (c) the center-to-center stiffener spacing, and (d) the locations of the "clamped edges".

Specimens CP-7, CP-8, CP-9, and CP-12 were mounted as described in Subsection 2.2 and as depicted in Fig. 11. Specimens SCP-1 and SCP-2 were mounted similarly except that steel spacer bars were placed between the specimen support collar and the 1 by 12 by 12-in steel mounting plate to provide ample clearance for the impact-induced deflection to take place without interference from the cited steel mounting plate.

3.3 Experimental Arrangement and Procedure

A schematic of the test arrangement is shown in Fig. 11. The steel sphere is launched vertically by "explosive propulsion" [1] and is intended to impact the panel (a) at the panel center location for the uniform-thickness models and (b) at the flat surface opposite a specific stiffener of the SCP models as indicated in Figs. 8, 9, and 10. At sphere/panel impact, an "impact switch" provides an electrical signal which starts the sweeps of the oscilloscopes employed to measure transient strains at various upper-surface locations. This impact switch consists of heavy-duty aluminum foil separated from the aluminum panel by a polyurethane foam pad insulator (0.5-in thick by 1.5-in by 2.5-in) of 6 lb/ft^3 density with a 5/8-in diameter hole in the pad at the location of intended impact. The sphere causes the aluminum foil to contact the aluminum panel specimen at the "instant of impact", thereby closing a circuit and causing an electrical signal which initiates the sweeping of the oscilloscope.

In order to produce panel responses ranging from moderate to very large permanent deformation (including specimen rupture), various steel-sphere

velocities were used in testing the panel specimens; these values and the associated results are described in Subsection 3.4.

In an effort to measure transient strains, type EP-08-125AD-120 high-elongation annealed constantan foil-type polyimide-backed strain gages (120 ohm $\pm$ .15%; gage factor 2.075 $\pm$ .5%) were oriented and attached at various locations on the non-impacted surface, as listed in Table 7. These gages were attached with Armstrong A-12 cement and cured at 200^{o}F for 60 minutes as advised by the gage manufacturer; according to the manufacturer, this system should permit one to measure strains (relative elongations) reliably up to about 20 per cent. One-foot long varnish-covered copper leads, type AWG36, were attached to each transient-strain gage, fed via shielded cable to a standard Wheatstone bridge, and the strain signal was recorded on a dual-beam Tektronix oscilloscope. As noted earlier, each scope sweep was initiated at the "instant of initial impact" by an electrical signal generated upon "closing of the impact switch". Each scope trace was set to sweep at a known rate; thus, all transient strains are correlatable to a common time. These strain traces were recorded on Polaroid type 47 film with a Tektronix 196A scope camera. In addition to measuring transient strain (attempted on 8 gages on each panel specimen), some additional gages were used to obtain permanent strain data. Permanent strain data were obtained on all surviving gages. Summarized in Table 7 are the strain gage locations, the gages used for transient strain measurements, and the permanent strain data on all surviving strain gages for the uniform-thickness panels. Similar strain gage location and permanent strain data are given in Tables 8 and 9 for integrally-stiffened panel specimens SCP-1 and SCP-2, respectively.

It should be noted that a circuit was designed so that upon closing of the "impact switch" a short-duration pulse would be applied to each transient strain channel as a "marker pulse" as indicated in Fig. 11. This design was tested and modified so that this impact pulse would have a duration of about 3 microseconds or less; in some cases this pulse persists up to 8 microseconds, depending on the response of the oscilloscope. Accordingly, only about the initial 8 microseconds or less of each transient strain pulse represents a "false strain reading"; thereafter, it is believed that valid transient strain

data were obtained until effects such as lead wire breakage, gage detachment, etc. occur.

Pre-test and post-test configuration measurements were made on typical models in this test series by mounting the specimen on a milling machine and employing a dial gage arrangement to determine the vertical location change z_ℓ of the impacted surface along x,y lines at 0.5-inch spacing as described in Subsection 2.3.3. Similar measurements were made along lines x=constant and/or y=constant near the "impact point" on each specimen.

3.4 Panel Response Results

Four uniform-thickness panels and two integrally-stiffened panels were subjected to impact by a 1-inch diameter steel sphere. Various impact velocities were employed for the first category of specimens, producing effects ranging from substantial permanent deformation to panel rupture. For the second specimen category, the impact velocities were such that only significant permanent deformation but no specimen rupture was produced. Summarized in Table 10 are the impact location, initial impact velocity, steel sphere weight, and the weight of the launching explosive for each of these tests. The listed impact velocity was determined from velocity calibration tests described in Subsection 3.5 of Ref. 1.

Post-test photographs of the impacted panel specimens are shown in the figures listed below; indicated also concisely are the principal observed effects on each specimen:

Nominal Impact Velocity (in/sec)	Comments	Specimen	Figure
	UNIFORM-THICKNESS PANELS		
2395	Moderate permanent deformation; no cracks	CP-12	12
2435	Large permanent deformation, slight crack	CP-8	13
2755	Panel ruptured	CP-9	14
2850	Panel ruptured	CP-7	15
	GEOMETRICALLY-STIFFENED PANELS		
2400	Large permanent deflection; thru crack observed	SCP-1	16
2125	Moderate permanent deflection; no thru crack	SCP-2	17

Deflection and strain results are discussed in the following.

3.4.1 Deflection Data

Since specimens CP-7 and CP-9 ruptured, post-test measurements on these models were not made to determine the change of the vertical location of the impacted surfaces of these models; the post-test photographs shown in Figs. 14 and 15 are believed to suffice for present purposes since they show reasonably well the locations of the rupture lines. Except in the immediate vicinity of impact and the rupture lines (and "petals"), the vertical permanent deflection along lines x=constant and y=constant through the center of impact is quite small and increases almost linearly over a distance of about 2.5 inches from each clamped edge of specimen CP-9, for example, reaching a value of about 0.15-in at that location.

Models CP-8 and CP-12 experienced considerable deformation. Model CP-12 did not rupture. However, model CP-8 has a crack on the photo-etched non-impacted side that runs along the x direction from $\bar{x}$ = -0.102" to $\bar{x}$ = +0.101" at $\bar{y}$ = +0.230", and its width is ≈0.003"; the normal to this crack points in the transverse direction of the material. This crack extends only partly through the thickness of the panel. Vertical location change measurements of the impacted surface were determined from pre-test and post-test measurements as described earlier. In these cases measurements were made along lines x=constant and y=constant spaced 0.5-in apart from the observed point of initial impact which is reported in Table 10 for each specimen. Shown in Tables 11 and 12 for specimens CP-8 and CP-12, respectively, are the vertical location change z_ℓ determinations of the impacted (lower) surface as a function of $\bar{x}$ and $\bar{y}$, where the $\bar{x},\bar{y}$ origin is at the observed "impact point", and these axes are parallel to the x,y axes of Fig. 2. In addition to the z_ℓ values determined at 0.5-in $\bar{x},\bar{y}$ spacings, values of z_ℓ were determined for more closely spaced points along $\bar{x}$=0 and $\bar{y}$=0; these values are included in the last page of each of Tables 11 and 12. Note that the region of severe deflection is highly localized about the point of impact. This deflection tends to be nearly symmetric about the point of initial impact.

For the geometrically-stiffened panel specimens SCP-1 and SCP-2, pre-test and post-test measurements were made to determine the vertical location change z_u of the (upper) non-impacted surface along lines x=constant and

y=constant spaced 0.5-in apart. Hence, these determinations were made both in the subpanel regions and along each stiffener. Note that an $\bar{x},\bar{y}$ system was not used, but that the location of the initial impact point is given for each model in Table 10. The resulting z_u values are given in Tables 13 and 14 for specimens SCP-1 and SCP-2, respectively. Values of z_u are given for each specimen along lines x=constant and/or y=constant near the "initial impact point".

Note from Table 10 and Fig. 16 that specimen SCP-1 suffered a through crack of 1.51-inch length located (next to the "impacted stiffener") at x = -2.13-in and extending from y = -0.65 to y = +0.86 inch. Specimen SCP-2 suffered only a small fracture extending only partly through the thickness of the panel; this "part-through" crack was about 0.24-in long and was located about x = 1.93-in extending from about y = -0.03 to +0.21 inch. The normal to each of these cracks points in the transverse direction of the material.

3.4.2 Transient and Permanent Strain Data

For the sphere-impacted specimens, attempts were made to measure transient and permanent strains at various locations on the non-impacted surface of each test specimen. Strain gage locations and permanent strain data are given in Table 7 for models CP-7, CP-8, CP-9, and CP-12; similar data are given in Tables 8 and 9 for models SCP-1 and SCP-2, respectively. Note that these permanent strain data represent the "corrected" relative elongation as determined from Eq. 2.1. It is seen that at the locations sensed, these permanent relative elongations ranged from a fraction of a per cent to about 1.2 per cent on the non-ruptured specimens and to nearly 7 per cent on the ruptured specimens. Confining attention to the non-ruptured and "slightly ruptured" specimens (CP-8, CP-12, and SCP-2) it is clear that much larger strains occurred near the impact point than those just cited. Diligent strain gage installation and protective measures were followed, but the Table 7, 8, and 9 results show successful permanent strain measurements by strain gages were not obtained at locations interestingly close to the point of initial impact.

In order to obtain permanent relative elongation data closer to the

point of impact, a 4-in by 4-in pattern of photo-etched* grid lines spaced 0.020-in apart and centered at $(x,y)=(0,0)$ was applied to specimens CP-7 and CP-8. Pre-test and post-test measurements of the grid spacing along lines $\bar{x}=0$ and $\bar{y}=0$ of model CP-8 provided the upper-surface permanent relative elongation data shown in Fig. 18 (also, see Table 7); these data represent average values along $\bar{x}=-$ and + (i.e., for $\bar{y}=0$) and $\bar{y}=+$ and - (i.e., for $\bar{x}=0$) as a function of distance from the center of impact $(\bar{x},\bar{y})=(0,0)$. Note that the largest measured permanent relative elongation is about 28.9 per cent and occurs at about 0.2-in from the center of impact. As the standard deviation bars show, these data are useful but are of limited reliability. In principle, similar measurements could be made from ruptured specimen CP-7; however, because of the complexity of reporting that information in a clear comprehensive way, these data are not included.

A grid pattern of mechanically lightly scribed lines was applied to specimen CP-9; however, since model CP-9 ruptured, the attendant permanent strain data are not reported.

Transient strain traces (some very good throughout, some good for a part of the time span, and others of questionable value) were obtained for all of the sphere-impacted panel specimens. The transient strain (actually relative elongation) traces included in this report are identified by model, gage number, and figure number as follows:

Nominal Impact Velocity (in/sec)	Specimen	Gages	Figure
2395	CP-12	1 2 4 5 7 8 10 11	19
2435	CP-8	1 2 4 5 7 8 10 11	20
2755	CP-9	1 2 4 5 7 8 10 11	21
2850	CP-7	1 2 4 7 10 11	22
2400	SCP-1	1 2 4 6 10 12 14 16	23
2125	SCP-2	1 2 4 6 10 12 14 16	24

For each of these strain traces, the sweep speed (time scale) and the as-read or nominal relative elongation in per cent with linear scales are given on each

*This gridding was applied by Tech-Etch Inc. of Plymouth, Mass.

figure. If desired, one can convert these uncorrected relative elongations to corrected relative elongations by using Eq. 2.1.

Note that, in general, two traces appear on each photograph. Identified for each trace are the strain gage number, the pre-test zero-strain position, and the "instant of impact". Unless noted explicitly to the contrary, both traces have the same sweep speed (in microseconds per division).

Certain strain traces appear to be valid throughout the recorded time history, while others vanish after a short time (probably because of broken lead wires), and still others drop rapidly to essentially zero strain after apparently behaving in a plausible fashion for an initial period. In the latter case, it is likely that the strain gage became detached from the specimen after a short time, thus resulting in a drop in indicated strain; in all cases, post-test observations confirmed that such a gage had become detached from the panel specimen.

The strain traces for models CP-8, CP-12, and SCP-2 should be useful to the analyst throughout the recorded time period (except for the previously cited types of "defective" traces) since all of these models survived in the sense of exhibiting substantial permanent deformation but little or no fracturing. Since specimens CP-7 and CP-9 ruptured at an unknown time during the response, one must interpret these strain traces with care; some early portion of each trace will apply to an "intact" specimen.

SECTION 4

STATIC UNIAXIAL STRESS-STRAIN TESTS OF 6061-T651 ALUMINUM SPECIMENS

4.1 Objectives and Procedure

Sought are uniaxial tensile stress-strain data for the 1.5-inch thick plate of 6061-T651 aluminum material from which the panel specimens were fabricated.

One type of test specimen employed had its axis parallel to the plate-roll (or longitudinal, L) direction; this is the same as the grain direction of the material. Another type was prepared with its axis perpendicular (or transverse, T) to the plate-roll direction. It was anticipated that the as-delivered 6061-T651 plate might exhibit somewhat different stress-strain properties along these directions, and it was desired to measure these differences, if any, as well as to determine the stress-strain behavior of this material over its entire strain range to fracture. Several types of tensile test specimens were prepared: (a) 0.5-in diameter with a 1.5-in long "working section", (b) 0.25 x 0.5-in rectangular cross-section with a 2.0-in long working section, (c) 0.25 x 0.35-in rectangular cross-section with a 2.0-in long working section, and (d) 0.06 x 0.6-in rectangular cross section with a 2.0-in long working section.

These specimens were instrumented with Micro-Measurements Inc. high elongation strain gages types either EP-08-125AD-120 or EP-08-250AF-120. The smaller one (EP-08-125AD-120) was used in the majority of cases. The outputs from strain gages on opposite sides of each specimen were combined in a Wheatstone bridge to cancel out inadvertent bending effects.

The resulting outputs were recorded on a Honeywell Visicorder Model 1508 for the circular cross-sectional-area specimens or on a Hewlett-Packard Moseley 7005B X,Y recorder for the rectangular cross-section specimens. These specimens were tested using a calibrated Baldwin Model FGT Testing Machine (screw driven) operating at its slowest rate. The output from the strain gage bridge, accounting for the changing gage factor as a function of the strain level at high strains (Refs. 10 and 11) provides a measure of

of the axial-direction extension (change of length per unit of original length -- called the relative elongation) E_1:

$$E_1 \equiv (\ell - \ell_o)/\ell_o \tag{4.1a}$$

Hence,

$$\frac{\ell}{\ell_o} = 1 + E_1 \tag{4.1b}$$

where $\ell(\ell_o)$ represents the current (original) gage length. One can compute the extensional strain components of different strain tensors from a knowledge of E_1. Various alternatives for describing uniaxial stress-strain behavior are described next.

4.2 Data Presentation Alternatives

The extensional strain component γ_{11} of the Green (Lagrangian) strain tensor (strain tensor referred to the original configuration) is related to E_1 by (see, for example, Ref. 12, page 165):

$$E_1 = \left[1 + 2\,\gamma_{11}\right]^{\frac{1}{2}} - 1 \tag{4.2a}$$

or

$$\gamma_{11} = \frac{1}{2}\left[(1+E_1)^2 - 1\right] = E_1 + \frac{1}{2}(E_1)^2 = \frac{1}{2}\left[\frac{\ell^2 - \ell_o^2}{\ell_o^2}\right] \tag{4.2b}$$

where, in usual tensor notation [Ref. 12, page 161]:

$$\gamma_{mn} = \frac{1}{2}\left[\frac{\partial u_m}{\partial X_n} + \frac{\partial u_n}{\partial X_m} + \frac{\partial u_k}{\partial X_m}\frac{\partial u_k}{\partial X_n}\right] \tag{4.2c}$$

In Eq. 4.2c the X_m are the rectangular Cartesian coordinates (m=1,2,3) which serve to define the "undeformed location" of any material particle in the body, and the u_m represent the displacement components for any given material point in the body: $u_m = x_m - X_m$ (the x_m are the spatial or Eulerian coordinates).

The extensional strain component e_{11} of the Almansi (Eulerian) strain tensor (strain tensor referred to the current configuration) is related from the basic definition of e_{ij} [12, page 158] to E_1 by:

$$e_{11} = \frac{1}{2}\left[1 - \frac{1}{(1+E_1)^2}\right] = \frac{1}{2}\left[\frac{\ell^2 - \ell_o^2}{\ell^2}\right] \tag{4.3}$$

The strain components e_{11} and γ_{11} are related to each other and to E_1 by

$$\gamma_{11} = e_{11}(1+E_1)^2 \tag{4.4}$$

Finally, it is clear that $$-1 < E_1 < +\infty \tag{4.5a}$$

and then $$-\frac{1}{2} < \gamma_{11} < +\infty \tag{4.5b}$$

and $$-\infty < e_{11} < +\frac{1}{2} \tag{4.5c}$$

From the measured axial load P applied to the specimen, its original (A_o) or current (A) cross-sectional area, and the extension E_1, one can determine the associated stress tensors as described next.

The Lagrange, or first Piola-Kirchhoff stress tensor T_{ij} gives the actual force dP_i acting on the deformed area dA, but it is reckoned per unit area dA_o of the undeformed body, and expresses the force in terms of the unit normal ν_o to dA_o [12, page 222]:

$$T_{ji}\, \nu_{o_j}\, dA_o = dP_i \tag{4.6}$$

The Lagrange, or first Piola-Kirchhoff stress tensor is also referred to as the "engineering stress" σ_E in uniaxial tests:

T_{11} = LAGRANGE STRESS = FIRST PIOLA-KIRCHHOFF STRESS

= "ENGINEERING STRESS" = $\sigma_E \equiv \frac{P}{A_o}$ (4.6a)

= $\frac{\text{actual force acting on deformed area}}{\text{undeformed area}}$

The second Piola-Kirchhoff stress tensor S_{ij} gives a pseudo force $d\tilde{\vec{P}}$ with components $\frac{\partial X_i}{\partial x_\alpha} dP_\alpha$, related to the actual force $d\vec{P}$ with components dP_α in the same way that a material (undeformed) vector dX_i at X_i is related by the deformation to the corresponding spatial (deformed) vector dx_α at x_α. It is reckoned per unit area dA_o of the undeformed body, and expresses the force in terms of the normal ν_o to dA_o [12, page 222]:

$$S_{ji}\,\nu_{o_j}\,dA_o = \frac{\partial X_i}{\partial x_\alpha}\,dP_\alpha \qquad (4.7)$$

In a uniaxial (and irrotational) deformation*: $\frac{\partial x_1}{\partial x_1} = \frac{1}{(1+E_1)}$

and hence $$S_{11} = \frac{P}{A_o(1+E_1)} = \frac{\sigma_E}{1+E_1} \qquad (4.7a)$$

S_{11} = SECOND PIOLA-KIRCHHOFF STRESS TENSOR COMPONENT

= $\frac{P/(1+E_1)}{A_o}$ = $\frac{\text{pseudo-force}}{\text{undeformed area}}$

The stress tensor S_{ij} can also be interpreted as the stress referred to a convected or intrinsic system of coordinates X_i (defined by the material coordinates as they deform with the body, in such a way that at each time t the numerical value of the coordinates x_α of a given point is the same as that of X_i), where S_{ij} is measured per unit area of the coordinate planes in the reference state. In order to calculate the second Piola-Kirchhoff stress, the axial extension E_1 is needed, in addition to the load P and the original area A_o.

*Since $x_m = u_m + X_n \delta_{nm}$, $\frac{\partial x_m}{\partial X_n} = \frac{\partial u_m}{\partial X_n} + \delta_{nm}$ and $u_1(X_1) = E_1 X_1$; hence, $\frac{\partial x_1}{\partial X_1} = E_1 + 1$

where $\delta_{nm}=1$ for $n=m$ and $\delta_{nm}=0$ for $n\neq m$.

The Cauchy stress tensor σ_{ij} [12, pages 77 and 222] gives the actual force dP_i acting on the deformed area dA, reckoned per unit area dA of the deformed body, expressing the force in terms of the unit outer normal ν to the deformed dA as $\sigma_{ji}\ \nu_j\ dA = dP_i$. The Cauchy stress tensor is also referred to as the "true stress" in uniaxial tests:

$$\sigma_{11} = \text{CAUCHY STRESS} = \text{"TRUE STRESS"} = \sigma_T \equiv \frac{P}{A} = \frac{\text{actual force acting on deformed area}}{\text{deformed area}} \tag{4.8}$$

Hence, in order to calculate the Cauchy stress, the actual (deformed) cross-sectional area is needed.

For the test specimens of circular cross-section, direct measurements of the "instantaneous diameter", D, were made using a displacement transducer (Hewlett-Packard Model 7DC DT-100) and recorded on a Honeywell Visicorder Model 1508 versus both extension E_1 and load P during each test. One can estimate the actual cross-sectional area as being $A = \frac{\pi}{4} D^2$. Also, one can relate the actual area A to the original area A_o through the use of the law of mass conservation which can be expressed for uniaxial deformation* by:

$$m_o = m \qquad \text{or} \qquad \rho_o A_o \ell_o = \rho A \ell \tag{4.9}$$

Hence, $\frac{A_o}{A} = \frac{\rho \ell}{\rho_o \ell_o}$ but $\frac{\ell}{\ell_o} = 1+E_1$ from Eq. 4.2. Thus,

$$\frac{A_o}{A} = \frac{\rho}{\rho_o}(1+E_1) \tag{4.10}$$

where m_o = original mass, m = current mass, ρ_o = original density = $m_o/(A_o \ell_o)$, and ρ = current density = $m/(A\ell)$. Note from Eq. 4.8 that

$$\sigma_T = \frac{P}{A} = \frac{P}{A_o}\frac{\rho}{\rho_o}(1+E_1) \tag{4.11a}$$

*Not necking.

or

$$\sigma_T = \sigma_E \frac{\rho}{\rho_o}(1 + E_1) \tag{4.11b}$$

If one assumes the material to be incompressible ($\frac{\rho}{\rho_o} = 1$), one can estimate the area ratio as

$$\frac{A_o}{A} = 1 + E_1 \tag{4.12}$$

It follows from Eq. 4.11b that

$$\sigma_T = \sigma_E (1 + E_1) \tag{4.13}$$

Aluminum is very nearly incompressible in the plastic region. The amount of compressibility that occurs in the elastic region is negligible since the material becomes plastic at very low levels of extension E_1. On the other hand, the material cross-sectional area did not deform in a circular fashion, but rather it became elliptical; such behavior has been noted often in similar past experiments (see Ref. 13, for example). This indicates material work-hardening anisotropy (as will be seen later by the somewhat different uniaxial stress-strain behavior and the significantly different fracture strain of the longitudinal vs. the transverse specimens). It turned out from the experimental measurements that meaningful diameter ratios ($\frac{D}{D_o}$) could be discerned only for extensions E_1 over 0.02, and this is significantly beyond the elastic region. Moreover, in order to calculate the true stress, the smallest cross-sectional area in the necked region should be measured. Since necking occurred at locations different from the extensometer location, these latter measurements could not be used for a true stress or (necked) cross-sectional area reduction determination once necking started.

For all of these reasons it is believed that Eq. 4.13 represents more accurately the Cauchy ("true") stress than the "true stress" obtained from employing direct diameter measurements using $\sigma_T = \frac{4P}{\pi D^2}$.

For the reader's convenience, plots of (1) Cauchy ("true") stress σ_T versus Green ("Lagrangian") strain γ_{11} (2) Lagrange (first Piola-Kirchhoff or "engineering") stress σ_E versus Green ("Lagrangian") strain γ_{11} and (3) 2nd Piola-Kirchhoff stress S_{11} versus Green ("Lagrangian") strain γ_{11} are included in this report. Other possible combinations of stress measures versus strain measures can be obtained readily from this information.

4.3 Uniaxial Stress-Strain Results

A total of 22 specimens was strain gaged and tested. The following table indicates their cross-sectional type (circular, C or rectangular, R) and their nominal cross-sectional dimensions as well as the figure number on which the associated stress-strain data appear:

Specimen Cross-Section Type	Nominal Dimensions	Specimen Type Longitudinal(L) or Transverse(T)	Specimen Identification Numbers	Associated Figures
R	0.5 in x 0.25 in	L	76-L1,-L2,-L3	25a,26a,27a
		T	76-T1,-T2,-T3,-T4,-T5	25b,26b,27b
R	0.35 in x 0.25 in	T	76-T7,-T8	25b,26b,27b
R	0.6 in x 0.06 in	L	76-L11,-L12	---
		T	76-T11,-T12	---
C	0.5 in D	L	CL-1,-2,-3,-4	28a,29a,30a
		T	CT-1,-2,-3,-4	28b,29b,30b

Stress-strain data were plotted up to the strain where the load began to decrease in value (in those areas where the strain gages were still attached to provide that information). Stress-strain data were not plotted after that point so as to ensure that the data represented actual uniaxial tensile behavior. It may be useful to note at this point that Miles [14] has proved that bifurcation (also called necking) cannot occur before the maximum load is attained. At bifurcation a complicated state of multiaxial stress develops in the necked region, and hence the state of stress is no longer uniaxial. Therefore, Eqs. 4.6a, 4.7a, and 4.8 are, strictly speaking, no longer valid.

It was found that the "post-elastic" stress-strain data for the circular cross-section specimens were somewhat different from those for the rectangular cross-section specimens. Accordingly, these two categories of data are plotted separately.

The data provided by the transverse specimens of rectangular cross-section measuring .35 in x .25 in (models 76-T7 and 76-T8) were very similar to that provided by the transverse specimens of rectangular cross-section measuring .5 in x .25 in (models 76-T1 through 76-T5). The .6 in x .06 in specimens (models 76-L11, 76-L12, 76-T11, and 76-T12) exhibited a larger spread than did the other specimens, but the mean of these data coincides with that of the remainder of the rectangular cross-section specimens; hence, these data points are not included here in present plots so as to avoid clutter.

It is believed that the deviation from stress-strain isotropy is sufficiently small for the rectangular cross-section specimens at strains lower than $\gamma_{11} \approx .18$, that is, before necking, that one can use the "average" properties as those for an isotropic material in that strain range.

The circular cross-section specimens (Figs. 28,29,30) exhibited more stress anisotropy (comparing the longitudinal versus the transverse specimens) and supported higher stresses than did the rectangular cross-section specimens (Figs. 25,26,27). However, further data are needed to permit one to make a definitive assessment of the implications of this behavior.

In 1973 the MIT-ASRL conducted tensile stress-strain tests of longitudinal specimens of 0.36 in diameter circular cross section of a very similar aluminum alloy: 6061-T6511. These specimens were prepared from 6-in diameter thick-wall drawn tubes, and are identified as specimens 73-L1 and 73-L2; the results are shown in Figs. 11 and 15 of Ref. 8. In comparing those earlier results with the present results it was found that the data for specimen 73-L1 (6061-T6511) are in good agreement with the present data shown in Figs. 28a, 29a, and 30 for the present circular cross-section specimens of 6061-T651: CL-1, CL-2, CL-3, and CL-4. However, the stress-strain data for circular cross-section specimen 73-L2 (6061-T6511) coincides with that of Figs. 25a, 26a, and 27 for the present rectangular cross-section specimens of 6061-T651: 76-L1, 76-L2, and 76-L3.

4.4 Stress-Strain Measurements Near Fracture

Two specimens of 6061-T651 aluminum with a rectangular cross-section of nominal dimensions 0.5 in by 0.25 in were lightly scribed with lines nominally .025 in apart and tested to tensile fracture.

One test specimen had its axis parallel to the plate-roll (or longitudinal, L, or material-grain) direction and was denoted as 76-L4. The other test specimen (denoted as 76-T6) was prepared with its axis parallel to the transverse (T) direction (or perpendicular to the plate-roll direction). Photographs of these two specimens are shown in Fig. 31.

The axial-direction extension, or relative elongation (E_1), was determined by measuring the distances between the lightly-scribed marks before (ℓ_o) and after (ℓ) the test, according to Eq. 4.1a; namely, $E_1 = \frac{\ell}{\ell_o} - 1$. These distances, ℓ_o and ℓ, were measured along the midwidth axis; along this axis the maximum elongations on the surface are present. The two 0.5 in wide faces along which extension measurements were made, were arbitrarily called "upper" and "lower" surfaces, in order to distinguish between the two sets of elongation (E_1) data shown in Fig. 32 for a given specimen.

Figures 32a and 32b show the permanent relative elongation (E_1) data as a function of pre-test distance (in inches) of the material points along the axis of the specimen, on the "upper" and "lower" surfaces of the longitudinal-direction specimen 76-L4. Fracture occurred at an angle of approximately 76° through the thickness. The thickness was measured as being 0.2365 in before the test, and .1970 in after the test (at the fracture location). The permanent relative elongation $[E_1]_F$ at the fracture location for specimen 76-L4 (tested in tension), as observed from the lightly scribed marks, is approximately $[E_1]_F \approx 0.89$. On the other hand, the ratio of the undeformed cross-sectional area (A_o) to the permanently deformed cross-sectional area (A_F) at the fracture location is $\frac{A_o}{A_F} \approx 1.73$. Using Eq. 4.10, one obtains $\frac{\rho_o}{\rho_F} \approx \frac{1.89}{1.73} \approx 1.09$. One must take into account that Eq. 4.10 assumes a uniaxial strain distribution at a given axial location (and hence constant over the entire neck cross-sectional area). In fact, the distribution is not constant over the neck cross-sectional area, the highest strains being located in the middle of the cross-sectional area (where fracture

starts). Therefore $(\frac{A_o}{A_F} - 1)$ gives only a cross-sectional average of the axial relative elongation at the neck, while $[E_1]_F$ measured on the middle axis at the surface gives the highest extension at that surface. This is part of the reason why $(1 + [E_1]_F) > \frac{A_o}{A_F}$. Also, the deformed cross-sectional area A_F and permanent relative elongation $[E_1]_F$ do not accurately represent the conditions at the initiation of fracture, there usually being some distortion incidental to the act of fracture ("springback" after fracture-induced unloading). Finally, there is considerable experimental error due to uncertainties in the measurements of distance and area; hence before any final conclusions are drawn for this material lot, more tests on similar specimens with lightly scribed marks should be performed.

Figures 32c and 32d show the permanent relative elongation E_1 as a function of pre-test distance (in inches) of the material points along the axis of the specimen on the "upper" and "lower" surfaces for the transverse-direction specimen, 76-T6. The permanent relative elongation $[E_1]_F$ at the fracture location, for specimen 76-T6, as observed from the lightly scribed marks, is approximately $[E_1]_F \approx 0.47$. The ratio of the undeformed cross-sectional area (A_o) to the permanently deformed cross-sectional area (A_F) at the fracture location is $\frac{A_o}{A_F} \approx 1.45$. Using Eq. 4.10 one obtains $\frac{\rho_o}{\rho_F} \approx \frac{1.47}{1.45} \approx 1.01$.

Nomenclature and definitions of relative elongation measures used to determine permanent "relative elongation" data at fracture for the rectangular and circular cross-section 6061-T651 aluminum specimens tested in tension to failure are given in Fig. 33. In Fig. 34 the circle symbols express the permanent "relative axial elongation" $[E_1]_F$ at the fracture location as derived from Eq. 4.12; that is, assuming incompressibility $(\frac{\rho_o}{\rho_F} \approx 1)$. It permits one to express the permanent relative axial elongation $[E_1]_F$ as a function of the ratio of the original cross-sectional area (A_o) to the final cross-sectional area (A_F) at the neck, or $[E_1]_F \approx \frac{A_o}{A_F} - 1$. It is evident from Fig. 34 that there is no difference for the fracture relative elongation $[E_1]_F$ between the circular and the rectangular cross-section specimens. Figure 34 also shows distinct work-hardening anisotropy of the aluminum

material. All transverse-direction specimens (irrespective of cross-sectional area type) fracture at strains considerably lower than the longitudinal-direction specimens.

The other two symbols (x and +) in Fig. 34 pertain to the unit contractions of the specimen cross-sections, measured in two orthogonal directions perpendicular to the axial direction. For the specimens with initially-circular cross-sectional area, these axes are oriented at right angles to each other according to the major (denoted by subscript 3) and minor (denoted by subscript 2) axis of the final elliptical shape of the cross-section (see Fig. 33). For the specimens with rectangular cross-sectional area, one axis (denoted by subscript 2) is oriented along the longest side of the rectangular cross-section, and the other axis (denoted by subscript 3) is oriented along the shortest side of the cross-section (see Fig. 33).

The permanent unit contractions ($[-E_2]_F$ and $[-E_3]_F$ as depicted in Fig. 34 are the average value over the entire side of the cross-section, calculated as $[-E_2]_F = 1 - \frac{(\ell_2)_F}{(\ell_2)_o}$ (denoted by symbol x in Fig. 34), and $[-E_3]_F = 1 - \frac{(\ell_3)_F}{(\ell_3)_o}$ (denoted by symbol + in Fig. 34), where $(\ell_{2,3})_o$, $(\ell_{2,3})_F$ are the original and permanent (final) lengths respectively, along axes 2 and 3. It is evident from Fig. 34 that the rectangular cross-section specimens experienced the largest unit contraction along the longest side on their cross-sections. If the ℓ_3 dimension for specimens of both rectangular and circular cross section were in the through-the-thickness direction of the 2.55-in thick rolled plate stock from which these specimens were made, one might conclude that the least strain occurred in this direction (which is the direction of imposed compression strains during rolling). However, the specimen-orientation data records are not sufficiently clear to permit making that conclusion.

Figures 35, 36, and 37 show the tensile static stress versus permanent strain data at the fracture location for the 6061-T651 aluminum specimens. These data are given in terms of the stress measures and Lagrangian strain tensor used previously for the uniaxial stress-strain data (Figs. 25 through 30). Since the state of stress at fracture is not uniaxial (the stress and

and strain being non-uniform over the cross-section), these stress measures (computed from quantities averaged over the cross-section) are only rough average measures of the true behavior.

Figures 35, 36, and 37 clearly indicate, that although there is no difference between the rectangular and the initially-circular cross-section specimens with respect to permanent strain at fracture, the initially-circular cross-section specimens did support higher stresses.

The axial (Lagrangian) Green strain tensor component at fracture ($[\gamma_{11}]_F$) was computed by assuming incompressibility ($\frac{\rho_o}{\rho_F} \approx 1$). Using Eqs. 4.2b and 4.12, one obtains $[\gamma_{11}]_F \approx \frac{1}{2}\left[\left(\frac{A_o}{A_F}\right)^2 - 1\right]$ where A_o (A_F) is the cross-sectional area at the fracture location before (after) the test. The testing machine provided the value of the load (P_F) supported by the specimen at the instant of fracture. From a knowledge of the load at fracture (P_F) and the original cross-sectional area (A_o) at the fracture location, one can compute the "engineering stress" at fracture. Using Eq. 4.6, one obtains $[\sigma_E]_F = \frac{P_F}{A_o}$ as shown in Fig. 35. Measuring the permanent cross-sectional area (A_F) at the fracture location (and hence neglecting the "springback" at fracture) one can compute the "true stress" at fracture by employing Eq. 4.8; hence, one obtains $[\sigma_T]_F = \frac{P_F}{A_F}$. Figure 36 shows the tensile static true stress versus permanent Green strain at the fracture location.

Finally, one can estimate the axial 2nd Piola-Kirchhoff stress by assuming incompressibility ($\frac{\rho_o}{\rho_F} \approx 1$), and neglecting the "springback" at fracture. Employing Eqs. 4.7 and 4.12, one obtains

$$\left[S_{11}\right]_F \approx \frac{P_F\, A_F}{(A_o)^2} \tag{4.14}$$

Figure 37 shows the correlation of this stress measure with the permanent Green strain $[\gamma_{11}]_F$ at the fracture location for the 6061-T651 aluminum specimens.

4.5 Comments

Although more than 20 tensile specimens of this lot of 6061-T651 aluminum plate material were tested to obtain uniaxial stress-strain data, this material characterization is incomplete but the needed further testing could not be done in the present effort because of fund limitations.

In addition to the tension tests already conducted, compression stress-strain measurements should be carried out in specimens with longitudinal-direction and transverse-direction axes, from the 6061-T651 aluminum plate stock. Specimens with circular cross-sections would be advisable for these tests.

Further tests are needed to characterize the material condition at tensile fracture. In this regard, the use of light mechanically-scribed grids on test specimens for pre-test and post-test spacing measurements is valuable since strain gages do not survive nor do they turn out to be located where the fracture level of strain is produced. In the present program, only one specimen from each the longitudinal (76-L4) and the transverse (76-T6) direction was employed to make these measurements and tested to fracture; further, these were specimens of 0.25 in by 0.50 in rectangular cross section. The relative elongation at fracture was found to be very different for the longitudinal vs. the transverse-direction specimen.

Longitudinal	76-L4	$(E_1)_F \doteq 0.89$
Transverse	76-T6	$(E_1)_F \doteq 0.47$

Perhaps 4 or 5 specimens of each type should be tested to obtain similar data in order to establish mean $(E_1)_F$ values for each type of specimen: L and T. Further, one should prepare, apply mechanical gridding, and test to fracture specimens of both circular cross section and rectangular cross section of several width-to-thickness ratios for axis orientation L and T. It may also be instructive to employ similar specimens with axes intermediate between the L and T directions.

These data are believed to be needed to provide fracture strain criteria and envelope information to permit rational predictions of fracture initiation in the 6061-T651 panels which have been subjected to impulse loads or to fragment impact.

SECTION 5

SUMMARY AND COMMENTS

The sheet explosive loading technique (SELT) has been employed to obtain elastic-plastic, large-deflection 3-d structural transient and/or permanent strain data on simple well-defined structural specimens and materials: initially-flat 6061-T651 aluminum panels with all four sides ideally clamped via integral construction. The SELT loading technique was chosen since it is both convenient and provides "forcing function information" of small uncertainty. These data will be useful for evaluating pertinent 3-d structural response prediction methods.

A second objective of the present study was to obtain high-quality transient-strain data for a well-defined structural/material model subjected to impact by a "rigid body" of known mass, impact velocity, and geometry; large-deflection, elastic-plastic transient 3-d response conditions are of primary interest. Accordingly, (a) uniform-thickness and integrally-stiffened panels with all four sides clamped and (b) a steel sphere as the impacting body were chosen. The steel sphere was launched vertically by explosive propulsion to achieve various desired impact velocities. The conducted sphere/panel impact tests produced a wide range of structural responses and permanent deformations, including rupture of the panel from excessive structural response in several cases. The transient and permanent strain data as well as the permanent deflection data obtained are of high quality and should be quite useful for checking and evaluating methods for predicting the 3-d structural responses of panels subjected to fragment (sphere) impact. Unfortunately, however, transient strain data very close to the point of impact were not obtained over as long a time as desirable because the gage(s) in that region became detached during the transient response. Nevertheless, a considerable amount of useful transient strain data and permanent strain data was obtained.

Both of these types of experimental structural response data will be valuable for checking structural response prediction methods. In particular, the present impact-induced structural response data will be employed to

evaluate the adequacy and accuracy of methods developed to predict the responses of protective structures undergoing 3-d structural deformations when subjected to impact by aircraft engine rotor fragments.

In order to assess the stress-strain behavior of the 6061-T651 aluminum thick-plate material from which the panel specimens were prepared, a number of tensile specimens of rectangular or circular cross-section were prepared and subjected to static uniaxial loading. Specimens with axes parallel to the 6061-T651 plate roll (or longitudinal, L,) direction as well as perpendicular (or transverse, T) to the plate-roll direction were used. To assess the "fracture strain" properties of this material, one L and one T specimen were marked lightly with mechanically-scribed closely-spaced grids, whose spacings before and after tensile testing to fracture were measured; further tests of this type are needed to provide statistically significant fracture strain data. Also, monotonic compression tests as well as yielding, unloading, reversed yielding, reloading tests -- of initial-tension yielding and of initial-compression yielding are needed for a fuller description of the mechanical behavior of this lot of 6061-T651 aluminum material.

REFERENCES

1. Witmer, E.A, Merlis, F. and Spilker, R.L., "Experimental Transient and Permanent Deformation Studies of Steel-Sphere-Impacted or Impulsively-Loaded Aluminum Beams with Clamped Ends", ASRL TR 154-11, Aeroelastic and Structures Research Laboratory, Massachusetts Institute of Technology, October 1975. (Available as NASA CR-134922.)

2. Stagliano, T.R., Spilker, R.L. and Witmer, E.A., "User's Guide to Computer Program CIVM-JET 4B to Calculate the Transient Structural Responses of Partial and/or Complete Structural Rings to Engine-Rotor Fragment Impact", ASRL TR 154-9, Aeroelastic and Structures Research Laboratory, Massachusetts Institute of Technology, September 1975. (Available as NASA CR-134907.)

3. Wu, Richard, W-H, Spilker, R.L., Stagliano, T.R. and Witmer, E.A., "User's Guide to Computer Programs JET 5A and CIVM-JET 5B to Calculate the Large Elastic-Plastic Dynamically-Induced Deformations of Multilayer Partial and/or Complete Structural Rings", ASRL TR 154-10, Aeroelastic and Structures Research Laboratory, Massachusetts Institute of Technology, February 1977 (in preparation).

4. Spilker, R.L., Witmer, E.A. and French, S.E., "Finite Element Nonlinear Transient Response Analysis of Panels Subjected to Impulse or Impact Loads", MIT ASRL TR 154-14 (in preparation).

5. Wu, Richard, W-H and Witmer, E.A., "Finite Element Analysis of Large Transient and Elastic-Plastic Deformations of Simple Structures, with Application to the Engine Rotor Fragment Containment/Deflection Problem", ASRL TR 154-4, Aeroelastic and Structures Research Laboratory, Massachusetts Institute of Technology, January 1972. (Available as NASA CR-120886.)

6. Wu, Richard W-H and Witmer, E.A., "Computer Program - JET 3 - To Calculate the Large Elastic-Plastic Dynamically-Induced Deformations of Free and Restrained, Partial and/or Complete Structural Rings", ASRL TR 154-7, Aeroelastic and Structures Research Laboratory, Massachusetts Institute of Technology, August 1972. (Available as NASA CR-120993.)

7. Wu, Richard W-H and Witmer, E.A., "Finite Element Predictions of Transient Elastic-Plastic Large Deflections of Stiffened and/or Unstiffened Rings and Cylindrical Shells", ASRL TR 171-4, Aeroelastic and Structures Research Laboratory, Massachusetts Institute of Technology, April 1974. (Available as AMMRC CTR 74-31).

8. Witmer, E.A., Wu, Richard W-H and Merlis, F., "Experimental Transient and Permanent Deformation Studies of Impulsively-Loaded Rings and Cylindrical Panels, both Stiffened and Unstiffened", ASRL TR 171-3, Aeroelastic and Structures Research Laboratory, Massachusetts Institute of Technology, April 1974. (Available as AMMRC CTR 74-29.)

9. Anon., "Du Pont Detasheet Flexible Explosive", E.I. du Pont de Nemours & Co., Inc., Wilmington, Delaware, 1971.

10. Murray, W.M., "Fundamental Concepts for Strain Gages", Department of Mechanical Engineering, Massachusetts Institute of Technology, 1973.

11. Private communcation 4-20-73 from J.F. Raudenbush, Senior Applications Engineer, Micro-Measurements, Inc., Romulus, Michigan; also, M-M Technical Note 137.

12. Malvern, L.E., Introduction to the Mechanics of a Continuous Medium, Prentice-Hall, Inc., Englewood Cliffs, N.J., 1969.

13. MacGregor, C.W., "Numerical Properties of Materials" in Section 5 of Marks' Standard Handbook for Mechanical Engineers, McGraw-Hill Book Co., 7th Edition, 1967, pp. 5-2 through 5-20.

14. Miles, J.P., "Bifurcation in Plastic Flow under Uniaxial Tension", J. Mech. Phys. Solids, Vol. 19, 1971, pp. 89-102.

TABLE 1

PRE-TEST DIMENSIONS OF THE UNIFORM-THICKNESS

6061-T651 ALUMINUM PANEL MODELS

Ident. No.	Panel Region				Support Collar	
	Thickness		Span (in)			
	Mean h (in)	% Std. Dev. from Mean	L_x	L_y	h_c (in)	L_c (in)
CP-1	.0636	.57	8.000	7.998	1.477	2.009
CP-2	.0623	.42	7.999	7.998	1.475	2.009
CP-7+	.0618	.43	8.003	8.000	1.462	1.999
CP-8+	.0633	.65	7.999	7.998	1.464	2.004
CP-9	.0607	2.61	7.999	7.999	1.464	2.003
CP-12	.0611	2.06	8.003	8.002	1.476	2.003

+Specimens with photo-etched grids spaced nominally 0.020-in apart over a centered 3-in x 3-in region on the upper surface.

TABLE 2

SHEET HE WEIGHT PER UNIT AREA AND INITIAL LATERAL VELOCITY IMPARTED TO EACH 6061-T651 IMPULSIVELY-LOADED PANEL MODEL

Model	CP-1	CP-2
HE Sheet Weight per Unit Area (gm/in^2)	0.6045	0.6323
Initial Velocity* (in/sec) of the 2-in by 2-in HE-Covered Region	15,216	16,325

*Based upon a specific impulse of 0.407 lb-sec/gm = 18.1×10^4 dyne-sec/gm and 6061-T651 aluminum material weight of 0.098 lb/in^3; see Ref. 8 for specific impulse data.

TABLE 3

STRAIN GAGE LOCATION AND PERMANENT STRAIN DATA

FOR THE IMPULSIVELY-LOADED 6061-T651 PANELS

Strain Gage Identif. Number	Location[a]				Permanent Strain[b] (per cent)	
	x(in)	y(in)	r(in)	θ(deg) Orient.	Model CP-1	Model CP-2
1	0	0.50	0.50	90	±*	-[c]
2	0	1.00	1.00	90	±*	±*
3	0	1.50	1.50	90	±*	+4.04*
4	0	2.00	2.00	90	+1.06	+1.82*
5	0.71	0.71	1.00	45	±*	±*
6	1.06	1.06	1.50	45	+3.22	+5.39*
7	1.50	1.50	2.12	45	+1.90*	+1.74*
8	2.00	2.00	2.83	45	+0.16*	+0.08*
9	0.25	0	0.25	0	-	Not Used
10	1.00	0	1.00	0	±*	-
11	+0.35	-0.35	0.50	315	-	-
12	+0.71	-0.71	1.00	315	-	-
13	+1.06	-1.06	1.50	315	+3.95	+4.10
14	+1.41	-1.41	2.00	315	+1.99	+2.46
15	0	-0.50	0.50	270	±*	-
16	0	-1.00	1.00	270	-	-
17	-0.35	-0.35	0.50	225	-	-
18	0	-1.50	1.50	270	Not Used	+4.85*

a: All gages are on the surface which was not loaded impulsively.

b: This permanent strain is the corrected relative elongation E_{r_c} along the ray denoted by θ (see Fig. 2 and Eq. 2.1).

c: A dash (-) indicates that the strain gage was found to be detached after the test.

*: Denotes that transient strain measurements were attempted.

TABLE 4

VERTICAL LOCATION CHANGE OF THE LOWER SURFACE OF

IMPULSIVELY-LOADED PLATE MODEL CP-1

Vertical Location Change z_ℓ (in)										
x(in)	y=-4.50	-4.00	-3.50	-3.00	-2.50	-2.00	-1.50	-1.00	-0.50	0
-4.50	-.0005	0	-.0008	-.0003	-.0006	-.0007	-.0008	-.0008	-.0008	-.0008
-4.00	-.0005	-.0005	-.0004	-.0003	0	0	.0002	.0003	.0006	.0008
-3.50	-.0003	-.0005	.0140	.0283	.0383	.0483	.0573	.0640	.0683	.0701
-3.00	-.0005	-.0006	.0283	.0576	.0759	.0915	.1070	.1204	.1283	.1323
-2.50	0	-.004	.0372	.0747	.0956	.1158	.1366	.1552	.1686	.1750
-2.00	-.0003	.0002	.0460	.0853	.1110	.1448	.1878	.2294	.2596	.2748
-1.50	-.0008	.0004	.0543	.0970	.1257	.1818	.2723	.3534	.4130	.4414
-1.00	-.0004	.0003	.0610	.1073	.1382	.2197	.3483	.4720	.5749	.6303
-0.50	-.0007	.0007	.0635	.1130	.1467	.2447	.4073	.5734	.7440	.8493
0	-.0005	.0003	.0638	.1148	.1493	.2530	.4343	.6263	.8521	1.015
0.50	0	.0015	.0635	.1126	.1455	.2450	.4117	.5820	.7633	.8765
1.00	.0003	.0012	.0615	.1078	.1380	.2209	.3553	.4829	.5930	.6496
1.50	.0003	.0012	.0564	.0973	.1253	.1838	.2786	.3653	.4268	.4574
2.00	.0003	.0011	.0470	.0852	.1110	.1468	.1942	.2406	.2707	.2847
2.50	.0005	.0007	.0381	.0748	.0956	.1165	.1383	.1575	.1713	.1780
3.00	.0007	.0010	.0290	.0580	.0758	.0914	.1067	.1185	.1252	.1292
3.50	.0010	.0011	.0153	.0296	.0395	.0497	.0582	.0641	.0672	.0683
4.00	.0010	.0013	.0013	.0012	.0013	.0018	.0020	.0021	.0023	.0028
4.50	.0011	.0013	.0017	.0016	.0017	.0016	.0018	.0018	.0017	.0017

Note: The center of the panel is at (x,y) = (0,0).

TABLE 4 -- CONTINUED (CP-1)

Vertical Location Change z_ℓ (in)									
x(in)	y=0.50	1.00	1.50	2.00	2.50	3.00	3.50	4.00	4.50
-4.50	-.0010	-.0005	-.0007	-.0008	-.0008	-.0008	-.0010	-.0011	-.0009
-4.00	.0004	.0003	0	0	-.0004	-.0004	-.0006	-.0007	-.0009
-3.50	.0700	.0666	.0588	.0488	.0380	.0267	.0112	-.0006	-.0010
-3.00	.1324	.1273	.1160	.0986	.0800	.0555	.0248	-.0006	-.0008
-2.50	.1766	.1712	.1577	.1376	.1133	.0812	.0373	-.0008	-.0010
-2.00	.2742	.2548	.2230	.1856	.1476	.1007	.0517	-.0004	-.0008
-1.50	.4250	.3803	.3167	.2457	.1872	.1344	.0667	-.0008	-.0009
-1.00	.5906	.5032	.4033	.3022	.2218	.1570	.0783	-.0003	-.0010
-0.50	.7704	.6167	.4733	.3456	.2467	.1697	.0844	0	-.0008
0	.8776	.6715	.5012	.3568	.2527	.1724	.0839	0	-.0008
0.50	.7813	.6193	.4733	.3416	.2400	.1662	.0817	0	-.0003
1.00	.6034	.5090	.4052	.2996	.2146	.1532	.0762	.0010	.0005
1.50	.4370	.3853	.3173	.2427	.1810	.1315	.0658	.0010	.0008
2.00	.2823	.2618	.2258	.1862	.1460	.1053	.0520	.0012	.0010
2.50	.1798	.1740	.1613	.1403	.1140	.0830	.0392	.0012	.0011
3.00	.1297	.1267	.1171	.1013	.0823	.0586	.0281	.0011	.0011
3.50	.0686	.0660	.0603	.0512	.0400	.0290	.0143	.0016	.0012
4.00	.0020	.0022	.0019	.0018	.0018	.0013	.0018	.0013	.0016
4.50	.0019	.0018	.0016	.0016	.0017	.0015	.0016	.0013	.0013

TABLE 4 -- CONCLUDED (CP-1)

Spanwise Location x(in) Along y=0	Vertical Location Change z_ℓ(in)	Spanwise Location x(in) Along y=0	Vertical Location Change z_ℓ(in)	Spanwise Location y(in) Along x=0	Vertical Location Change z_ℓ(in)	Spanwise Location y(in) Along x=0	Vertical Location Change z_ℓ(in)
-4.50	-.0003	4.50	+.0001	-4.50	-.0006	4.50	-.0006
-4.25	-.0003	4.25	+.0002	-4.25	-.0002	4.25	-.0005
-4.00	+.0007	4.00	+.0015	-4.00	+.0005	4.00	0
-3.75	+.0327	3.75	+.0325	-3.75	+.0310	3.75	+.0360
-3.50	+.0699	3.50	+.0678	-3.50	+.0643	3.50	+.0837
-3.25	+.1049	3.25	+.1009	-3.25	+.0953	3.25	+.1314
-3.00	+.1321	3.00	+.1281	-3.00	+.1153	3.00	+.1726
-2.75	+.1498	2.75	+.1479	-2.75	+.1282	2.75	+.2100
-2.50	+.1747	2.50	+.1778	-2.50	+.1497	2.50	+.2534
-2.25	+.2129	2.25	+.2215	-2.25	+.1876	2.25	+.3002
-2.00	+.2738	2.00	+.2843	-2.00	+.2524	2.00	+.3577
-1.75	+.3551	1.75	+.3689	-1.75	+.3413	1.75	+.4243
-1.50	+.4408	1.50	+.4570	-1.50	+.4347	1.50	+.5009
-1.25	+.5324	1.25	+.5496	-1.25	+.5302	1.25	+.5842
-1.00	+.6298	1.00	+.6508	-1.00	+.6267	1.00	+.6715
-0.80	+.7158	0.80	+.7370	-0.80	+.7142	0.80	+.7522
-0.60	+.8061	0.60	+.8287	-0.60	+.8045	0.60	+.8358
-0.40	+.8938	0.40	+.9201	-0.40	+.8963	0.40	+.9219
-0.20	+.9724	0.20	+.9918	-0.20	+.9753	0.20	+.9954
-0.10	+1.0009	0.10	+1.0128	-0.10	+1.0033	0.10	+1.0128
0	+1.0147	0	+1.0147	0	+1.0153	0	+1.0153

TABLE 5

VERTICAL LOCATION CHANGE OF THE LOWER SURFACE OF

IMPULSIVELY-LOADED PLATE MODEL CP-2

Vertical Location Change z_ℓ (in)										
x(in)	y=-4.50	-4.00	-3.50	-3.00	-2.50	-2.00	-1.50	-1.00	-0.50	0
-4.50	0	0	-.0003	-.0001	-.0002	-.0002	0	0	0	0
-4.00	-.0002	-.0002	0	0	0	+.0004	+.0008	+.0010	+.0011	+.0018
-3.50	-.0004	0	+.0148	+.031	+.0435	+.0538	+.0632	+.0707	+.0743	+.0753
-3.00	-.0002	0	+.0303	+.0636	+.0838	+.0990	+.1153	+.1288	+.1381	+.1432
-2.50	-.0004	0	+.0417	+.0823	+.1036	+.1238	+.1460	+.1650	+.1793	+.1862
-2.00	-.0006	0	+.0522	+.0956	+.1191	+.1535	+.2014	+.2433	+.2673	+.2787
-1.50	-.0006	-.0002	+.0624	+.1097	+.1342	+.1958	+.2927	+.3736	+.4408	+.4783
-1.00	-.0008	-.0001	+.0715	+.1203	+.1480	+.2393	+.3772	+.5084	+.6356	+.7123
-0.50	-.0008	0	+.0762	+.1264	+.1578	+.2700	+.4403	+.6278	+.8490	+.9726
0	-.0008	+.0002	+.0770	+.1290	+.1616	+.2793	+.4644	+.6797	+.9390	+1.1013
0.50	-.0006	0	+.0760	+.1267	+.1590	+.2671	+.4354	+.6194	+.8163	+.9318
1.00	-.0008	-.0002	+.0713	+.1207	+.1497	+.2360	+.3722	+.5004	+.6155	+.6790
1.50	-.0006	-.0003	+.0624	+.1096	+.1362	+.1935	+.2872	+.3702	+.4355	+.4701
2.00	-.0008	-.0003	+.0517	+.0953	+.1203	+.1533	+.1978	+.2390	+.2672	+.2832
2.50	-.0006	-.0007	+.0403	+.0820	+.1048	+.1228	+.1438	+.1626	+.1770	+.1845
3.00	-.0009	-.0006	+.0292	+.0626	+.0833	+.0986	+.1150	+.1293	+.1384	+.1430
3.50	-.0008	-.0006	+.0140	+.0298	+.0420	+.0530	+.0628	+.0703	+.0742	+.0750
4.00	-.0008	-.0004	0	0	0	0	+.0007	+.0009	+.0009	+.0010
4.50	-.0008	-.0002	-.0002	0	0	0	0	0	+.0002	0

Note: The center of the panel is at (x,y) = (0,0).

TABLE 5 -- CONTINUED (CP-2)

Vertical Location Change z_ℓ (in)									
x(in)	y=0.50	1.00	1.50	2.00	2.50	3.00	3.50	4.00	4.50
-4.50	-.0002	-.0002	0	0	-.0003	-.0004	-.0004	-.0003	-.0007
-4.00	+.0016	+.0013	+.0010	+.0008	+.0002	0	-.0002	-.0006	-.0007
-3.50	+.0752	+.0713	+.0640	+.0543	+.0447	+.0322	+.0157	-.0007	-.0010
-3.00	+.1417	+.1362	+.1240	+.1080	+.0903	+.0668	+.0310	-.0006	-.0009
-2.50	+.1867	+.1802	+.1677	+.1467	+.1232	+.0928	+.0450	-.0007	-.0009
-2.00	+.2788	+.2641	+.2338	+.1973	+.1593	+.1198	+.0603	-.0002	-.0009
-1.50	+.4538	+.3990	+.3330	+.2604	+.2013	+.1505	+.0766	0	-.0010
-1.00	+.6485	+.5374	+.4282	+.3260	+.2400	+.1733	+.0898	+.0008	-.0008
-0.50	+.8604	+.6623	+.5003	+.3718	+.2690	+.1880	+.0963	+.0020	-.0005
0	+.9486	+.7119	+.5287	+.3863	+.2774	+.1920	+.0972	+.0012	-.0007
0.50	+.8320	+.6540	+.4991	+.3710	+.2672	+.1860	+.0943	+.0009	-.0005
1.00	+.6316	+.5348	+.4303	+.3270	+.2390	+.1698	+.0872	+.0011	-.0002
1.50	+.4510	+.4015	+.3353	+.2632	+.2000	+.1448	+.0738	+.0008	-.0003
2.00	+.2838	+.2688	+.2392	+.2003	+.1587	+.1148	+.0567	+.0005	0
2.50	+.1870	+.1833	+.1702	+.1483	+.1216	+.0873	+.0411	+.0003	0
3.00	+.1428	+.1369	+.1238	+.1063	+.0866	+.0606	+.0282	+.0003	0
3.50	+.0742	+.0703	+.0627	+.0523	+.0405	+.0284	+.0138	+.0002	0
4.00	+.0010	+.0010	+.0008	+.0008	+.0003	+.0005	0	+.0002	0
4.50	+.0002	+.0005	+.0002	+.0002	+.0002	+.0002	0	+.0002	-.0002

TABLE 5 -- CONCLUDED (CP-2)

Spanwise Location x(in) Along y=0	Vertical Location Change z_ℓ(in)	Spanwise Location x(in) Along y=0	Vertical Location Change z_ℓ(in)	Spanwise Location y(in) Along x=0	Vertical Location Change z_ℓ(in)	Spanwise Location y(in) Along x=0	Vertical Location Change z_ℓ(in)
-4.50	0	4.50	+.0005	-4.50	-.0008	4.50	-.0005
-4.25	+.0005	4.25	+.0007	-4.25	-.0004	4.25	-.0003
-4.00	+.0011	4.00	+.0019	-4.00	+.0001	4.00	+.0013
-3.75	+.0371	3.75	+.0363	-3.75	+.0358	3.75	+.0440
-3.50	+.0759	3.50	+.0758	-3.50	+.0770	3.50	+.0977
-3.25	+.1125	3.25	+.1138	-3.25	+.1093	3.25	+.1500
-3.00	+.1433	3.00	+.1437	-3.00	+.1291	3.00	+.1922
-2.75	+.1622	2.75	+.1619	-2.75	+.1410	2.75	+.2316
-2.50	+.1860	2.50	+.1850	-2.50	+.1617	2.50	+.2780
-2.25	+.2209	2.25	+.2220	-2.25	+.2037	2.25	+.3278
-2.00	+.2781	2.00	+.2840	-2.00	+.2793	2.00	+.3868
-1.75	+.3657	1.75	+.3712	-1.75	+.3710	1.75	+.4520
-1.50	+.4769	1.50	+.4709	-1.50	+.4645	1.50	+.5283
-1.25	+.5915	1.25	+.5712	-1.25	+.5712	1.25	+.6175
-1.00	+.7111	1.00	+.6794	-1.00	+.6800	1.00	+.7128
-0.80	+.8098	0.80	+.7800	-0.80	+.7790	0.80	+.8050
-0.60	+.9328	0.60	+.8799	-0.60	+.8818	0.60	+.9010
-0.40	+1.0109	0.40	+.9826	-0.40	+.9843	0.40	+.9970
-0.20	+1.0759	0.20	+1.0712	-0.20	+1.0671	0.20	+1.0760
-0.10	+1.0962	0.10	+1.0941	-0.10	+1.0932	0.10	+1.1008
0	+1.1019	0	+1.1019	0	+1.1012	0	+1.1012

TABLE 6

PRE-TEST DIMENSIONS OF THE INTEGRALLY-STIFFENED

6061-T651 PANEL MODELS

Ident. No.	Panel Region				Stiffener		Support Collar	
	Thickness		Span (in)		h^*_{sp} (in)	Width (in)	h_c (in)	L_c (in)
	Mean h (in)	% Std. Dev. from Mean	L_x	L_y				
SCP-1	.0640	2.17	8.005	7.999	.240	.126	1.483	2.005
SCP-2	.0620	.68	8.014	7.997	.240	.121	1.478	2.000

*Total thickness (or depth) of panel and stiffener.

TABLE 7

STRAIN GAGE LOCATIONS AND PERMANENT STRAIN DATA
FOR THE STEEL-SPHERE-IMPACTED UNIFORM
THICKNESS 6061-T651 PANEL SPECIMENS

Strain Gage Identif. Number	Location[a]			Permanent Strain[b] (per cent)			
				Model			
	x(in)	y(in)	Orient. θ(deg)	CP-7 (ruptured)	CP-8	CP-9 (ruptured)	CP-12
1	0	0.50	90	-6.88*	-1.20*	*	+0.22*
2	0	1.00	90	-0.40*	-0.16*	-0.04*	-0.26*
3	0.71	0.71	45	-[c]	-0.61	-	+0.34
4	0.50	0	0	*	-0.06*	*	*
5	1.00	0	0	*	-0.03*	-0.91*	-0.32*
6	0.71	-0.71	315	-	-0.01	-	+0.46
7	0	-.50	270	*	*	+0.38*	-0.32*
8	0	-1.00	270	-0.50*	-0.03*	+0.38*	-0.14*
9	-0.71	-0.71	225	-3.95	-0.01	-3.38	-1.13
10	-0.50	0	180	-2.61*	-0.54*	-3.01*	-1.19*
11	-1.00	0	180	-0.67*	-0.18*	-0.38*	-0.06*
12	-0.71	0.71	135	-4.66	-1.15	+0.36	-0.56

a: All gages are on the non-impacted surface (see Fig. 2 for the definition of θ).

b: The permanent strain is the corrected relative elongation E_{rc} along the ray denoted by θ (see Eq. 2.1).

c: A dash (-) indicates that the strain gage was found to be detached after the test.

*: Denotes that transient strain measurements were attempted.

TABLE 8

STRAIN GAGE LOCATIONS AND PERMANENT STRAIN DATA FOR THE STEEL-SPHERE-IMPACTED INTEGRALLY-STIFFENED 6061-T651 PANEL SPECIMEN SCP-1

Strain Gage Identif. Number	Location[a]			Permanent Strain[b] (per cent)
	x(in)	y(in)	Orient. θ(deg)	Model SCP-1
1[d]	-1.98	0	270	±
2[d]	-1.98	-.50	270	-0.68*
3[d]	-1.98	-1.00	270	-0.92
4	-2.33	-.35	225	+0.42*
5	-2.69	-.71	225	-0.18
6	-2.48	0	180	+0.02*
7	-2.98	0	180	+0.02
8	-2.33	.35	135	+0.36
9	-2.69	.71	135	-0.16
10[d]	-1.98	.50	90	+1.08*
11[d]	-1.98	1.00	90	-0.84
12	-1.63	.35	45	0*
13	-1.27	.71	45	-0.34
14	-1.48	0	0	-0.30*
15	-0.98	0	0	-0.46
16	-1.63	-.35	315	-0.22*
17	-1.27	-.71	315	-0.36

a: All gages are on the surface not impacted; gages 1, 2, 3, 10, and 11 are on stiffener upper surface.

b: The permanent strain is the corrected relative elongation E_{rc} along the ray denoted by θ (see Eq. 2.1).

c: A dash (-) indicates that the strain gage was found to be detached after the test.

d: These gages are on the upper face of a stiffener.

*: Denotes that transient strain measurements were attempted.

TABLE 9

STRAIN GAGE LOCATIONS AND PERMANENT STRAIN DATA FOR THE STEEL-SPHERE-IMPACTED INTEGRALLY-STIFFENED 6061-T651 PANEL SPECIMEN SCP-2

Strain Gage Identif. Number	Location[a]			Permanent Strain[b] (per cent)
	x(in)	y(in)	Orient. θ(deg)	Model SCP-2
1[d]	2.01	0	90	+13.64*
2[d]	2.01	.50	90	+0.55*
3[d]	2.01	1.00	90	-0.67
4	2.36	.35	45	-0.22*
5	2.72	.71	45	-0.06
6	2.51	0	0	-0.32*
7	3.01	0	0	+0.20
8	2.36	-.35	315	-0.28
9	2.72	-.71	315	+0.02
10[d]	2.01	-.50	270	-0.63*
11[d]	2.01	-1.00	270	-0.69
12	1.66	-.35	225	-0.20*
13	2.70	-.71	225	-0.16
14	1.51	0	180	-
15	1.01	0	180	-0.46
16	1.66	.35	135	-
17	2.70	.71	135	-0.38

a: All gages are on the non-impacted surface; gages 1, 2, 3, 10, and 11 are on stiffener upper surface.

b: The permanent strain is the corrected relative elongation E_{rc} along the ray denoted by θ (see Eq. 2.1).

c: A dash (-) indicates that the strain gage was found to be detached after the test.

d: These gages are on the upper face of a stiffener.

*: Denotes that transient strain measurements were attempted.

TABLE 10

IMPACT LOCATION, IMPACT VELOCITY, AND WEIGHT OF LAUNCHING EXPLOSIVE FOR THE STEEL-SPHERE-IMPACTED 6061-T651 PANEL SPECIMENS

Model	Impact Location		Sphere Weight (gm)	Impact Velocity (in/sec)	HE Weight (gm)	Remarks
	x(in)	y(in)				
CP-7	+0.30	-0.10	66.805	2850	4.499	Too fast -- model ruptured.
CP-8	+0.041	-0.092	66.799	2435	3.105	Large permanent deflection. Upper surface photo-etch gridded.
CP-9	+0.016	+0.011	66.811	2755	3.999	Too fast -- model ruptured.
CP-12	+0.210	+0.087	66.809	2395	3.009	Large permanent deflection.
SCP-1	-1.98	+0.09	66.795	2400	3.019	Model exhibits a 1.51-in long through crack (along stiffener) located at x=-2.13 and extending from y=-.65 to +0.86-in.
SCP-2	+1.79	+0.12	66.785	2125	2.505	Tiny part-through crack produced next to stiffener on non-impacted side.

TABLE 11

VERTICAL LOCATION CHANGE OF THE LOWER SURFACE OF

STEEL-SPHERE IMPACTED PLATE MODEL CP-8

Vertical Location Change z_ℓ (in)										
$\bar{x}$(in)*	$\bar{y}$=-4.50*	-4.00	-3.50	-3.00	-2.50	-2.00	-1.50	-1.00	-0.50	0
-4.50	+.0007	+.0008	+.0003	+.0008	+.0007	+.0007	+.0006	+.0005	+.0003	+.0008
-4.00	+.0002	+.0006	+.0006	+.0008	+.0012	+.0016	+.0018	+.0020	+.0021	+.0022
-3.50	+.0007	+.0011	+.0043	+.0120	+.0180	+.0222	+.0248	+.0255	+.0258	+.0255
-3.00	+.0002	+.0003	+.0088	+.0218	+.0328	+.0410	+.0451	+.0477	+.0490	+.0495
-2.50	+.0005	+.0002	+.0128	+.0298	+.0460	+.0568	+.0642	+.0682	+.0703	+.0717
-2.00	+.0002	+.0002	+.0150	+.0353	+.0532	+.0678	+.0780	+.0850	+.0892	+.0903
-1.50	0	0	+.0162	+.0385	+.0596	+.0763	+.0900	+.1007	+.1081	+.1100
-1.00	0	+.0002	+.0168	+.0403	+.0635	+.0828	+.1002	+.1178	+.1322	+.1371
-0.50	0	0	+.0171	+.0426	+.0664	+.0877	+.1088	+.1368	+.1783	+.2170
0	+.0003	+.0001	+.0170	+.0420	+.0666	+.0890	+.1122	+.1471	+.2240	+.3873
0.50	+.0001	0	+.0169	+.0411	+.0660	+.0872	+.1092	+.1382	+.1811	+.2171
1.00	+.0003	-.0002	+.0166	+.0397	+.0628	+.0822	+.1009	+.1193	+.1360	+.1417
1.50	+.0002	+.0006	+.0160	+.0376	+.0583	+.0753	+.0893	+.1006	+.1086	+.1111
2.00	+.0003	+.0007	+.0147	+.0338	+.0519	+.0662	+.0767	+.0837	+.0880	+.0893
2.50	+.0002	+.0003	+.0128	+.0278	+.0429	+.0534	+.0606	+.0653	+.0676	+.0690
3.00	+.0003	+.0002	+.0080	+.0196	+.0292	+.0367	+.0409	+.0437	+.0450	+.0454
3.50	+.0003	+.0003	+.0033	+.0091	+.0142	+.0180	+.0202	+.0210	+.0214	+.0212
4.00	+.0008	+.0007	+.0008	+.0010	+.0011	+.0015	+.0016	+.0016	+.0016	+.0017
4.50	+.0003	+.0008	+.0008	+.0011	+.0012	+.0013	+.0014	+.0013	+.0017	+.0018

*: $\bar{x}$ and $\bar{y}$ are measured from the center of impact; see Table 10 for the x,y location of the center of impact.

TABLE 11 -- CONTINUED (CP-8)

Vertical Location Change z_ℓ (in)									
$\bar{x}$(in)	$\bar{y}$=0.50	1.00	1.50	2.00	2.50	3.00	3.50	4.00	4.50
-4.50	+.0007	+.0003	+.0006	+.0004	+.0003	+.0002	+.0002	+.0002	0
-4.00	+.0021	+.0018	+.0018	+.0016	+.0010	+.0005	+.0003	+.0004	+.0002
-3.50	+.0248	+.0242	+.0233	+.0218	+.0186	+.0133	+.0067	+.0007	+.0002
-3.00	+.0486	+.0463	+.0439	+.0400	+.0339	+.0242	+.0132	+.0008	+.0002
-2.50	+.0700	+.0668	+.0626	+.0560	+.0475	+.0340	+.0187	+.0016	+.0003
-2.00	+.0882	+.0832	+.0770	+.0676	+.0560	+.0400	+.0223	+.0018	0
-1.50	+.1060	+.0979	+.0878	+.0762	+.0618	+.0440	+.0237	+.0020	+.0002
-1.00	+.1267	+.1118	+.0968	+.0818	+.0661	+.0460	+.0247	+.0022	+.0002
-0.50	+.1643	+.1248	+.1035	+.0862	+.0688	+.0478	+.0250	+.0021	0
0	+.2110	+.1326	+.1063	+.0877	+.0700	+.0488	+.0254	+.0027	+.0002
0.50	+.1673	+.1261	+.1041	+.0868	+.0691	+.0482	+.0257	+.0028	+.0008
1.00	+.1298	+.1133	+.0980	+.0826	+.0663	+.0466	+.0257	+.0028	+.0005
1.50	+.1068	+.0987	+.0880	+.0760	+.0621	+.0422	+.0247	+.0028	+.0007
2.00	+.0873	+.0822	+.0758	+.0672	+.0561	+.0402	+.0224	+.0025	+.0008
2.50	+.0678	+.0648	+.0608	+.0543	+.0460	+.0337	+.0188	+.0022	+.0009
3.00	+.0449	+.0430	+.0410	+.0378	+.0318	+.0236	+.0133	+.0018	+.0012
3.50	+.0208	+.0201	+.0198	+.0188	+.0160	+.0118	+.0062	+.0018	+.0012
4.00	+.0016	+.0017	+.0018	+.0018	+.0013	+.0013	+.0012	+.0013	+.0012
4.50	+.0016	+.0016	+.0016	+.0013	+.0013	+.0017	+.0012	+.0012	+.0012

TABLE 11 -- CONTINUED (CP-8)

Spanwise Location* $\bar{x}$(in) Along $\bar{y}$=0	Vertical Location Change z_ℓ(in)	Spanwise Location $\bar{x}$(in) Along $\bar{y}$=0	Vertical Location Change z_ℓ(in)	Spanwise Location $\bar{y}$(in) Along $\bar{x}$=0	Vertical Location Change z_ℓ(in)	Spanwise Location $\bar{y}$(in) Along $\bar{x}$=0	Vertical Location Change z_ℓ(in)
-4.50	+.0006	4.50	+.0013	-4.50	0	4.50	0
-4.25	+.0010	4.25	+.0012	-4.25	0	4.25	0
-4.00	+.0022	4.00	+.0011	-4.00	-.0002	4.00	+.0021
-3.75	+.0132	3.75	+.0093	-3.75	+.0039	3.75	+.0140
-3.50	+.0253	3.50	+.0210	-3.50	+.0167	3.50	+.0252
-3.25	+.0376	3.25	+.0332	-3.25	+.0289	3.25	+.0368
-3.00	+.0495	3.00	+.0455	-3.00	+.0417	3.00	+.0484
-2.75	+.0614	2.75	+.0580	-2.75	+.0549	2.75	+.0600
-2.50	+.0719	2.50	+.0698	-2.50	+.0671	2.50	+.0698
-2.25	+.0812	2.25	+.0798	-2.25	+.0783	2.25	+.0790
-2.00	+.0902	2.00	+.0900	-2.00	+.0888	2.00	+.0876
-1.75	+.0994	1.75	+.1000	-1.75	+.0998	1.75	+.0969
-1.50	+.1099	1.50	+.1117	-1.50	+.1120	1.50	+.1062
-1.25	+.1219	1.25	+.1250	-1.25	+.1277	1.25	+.1170
-1.00	+.1373	1.00	+.1421	-1.00	+.1470	1.00	+.1313
-0.90	+.1459	0.90	+.1510	-0.90	+.1570	0.90	+.1393
-0.80	+.1565	0.80	+.1618	-0.80	+.1688	0.80	+.1498
-0.75	+.1629	0.75	+.1681	-0.75	+.1760	0.75	+.1568
-0.70	+.1710	0.70	+.1760	-0.70	+.1830	0.70	+.1640
-0.65	+.1801	0.65	+.1847	-0.65	+.1920	0.65	+.1730

*: $\bar{x}$ and $\bar{y}$ are measured from the center of impact; see Table 10 for the x,y location of the center of impact.

TABLE 11 -- CONCLUDED (CP-8)

Spanwise Location* $\bar{x}$(in) Along $\bar{y}$=0	Vertical Location Change z_ℓ(in)	Spanwise Location $\bar{x}$(in) Along $\bar{y}$=0	Vertical Location Change z_ℓ(in)	Spanwise Location $\bar{y}$(in) Along $\bar{x}$=0	Vertical Location Change z_ℓ(in)	Spanwise Location $\bar{y}$(in) Along $\bar{x}$=0	Vertical Location Change z_ℓ(in)
-0.60	+.1908	0.60	+.1942	-0.60	+.2018	0.60	+.1842
-0.55	+.2030	0.55	+.2052	-0.55	+.2119	0.55	+.1973
-0.50	+.2167	0.50	+.2183	-0.50	+.2240	0.50	+.2113
-0.45	+.2322	0.45	+.2326	-0.45	+.2373	0.45	+.2280
-0.40	+.2499	0.40	+.2489	-0.40	+.2536	0.40	+.2465
-0.35	+.2703	0.35	+.2676	-0.35	+.2720	0.35	+.2678
-0.30	+.2950	0.30	+.2903	-0.30	+.2942	0.30	+.2920
-0.25	+.3241	0.25	+.3174	-0.25	+.3168	0.25	+.3216
-0.20	+.3482	0.20	+.3438	-0.20	+.3433	0.20	+.3470
-0.15	+.3660	0.15	+.3629	-0.15	+.3622	0.15	+.3660
-0.10	+.3780	0.10	+.3771	-0.10	+.3762	0.10	+.3783
-0.05	+.3855	0.05	+.3850	-0.05	+.3843	0.05	+.3851
0	+.3878	0	+.3878	0	+.3877	0	+.3877

TABLE 12

VERTICAL LOCATION CHANGE OF THE LOWER SURFACE

OF STEEL-SPHERE IMPACTED PLATE MODEL CP-12

	Vertical Location Change z_ℓ (in)									
$\bar{x}$(in)*	$\bar{y}$=-4.50*	-4.00	-3.50	-3.00	-2.50	-2.00	-1.50	-1.00	-0.50	0
-4.50	0	0	0	0	-.0002	0	0	0	0	0
-4.00	-.0001	-.0002	.0010	.0031	.0050	.0061	.0068	.0068	.0073	.0072
-3.50	-.0002	0	.0082	.0179	.0245	.0293	.0317	.0329	.0334	.0329
-3.00	-.0007	-.0002	.0149	.0289	.0404	.0478	.0517	.0537	.0552	.0551
-2.50	0	0	.0198	.0374	.0521	.0615	.0677	.0700	.0712	.0707
-2.00	-.0006	.0001	.0226	.0421	.0584	.0701	.0777	.0816	.0832	.0824
-1.50	-.0007	0	.0234	.0444	.0626	.0759	.0857	.0922	.0959	.0959
-1.00	-.0008	0	.0234	.0458	.0654	.0806	.0933	.1048	.1141	.1190
-0.50	-.0008	.0002	.0231	.0470	.0674	.0846	.1006	.1202	.1594	.2110
0	-.0004	.0005	.0229	.0467	.0675	.0871	.1053	.1328	.2163	.3816
0.50	-.0005	.0003	.0229	.0458	.0667	.0853	.1040	.1294	.1751	.2162
1.00	-.0008	0	.0232	.0446	.0646	.0811	.0976	.1139	.1317	.1409
1.50	-.0008	0	.0226	.0429	.0606	.0758	.0879	.0980	.1049	.1068
2.00	-.0008	0	.0203	.0388	.0547	.0657	.0748	.0816	.0854	.0858
2.50	-.0009	-.0002	.0159	.0306	.0429	.0515	.0580	.0622	.0655	.0655
3.00	-.0009	-.0004	.0098	.0196	.0270	.0328	.0370	.0391	.0407	.0408
3.50	-.0008	-.0004	.0017	.0057	.0081	.0103	.0116	.0127	.0131	.0134
4.00	-.0010	-.0007	-.0008	-.0006	-.0006	-.0004	-.0006	-.0003	-.0004	-.0003
4.50	-.0011	-.0009	-.0008	-.0008	-.0006	-.0005	-.0005	-.0006	-.0003	-.0006

*: $\bar{x}$ and $\bar{y}$ are measured from the center of impact; see Table 10 for the x,y location of the center of impact.

TABLE 12 -- CONTINUED (CP-12)

Vertical Location Change z_ℓ (in)									
$\bar{x}$(in)	$\bar{y}$=0.50	1.00	1.50	2.00	2.50	3.00	3.50	4.00	4.50
-4.50	0	0	0	-.0002	0	0	0	-.0003	-.0006
-4.00	.0071	.0066	.0060	.0052	.0040	.0020	0	-.0008	-.0008
-3.50	.0314	.0301	.0279	.0247	.0197	.0123	.0040	-.0005	-.0007
-3.00	.0519	.0485	.0441	.0378	.0293	.0181	.0067	-.0007	-.0007
-2.50	.0666	.0671	.0550	.0456	.0343	.0204	.0068	-.0007	-.0007
-2.00	.0783	.0715	.0624	.0501	.0351	.0183	.0039	-.0007	-.0007
-1.50	.0913	.0815	.0687	.0542	.0383	.0200	.0043	-.0006	-.0008
-1.00	.1110	.0948	.0765	.0586	.0399	.0216	.0072	-.0007	-.0005
-0.50	.1598	.1133	.0844	.0619	.0424	.0232	.0087	-.0006	-.0005
0	.2153	.1281	.0994	.0633	.0420	.0228	.0070	-.0003	-.0002
0.50	.1732	.1219	.0875	.0635	.0409	.0196	.0039	0	0
1.00	.1280	.1049	.0816	.0599	.0399	.0189	0	0	0
1.50	.1002	.0875	.0727	.0562	.0388	.0211	.0054	0	0
2.00	.0805	.0725	.0623	.0507	.0380	.0231	.0096	0	0
2.50	.0613	.0560	.0489	.0414	.0328	.0218	.0089	0	-.0002
3.00	.0384	.0357	.0314	.0269	.0213	.0149	.0060	-.0003	-.0003
3.50	.0124	.0110	.0097	.0086	.0066	.0038	.0006	-.0005	-.0008
4.00	-.0003	-.0005	-.0008	-.0006	-.0005	-.0006	-.0008	-.0008	-.0008
4.50	-.0006	-.0007	-	-.0009	-.0008	-.0010	-.0008	-.0008	-.0010

TABLE 12 -- CONTINUED (CP-12)

Spanwise Location* $\bar{x}$(in) Along $\bar{y}$=0	Vertical Location Change z_ℓ(in)	Spanwise Location $\bar{x}$(in) Along $\bar{y}$=0	Vertical Location Change z_ℓ(in)	Spanwise Location $\bar{y}$(in) Along $\bar{x}$=0	Vertical Location Change z_ℓ(in)	Spanwise Location $\bar{y}$(in) Along $\bar{x}$=0	Vertical Location Change z_ℓ(in)
-4.50	-.0007	4.50	-.0001	-4.50	-.0006	4.50	0
-4.25	.0001	4.25	-.0003	-4.25	-.0004	4.25	0
-4.00	.0077	4.00	-.0001	-4.00	.0004	4.00	-.0003
-3.75	.0210	3.75	.0006	-3.75	.0111	3.75	.0033
-3.50	.0234	3.50	.0134	-3.50	.0231	3.50	.0071
-3.25	.0450	3.25	.0277	-3.25	.0344	3.25	.0163
-3.00	.0557	3.00	.0408	-3.00	.0466	3.00	.0231
-2.75	.0640	2.75	.0539	-2.75	.0573	2.75	.0329
-2.50	.0710	2.50	.0657	-2.50	.0673	2.50	.0422
-2.25	.0792	2.25	.0759	-2.25	.0772	2.25	.0529
-2.00	.0829	2.00	.0858	-2.00	.0866	2.00	.0633
-1.75	.0889	1.75	.0957	-1.75	.0952	1.75	.0760
-1.50	.0961	1.50	.1069	-1.50	.1047	1.50	.0894
-1.25	.1053	1.25	.1214	-1.25	.1170	1.25	.1063
-1.00	.1189	1.00	.1409	-1.00	.1330	1.00	.1281
-0.90	.1270	0.90	.1513	-0.90	.1416	0.90	.1398
-0.80	.1395	0.80	.1635	-0.80	.1538	0.80	.1532
-0.75	.1469	0.75	.1702	-0.75	.1613	0.75	.1613
-0.70	.1561	0.70	.1776	-0.70	.1695	0.70	.1705
-0.65	.1674	0.65	.1852	-0.65	.1792	0.65	.1794

*: $\bar{x}$ and $\bar{y}$ are measured from the center of impact; see Table 10 for the x,y location of the center of impact.

TABLE 12 -- CONCLUDED (CP-12)

Spanwise Location* $\bar{x}$ (in) Along $\bar{y}$=0	Vertical Location Change z_ℓ (in)	Spanwise Location $\bar{x}$ (in) Along $\bar{y}$=0	Vertical Location Change z_ℓ (in)	Spanwise Location $\bar{y}$ (in) Along $\bar{x}$=0	Vertical Location Change z_ℓ (in)	Spanwise Location $\bar{y}$ (in) Along $\bar{x}$=0	Vertical Location Change z_ℓ (in)
-0.60	.1797	0.60	.1948	-0.60	.1903	0.60	.1907
-0.55	.1940	0.55	.2048	-0.55	.2029	0.55	.2026
-0.50	.2100	0.50	.2169	-0.50	.2162	0.50	.2157
-0.45	.2277	0.45	.2297	-0.45	.2313	0.45	.2314
-0.40	.2490	0.40	.2444	-0.40	.2483	0.40	.2491
-0.35	.2728	0.35	.2630	-0.35	.2682	0.35	.2698
-0.30	.3025	0.30	.2832	-0.30	.2911	0.30	.2937
-0.25	.3302	0.25	.3067	-0.25	.3193	0.25	.3181
-0.20	.3517	0.20	.3320	-0.20	.3426	0.20	.3426
-0.15	.3672	0.15	.3568	-0.15	.3605	0.15	.3556
-0.10	.3772	0.10	.3682	-0.10	.3723	0.10	.3685
-0.05	.3813	0.05	.3757	-0.05	.3770	0.05	.3773
0	.3817	0	.3817	0	.3817	0	.3817

TABLE 13

VERTICAL LOCATION CHANGE OF THE UPPER (NON-IMPACTED) SURFACE OF THE STEEL-SPHERE-IMPACTED INTEGRALLY-STIFFENED PLATE MODEL SCP-1

Vertical Location Change z_u (in)											
x(in)*	y=-4.50*	-4.10	-3.90	-3.50	-3.00	-2.50	-2.00	-1.50	-1.00	-0.50	0
-4.50	0	0	0	0	0	0	0	0	0	0	0
-4.10	0	0	0	0	0	0	0	0	0	0	0
-3.90	0	0	+.001	0	+.001	+.001	+.004?	+.002	+.002	+.002	+.003
-3.50	0	0	+.001	+.002	+.005	+.010	+.018	+.028	+.039	+.049	+.055
-3.00	0	0	+.001	+.005	+.014	+.026	+.041	+.061	+.088	+.112	+.123
-2.50	0	0	+.001	+.009	+.024	+.041	+.062	+.094	+.137	+.188	+.226
-2.00	0	0	+.002	+.013	+.030	+.050	+.076	+.113	+.172	+.269	+.374
-1.50	0	0	+.001	+.015	+.035	+.055	+.078	+.111	+.154	+.211	+.258
-1.00	0	0	+.001	+.017	+.037	+.057	+.075	+.097	+.121	+.144	+.157
-0.50	0	0	+.001	+.018	+.036	+.053	+.067	+.081	+.093	+.104	+.109
0	0	0	+.001	+.016	+.033	+.046	+.056	+.067	+.075	+.079	+.081
0.50	0	0	+.001	+.013	+.027	+.038	+.047	+.055	+.059	+.063	+.064
1.00	0	0	+.001	+.010	+.021	+.030	+.038	+.044	+.048	+.052	+.054
1.50	0	0	+.001	+.008	+.016	+.024	+.030	+.037	+.042	+.045	+.046
2.00	0	0	+.001	+.005	+.011	+.017	+.023	+.029	+.035	+.039	+.040
2.50	0	0	+.001	+.002	+.007	+.011	+.017	+.023	+.029	+.033	+.034
3.00	0	0	+.001	+.002	+.004	+.008	+.011	+.016	+.020	+.024	+.025
3.50	0	0	-.001	0	+.001	+.002	+.004	+.007	+.009	+.012	+.012
3.90	0	0	0	+.002	+.002	+.002	+.001	+.001	+.002	+.002	+.002
4.10	0	0	0	0	0	0	0	0	0	0	0
4.50	0	0	0	0	0	0	0	0	0	0	0

*The origin of these x,y coordinates is at the center of the panel; see Fig. 9.

TABLE 13 -- CONTINUED (SCP-1)

Vertical Location Change z_u (in)										
x(in)	y=0.50	1.00	1.50	2.00	2.50	3.00	3.50	3.90	4.10	4.50
-4.50	0	0	0	0	0	0	0	0	0	0
-4.10	0	0	0	0	0	0	0	0	0	0
-3.90	+.003	+.002	+.001	+.003	0	0	0	-	0	0
-3.50	+.051	+.041	+.030	+.019	+.011	+.006	+.002	-	0	0
-3.00	+.117	+.094	+.067	+.045	+.029	+.016	+.006	-	0	0
-2.50	+.204	+.154	+.104	+.068	+.045	+.026	+.010	-	0	0
-2.00	+.310	+.201	+.128	+.083	+.055	+.032	+.013	+.002	0	0
-1.50	+.232	+.173	+.121	+.085	+.059	+.037	+.016	-	0	0
-1.00	+.152	+.130	+.103	+.079	+.058	+.038	+.017	-	0	0
-0.50	+.107	+.097	+.084	+.069	+.054	+.037	+.017	-	0	0
0	+.079	+.075	+.067	+.058	+.046	+.032	+.016	-	0	0
0.50	+.063	+.059	+.055	+.047	+.038	+.026	+.013	-	0	0
1.00	+.051	+.048	+.044	+.038	+.030	+.020	+.009	-	0	0
1.50	+.044	+.040	+.036	+.029	+.023	+.016	+.007	-	0	0
2.00	+.037	+.033	+.028	+.023	+.016	+.010	+.004	+.001	0	0
2.50	+.031	+.026	+.021	+.017	+.012	+.008	+.003	-	0	0
3.00	+.023	+.019	+.015	+.010	+.007	+.005	+.002	-	0	0
3.50	+.012	+.010	+.006	+.004	+.002	+.001	+.001	-	0	0
3.90	+.002	+.003	+.002	+.001	+.002	+.002	+.001	-	0	0
4.10	0	0	0	0	0	0	0	0	0	0
4.50	0	0	0	0	0	0	0	0	0	0

TABLE 13 -- CONTINUED (SCP-1)

Spanwise Location x(in) Along x=-2.25	Vertical Location Change z_u(in)	Spanwise Location y(in) Along x=-2.25	Vertical Location Change z_u(in)	Spanwise Location y(in) Along x=-1.75	Vertical Location Change z_u(in)	Spanwise Location y(in) Along x=-1.75	Vertical Location Change z_u(in)
-4.50	0	4.50	0	-4.50	0	4.50	0
-4.10	0	4.10	0	-4.10	0	4.10	0
-3.90	+.001	3.90	-	-3.90	+.001	3.90	-
-3.75	+.004	3.75	+.002	-3.75	+.006	3.75	+.007
-3.50	+.011	3.50	+.012	-3.50	+.014	3.50	+.016
-3.25	+.019	3.25	+.021	-3.25	+.023	3.25	+.026
-3.00	+.028	3.00	+.030	-3.00	+.034	3.00	+.036
-2.75	+.037	2.75	+.040	-2.75	+.044	2.75	+.047
-2.50	+.047	2.50	+.051	-2.50	+.055	2.50	+.059
-2.25	+.058	2.25	+.063	-2.25	+.068	2.25	+.073
-2.00	+.070	2.00	+.078	-2.00	+.078	2.00	+.085
-1.75	+.086	1.75	+.096	-1.75	+.096	1.75	+.103
-1.50	+.108	1.50	+.121	-1.50	+.116	1.50	+.127
-1.25	+.132	1.25	+.150	-1.25	+.140	1.25	+.158
-1.00	+.162	1.00	+.183	-1.00	+.169	1.00	+.194
-0.90	+.175	0.90	+.199	-0.90	+.183	0.90	+.211
-0.80	+.188	0.80	+.215	-0.80	+.198	0.80	+.229
-0.75	+.196	0.75	+.223	-0.75	+.206	0.75	+.238
-0.70	+.203	0.70	+.231	-0.70	+.215	0.70	+.247
-0.65	+.210	0.65	+.239	-0.65	+.222	0.65	+.257
-0.60	+.219	0.60	+.247	-0.60	+.231	0.60	+.267

TABLE 13 -- CONCLUDED (SCP-1)

Spanwise Location y(in) Along x=-2.25	Vertical Location Change z_u(in)	Spanwise Location y(in) Along x=-2.25	Vertical Location Change z_u(in)	Spanwise Location y(in) Along x=-1.75	Vertical Location Change z_u(in)	Spanwise Location y(in) Along x=-1.75	Vertical Location Change z_u(in)
-0.55	+.226	0.55	+.255	-0.55	+.240	0.55	+.276
-0.50	+.234	0.50	+.264	-0.50	+.249	0.50	+.286
-0.45	+.243	0.45	+.271	-0.45	+.259	0.45	+.296
-0.40	+.250	0.40	+.279	-0.40	+.269	0.40	+.307
-0.35	+.258	0.35	+.289	-0.35	+.279	0.35	+.317
-0.30	+.266	0.30	+.297	-0.30	+.289	0.30	+.328
-0.25	+.275	0.25	+.305	-0.25	+.299	0.25	+.339
-0.20	+.285	0.20	+.314	-0.20	+.309	0.20	+.347
-0.15	+.293	0.15	+.320	-0.15	+.320	0.15	+.353
-0.10	+.301	0.10	+.323	-0.10	+.329	0.10	+.355
-0.05	+.310	0.05	+.322	-0.05	+.339	0.05	+.352
0	+.317	0	+.317	0	+.347	0	+.347

TABLE 14

VERTICAL LOCATION CHANGE OF THE UPPER (NON-IMPACTED) SURFACE OF THE STEEL-SPHERE-IMPACTED INTEGRALLY-STIFFENED PLATE MODEL SCP-2

Vertical Location Change z_u (in)											
x(in)*	y=-4.50*	-4.10	-3.90	-3.50	-3.00	-2.50	-2.00	-1.50	-1.00	-0.50	0
-4.50	0	0	0	0	0	0	0	0	0	0	0
-4.10	0	0	0	0	0	0	0	0	0	0	0
-3.90	0	0	0	0	-.001	0	+.001	0	0	+.001	0
-3.50	0	0	0	+.001	+.001	+.002	+.003	+.005	+.006	.006	.007
-3.00	0	0	-.001	+.001	+.003	+.005	+.008	+.010	.012	.012	.012
-2.50	0	0	-.001	+.002	+.005	+.009	+.013	+.016	.019	.022	.022
-2.00	0	0	+.001	+.003	+.008	+.013	+.018	+.022	.027	.029	.030
-1.50	0	0	-	+.006	+.012	+.018	+.023	+.029	.034	.038	.039
-1.00	0	0	-	+.007	+.016	+.023	+.030	+.036	.041	.045	.047
-0.50	0	0	-	+.009	+.020	+.029	+.037	+.044	.050	.054	.056
0	0	0	-	+.012	+.025	+.036	+.045	+.053	.060	.065	.078
0.50	0	0	-	+.013	+.028	+.040	+.053	+.064	.074	.082	.087
1.00	0	0	-	+.014	+.029	+.044	+.058	+.075	.092	.109	.122
1.50	0	0	-	+.012	+.026	+.042	+.059	+.081	.108	.145	.212
2.00	0	0	+.002	+.009	+.021	+.036	+.053	+.077	.108	.150	.199
2.50	0	0	0	+.006	+.016	+.027	+.042	+.061	.085	.110	.128
3.00	0	0	0	+.003	+.009	+.017	+.027	+.041	.056	.070	.077
3.50	0	0	0	+.001	+.003	+.007	+.012	+.019	.027	.034	.037
3.90	0	0	0	0	0	+.001	+.003	+.002	.002	.003	.004
4.10	0	0	0	0	0	0	0	0	0	0	0
4.50	0	0	0	0	0	0	0	0	0	0	0

*The origin of these x,y coordinates is at the center of the panel; see Fig. 10.

TABLE 14 -- CONTINUED (SCP-2)

Vertical Location Change z_u (in)										
x(in)	y=0.50	1.00	1.50	2.00	2.50	3.00	3.50	3.90	4.10	4.50
-4.50	0	0	0	0	0	0	0	0	0	0
-4.10	0	0	0	0	0	0	0	0	0	0
-3.90	0	.001	.001	0	0	.001	0	0	0	0
-3.50	.007	.006	.005	.003	.002	.001	.001	0	0	0
-3.00	.013	.013	.011	.008	.005	.003	.001	0	0	0
-2.50	.022	.020	.017	.014	.010	.006	.002	0	0	0
-2.00	.029	.027	.023	.020	.014	.009	.004	0	0	0
-1.50	.038	.035	.030	.026	.020	.013	.006	0	0	0
-1.00	.046	.043	.038	.033	.025	.018	.010	0	0	0
-0.50	.055	.052	.047	.040	.032	.022	.010	0	0	0
0	.067	.063	.058	.049	.039	.027	.013	0	0	0
0.50	.085	.078	.069	.057	.045	.031	.015	0	0	0
1.00	.117	.100	.082	.064	.048	.032	.015	.001	0	0
1.50	.174	.124	.092	.066	.047	.029	.013	.001	0	0
2.00	.176	.126	.089	.061	.042	.025	.010	0	0	0
2.50	.120	.095	.070	.049	.032	.018	.007	0	0	0
3.00	.074	.062	.046	.031	.020	.011	.003	0	0	0
3.50	.035	.030	.022	.014	.008	.004	.001	0	0	0
3.90	.004	.003	.002	.003	0	0	0	0	0	0
4.10	0	0	0	0	0	0	0	0	0	0
4.50	0	0	0	0	0	0	0	0	0	0

TABLE 14 -- CONTINUED (SCP-2)

Spanwise Location y(in) Along x=+1.75	Vertical Location Change z_u(in)	Spanwise Location y(in) Along x=+1.75	Vertical Location Change z_u(in)	Spanwise Location y(in) Along x=+2.01	Vertical Location Change z_u(in)	Spanwise Location y(in) Along x=+2.01	Vertical Location Change z_u(in)
-4.50	0	4.50	0	-4.50	0	4.50	0
-4.10	0	4.10	0	-4.10	0	4.10	0
-3.90	-.002	3.90	.001	-3.90	.002	3.90	.002
-3.75	+.001	3.75	.005	-3.75	-	3.75	-
-3.50	.011	3.50	.012	-3.50	.009	3.50	.010
-3.25	.017	3.25	.020	-3.25	-	3.25	-
-3.00	.023	3.00	.027	-3.00	.021	3.00	.025
-2.75	.031	2.75	.036	-2.75	-	2.75	-
-2.50	.039	2.50	.045	-2.50	.036	2.50	.041
-2.25	.047	2.25	.054	-2.25	-	2.25	-
-2.00	.056	2.00	.065	-2.00	.053	2.00	.061
-1.75	.068	1.75	.078	-1.75	-	1.75	-
-1.50	.080	1.50	.093	-1.50	.076	1.50	.087
-1.25	.095	1.25	.110	-1.25	-	1.25	-
-1.00	.112	1.00	.130	-1.00	.107	1.00	.123
-0.90	.120	0.90	.140	-0.90	-	0.90	-
-0.80	.128	0.80	.151	-0.80	-	0.80	-
-0.75	.132	0.75	.157	-0.75	-	0.75	-
-0.70	.136	0.70	.163	-0.70	-	0.70	-
-0.65	.141	0.65	.169	-0.65	-	0.65	-
-0.60	.146	0.60	.176	-0.60	-	0.60	-

TABLE 14 -- CONTINUED (SCP-2)

Spanwise Location y(in) Along x=+1.75	Vertical Location Change z_u(in)	Spanwise Location y(in) Along x=+1.75	Vertical Location Change z_u(in)	Spanwise Location y(in) Along x=+2.01	Vertical Location Change z_u(in)	Spanwise Location y(in) Along x=+2.01	Vertical Location Change z_u(in)
-0.55	.152	0.55	.185	-0.55	-	0.55	-
-0.50	.157	0.50	.195	-0.50	.148	0.50	.174
-0.45	.163	0.45	.207	-0.45	-	0.45	-
-0.40	.170	0.40	.220	-0.40	-	0.40	-
-0.35	.177	0.35	.234	-0.35	-	0.35	-
-0.30	.186	0.30	.247	-0.30	-	0.30	-
-0.25	.195	0.25	.258	-0.25	-	0.25	-
-0.20	.207	0.20	.266	-0.20	-	0.20	-
-0.15	.220	0.15	.271	-0.15	-	0.15	-
-0.10	.233	0.10	.271	-0.10	-	0.10	-
-0.05	.248	0.05	.267	-0.05	-	0.05	-
0	.259	0	.259	0	.198	0	.198

TABLE 14 -- CONTINUED (SCP-2)

Spanwise Location x(in) Along y=+0.12	Vertical Location Change z_u (in)	Spanwise Location x(in) Along y=+0.12	Vertical Location Change z_u (in)	Spanwise Location x(in) Along y=+0.25	Vertical Location Change z_u (in)	Spanwise Location x(in) Along y=+0.25	Vertical Location Change z_u (in)
-4.50	0	-	-	-4.50	0	-	-
-4.10	0	-	-	-4.10	0	-	-
-3.90	0	4.50	0	-3.90	.001	4.50	0
-3.50	.007	4.10	0	-3.50	.007	4.10	0
-3.00	.012	3.90	.004	-3.00	.013	3.90	.004
-2.50	.022	3.75	.017	-2.50	.022	3.75	.017
-2.00	.030	3.50	.037	-2.00	.030	3.50	.037
-1.50	.039	3.25	.056	-1.50	.039	3.25	.056
-1.00	0.46	3.00	.075	-1.00	.046	3.00	.077
-0.75	.051	2.90	.085	-0.75	.051	2.90	.085
-0.50	.056	2.80	.094	-0.50	.056	2.80	.094
-0.25	.061	2.75	.099	-0.25	.061	2.75	.099
0	.067	2.70	.104	0	.068	2.70	.104
0.25	.075	2.65	.110	0.25	.076	2.65	.109
0.50	.086	2.60	.116	0.50	.086	2.60	.115
0.75	.100	2.55	.122	0.75	.100	2.55	.121
1.00	.122	2.50	.129	1.00	.121	2.50	.127
1.05	.127	2.45	.136	1.05	.126	2.45	.134
1.10	.133	2.40	.143	1.10	.132	2.40	.141
1.15	.140	2.35	.151	1.15	.139	2.35	.149

TABLE 14 -- CONCLUDED (SCP-2)

Spanwise Location x(in) Along y=+0.12	Vertical Location Change z_u(in)	Spanwise Location x(in) Along y=+0.12	Vertical Location Change z_u(in)	Spanwise Location x(in) Along y=+0.25	Vertical Location Change z_u(in)	Spanwise Location x(in) Along y=+0.25	Vertical Location Change z_u(in)
1.20	.147	2.30	.160	1.20	.146	2.30	.157
1.25	.155	2.25	.169	1.25	.153	2.25	.166
1.30	.164	2.20	.178	1.30	.162	2.20	.174
1.35	.175	2.15	-	1.35	.172	2.15	-
1.40	.187	2.10	.188	1.40	.182	2.10	.185
1.45	.203	2.05	.197	1.45	.195	2.05	.194
1.50	.219	2.00	-	1.50	.210	2.00	-
1.55	.235	1.95	-	1.55	.224	1.95	-
1.60	.249	1.90	.261	1.60	.237	1.90	.242
1.65	.259	1.85	.268	1.65	.248	1.85	.252
1.70	.267	1.80	.271	1.70	.256	1.80	.258
1.75	.271	1.75	.271	1.75	.258	1.75	.258

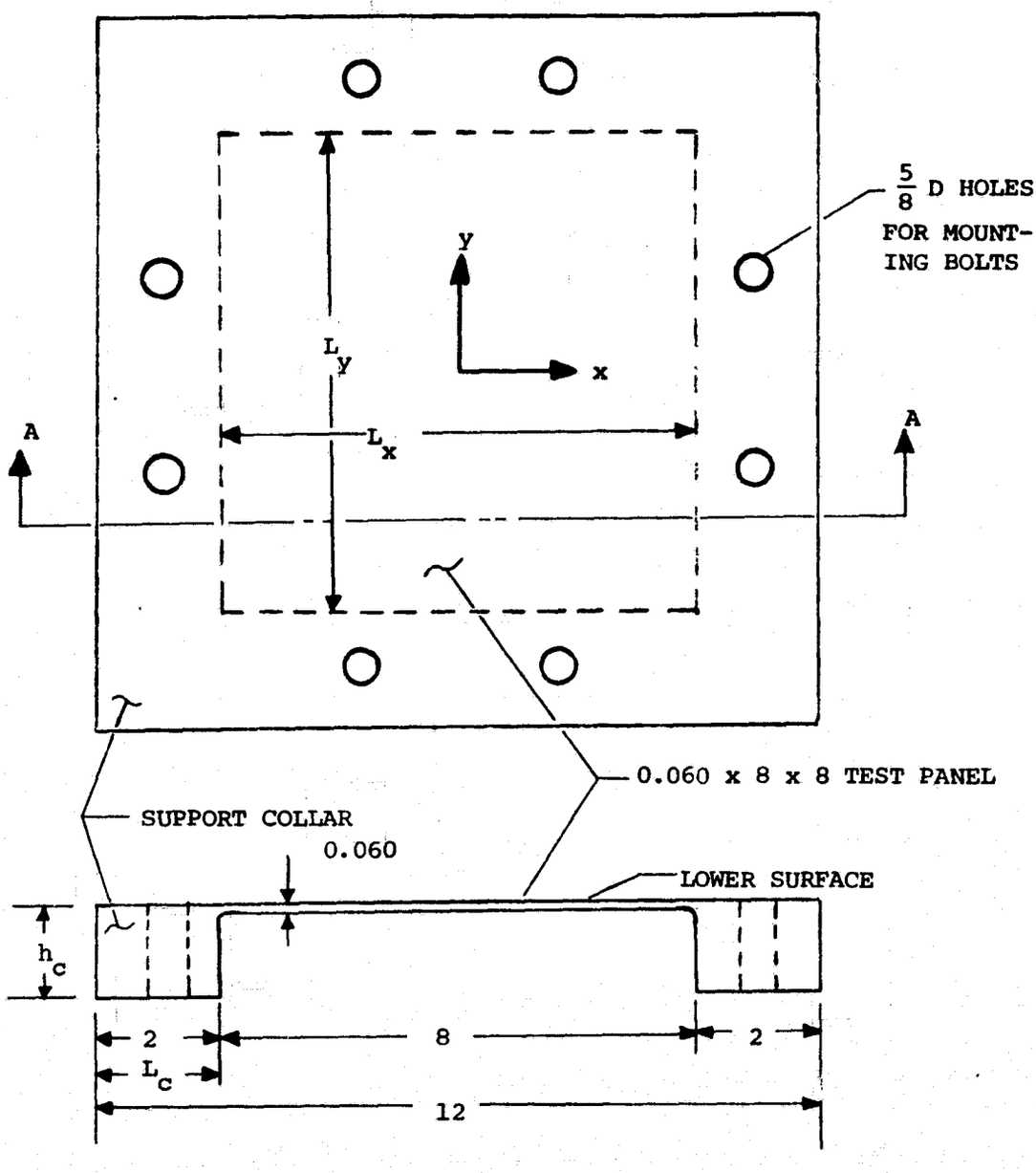

VIEW A-A

FIG. 1 GEOMETRY AND NOMINAL DIMENSIONS OF THE UNIFORM-THICKNESS 6061-T651 ALUMINUM PANEL MODELS

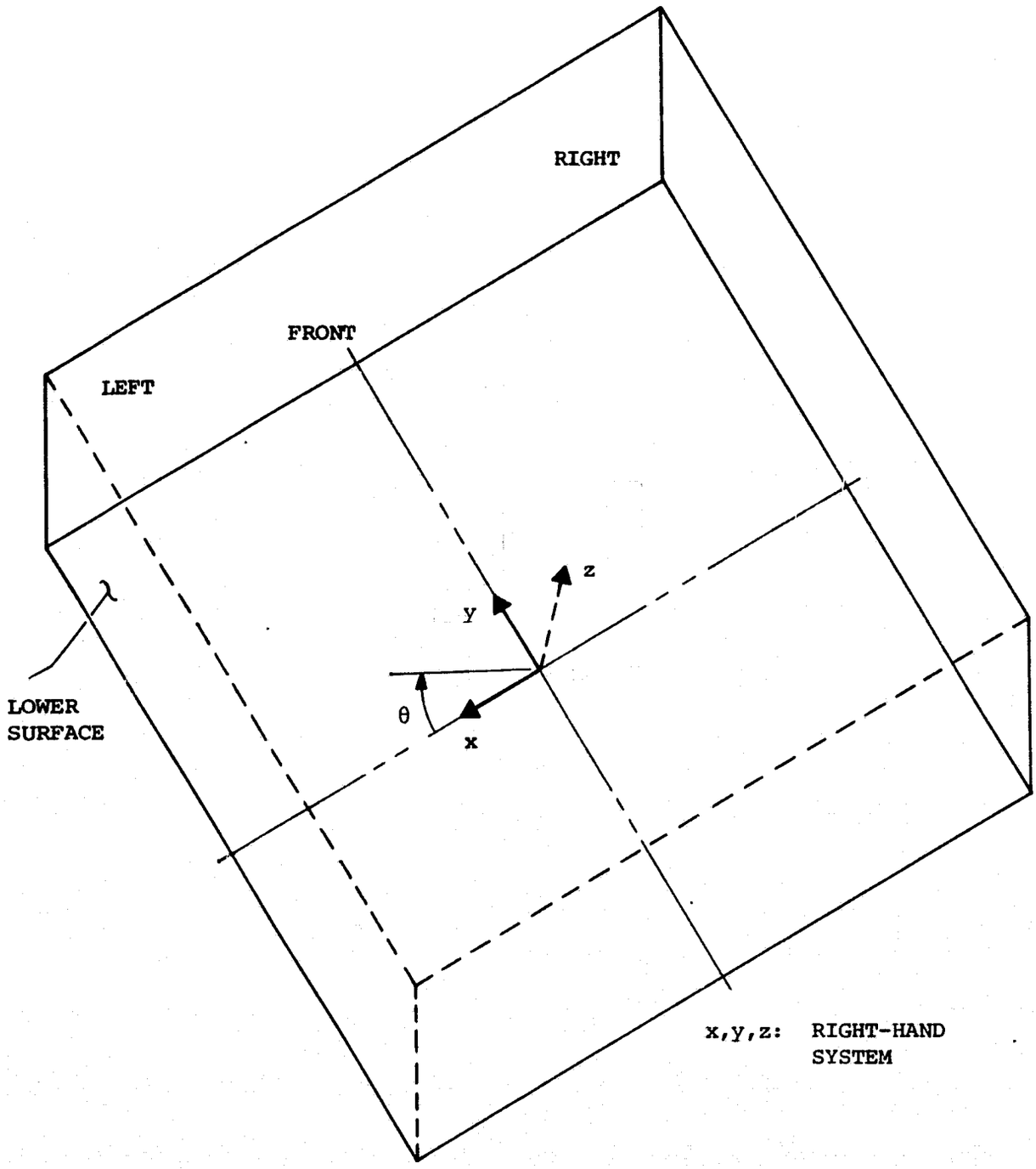

FIG. 2 PANEL MODEL COORDINATES AND NOMENCLATURE

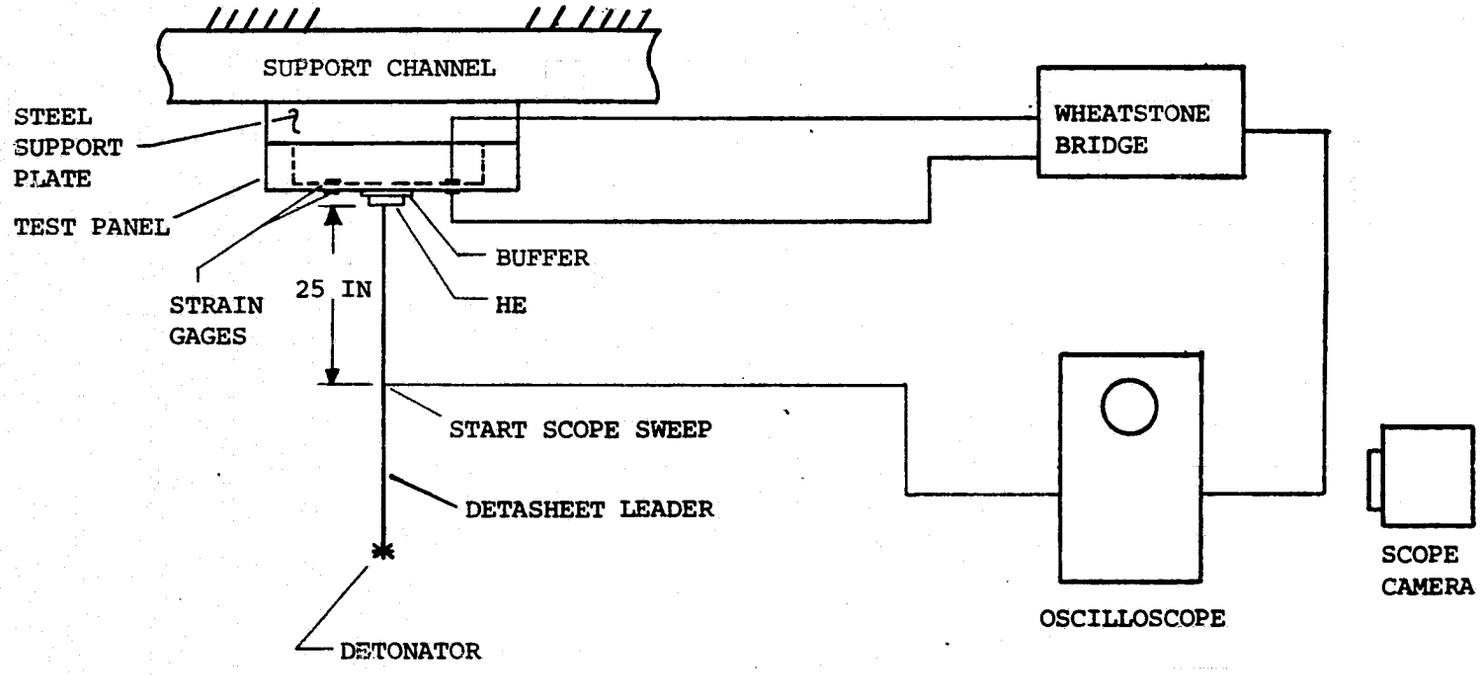

FIG. 3 SCHEMATIC OF IMPULSIVE-LOADING TESTS ON 6061-T651 PANELS WITH CLAMPED SIDES

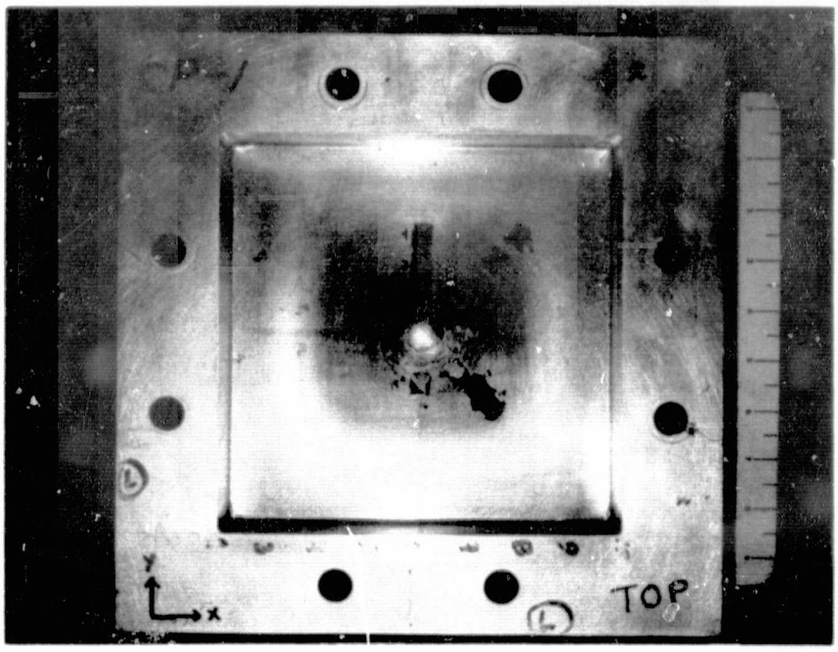

Model CP-1

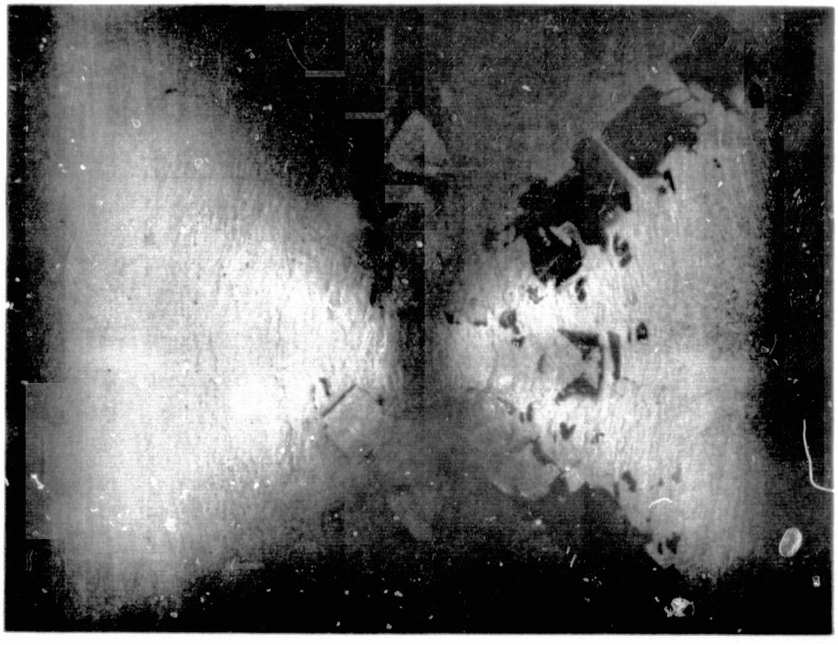

TOP
CLOSEUP

Model CP-1

FIG. 4 POST-TEST PHOTOGRAPHS OF THE IMPULSIVELY-LOADED 6061-T651 UNIFORM-THICKNESS PANEL MODELS

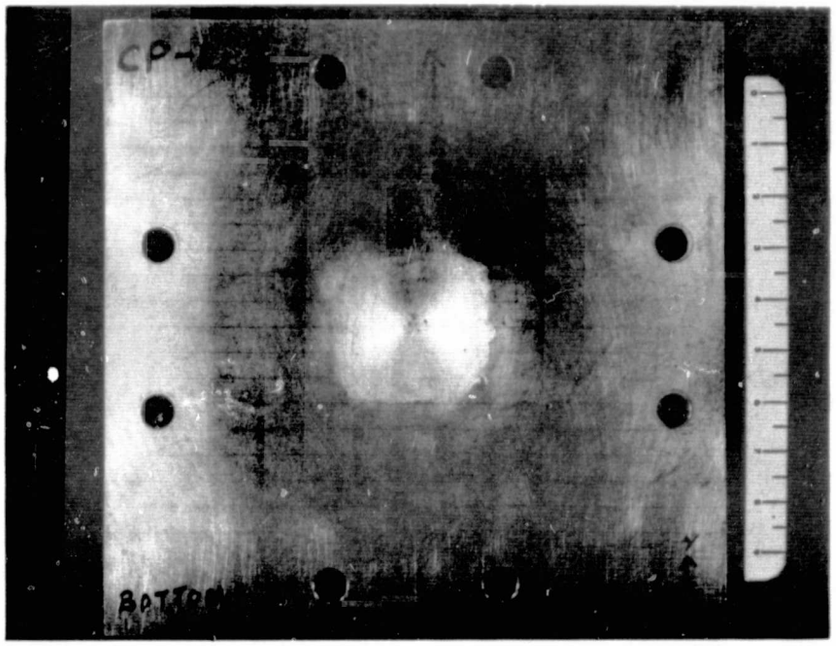

Model CP-1

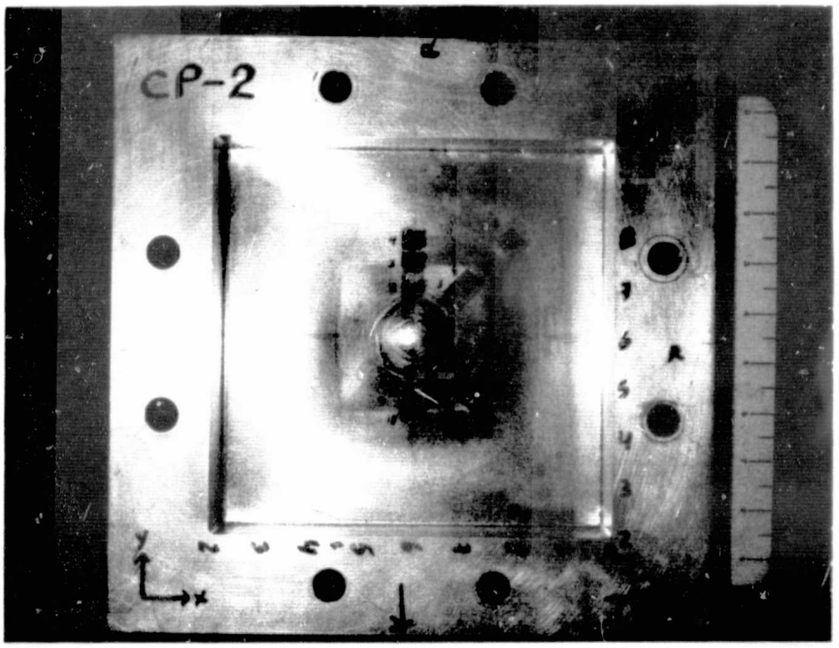

Model CP-2

FIG. 4 CONTINUED

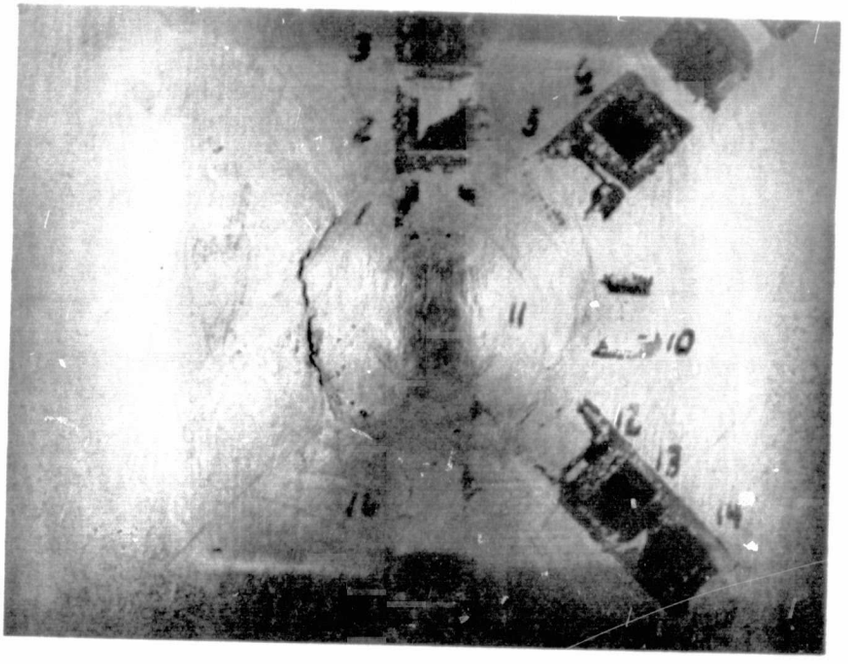

TOP
CLOSEUP

Model CP-2

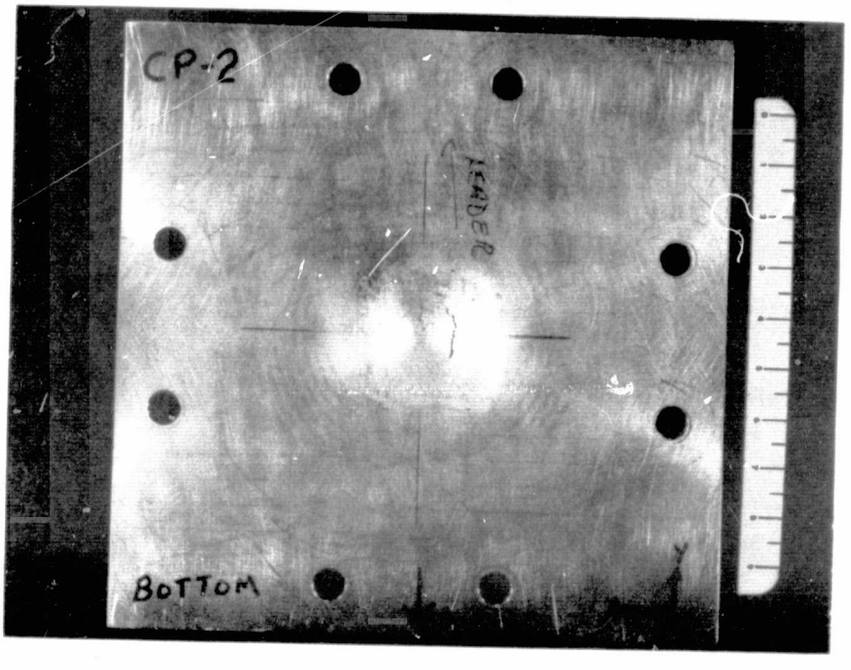

Model CP-2

FIG. 4 CONCLUDED

ABSCISSA: TIME, 50 μSEC/DIV
ORDINATE: UNCORRECTED RELATIVE ELONGATION IN PER CENT

\+ = TENSION (UP)
\- = COMPRESSION (DOWN)

∇: TIME = 0

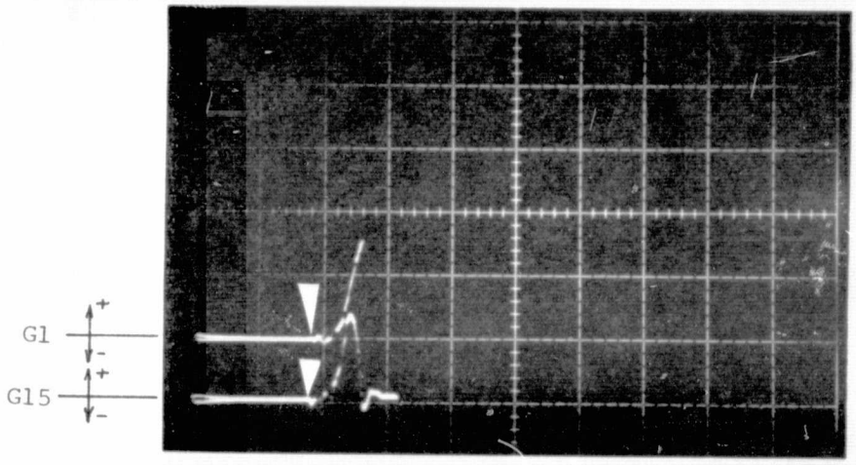

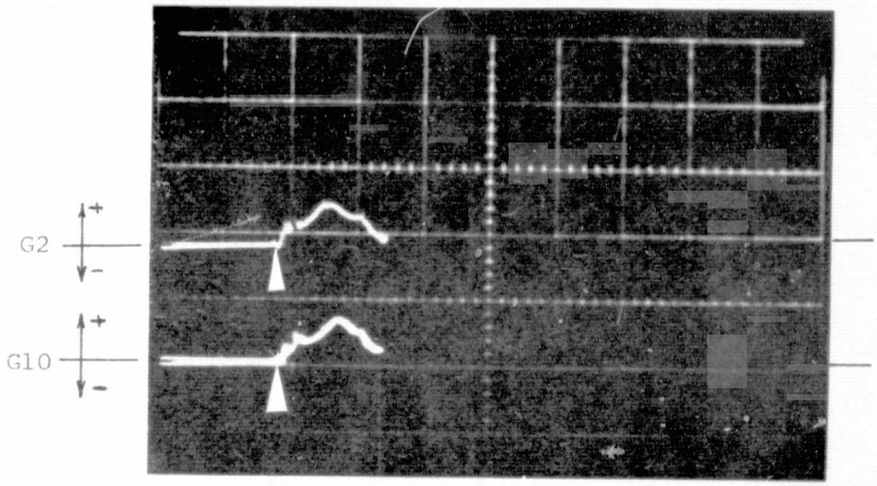

FIG. 5 UNCORRECTED TRANSIENT RELATIVE ELONGATION RECORDS FOR IMPULSIVELY-LOADED 6061-T651 PANEL MODEL CP-1 WITH CLAMPED EDGES

ABSCISSA: TIME
ORDINATE: UNCORRECTED RELATIVE ELONGATION IN PER CENT

\+ = TENSION (UP)
\- = COMPRESSION (DOWN)

∇: TIME = 0

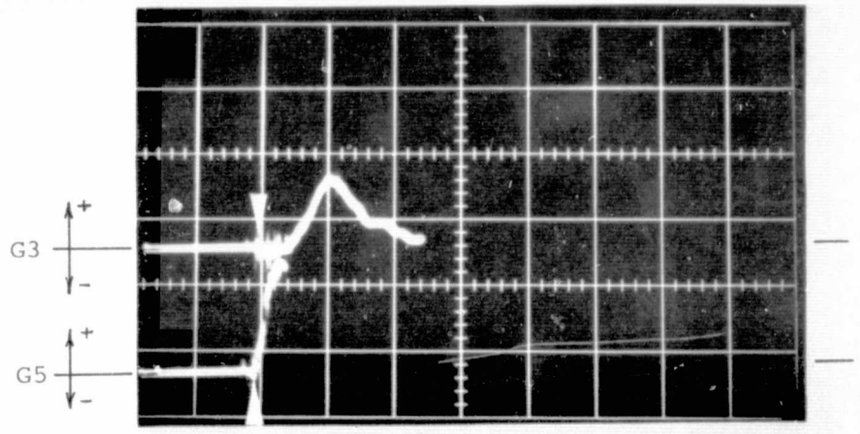

50 µSEC/DIV

GAGE 3
4%/DIV

GAGE 5
4%/DIV

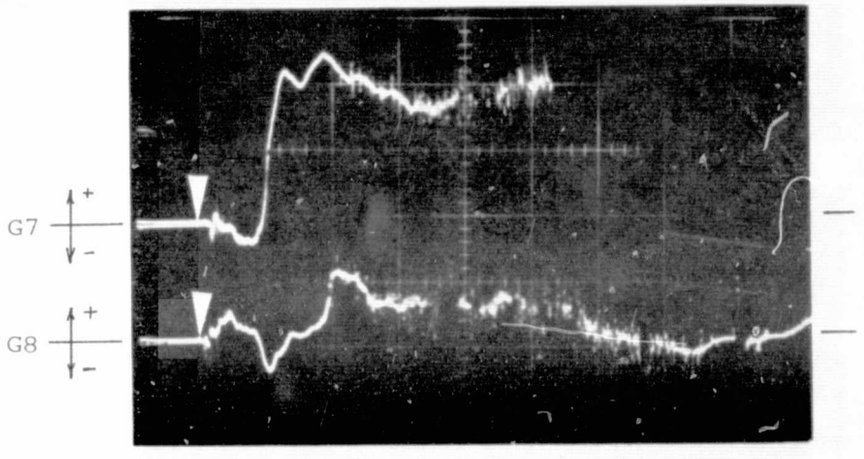

100 µSEC/DIV

GAGE 7
1%/DIV

GAGE 8
1%/DIV

FIG. 5 CONCLUDED (CP-1)

ABSCISSA: TIME, 50 μSEC/DIV
ORDINATE: UNCORRECTED RELATIVE ELONGATION IN PER CENT

\+ = TENSION (UP)
\- = COMPRESSION (DOWN)

∇: TIME = 0

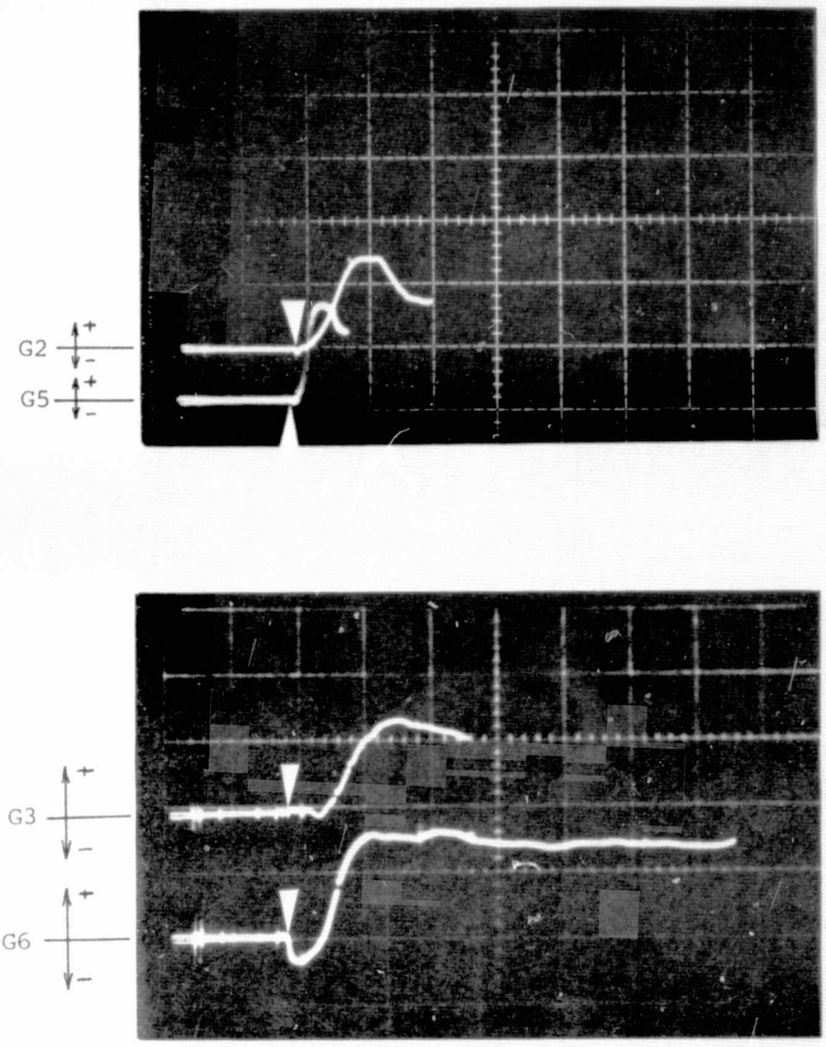

FIG. 6 UNCORRECTED TRANSIENT RELATIVE ELONGATION RECORDS FOR IMPULSIVELY-LOADED 6061-T651 PANEL MODEL CP-2 WITH CLAMPED EDGES

ABSCISSA: TIME
ORDINATE: UNCORRECTED RELATIVE ELONGATION IN PER CENT
+ = TENSION (UP)
- = COMPRESSION (DOWN)
∇: TIME = 0

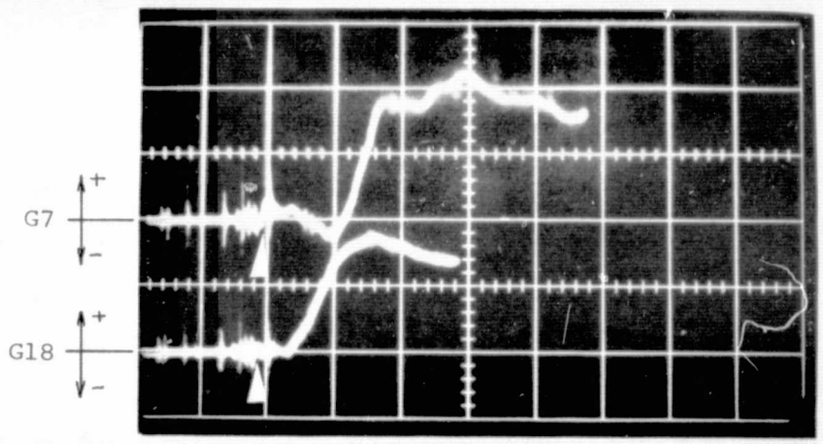

50 µSEC/DIV

GAGE 7
1%/DIV

GAGE 18
4%/DIV

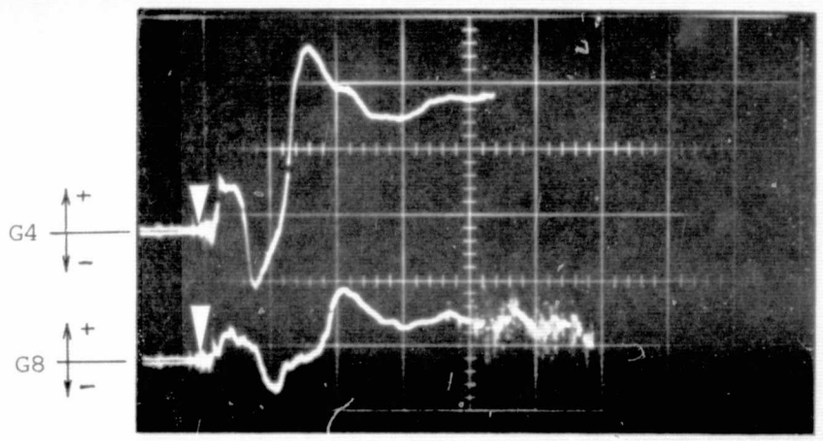

100 µSEC/DIV

GAGE 4
1%/DIV

GAGE 8
1%/DIV

FIG. 6 CONCLUDED (CP-2)

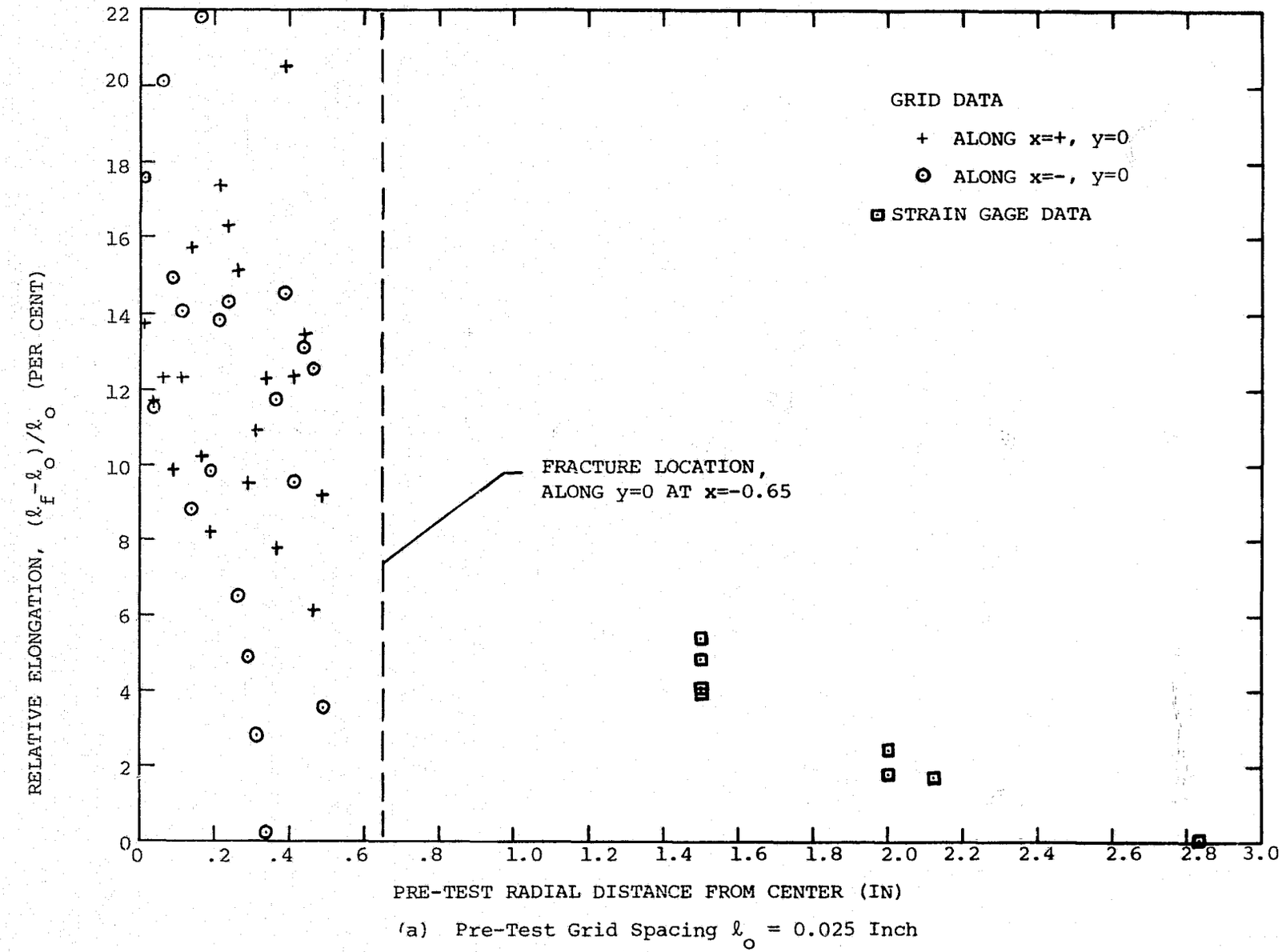

(a) Pre-Test Grid Spacing ℓ_o = 0.025 Inch

FIG. 7 MEASURED UPPER-SURFACE PERMANENT RELATIVE ELONGATION DATA ON IMPULSIVELY-LOADED 6061-T651 PANEL MODEL CP-2

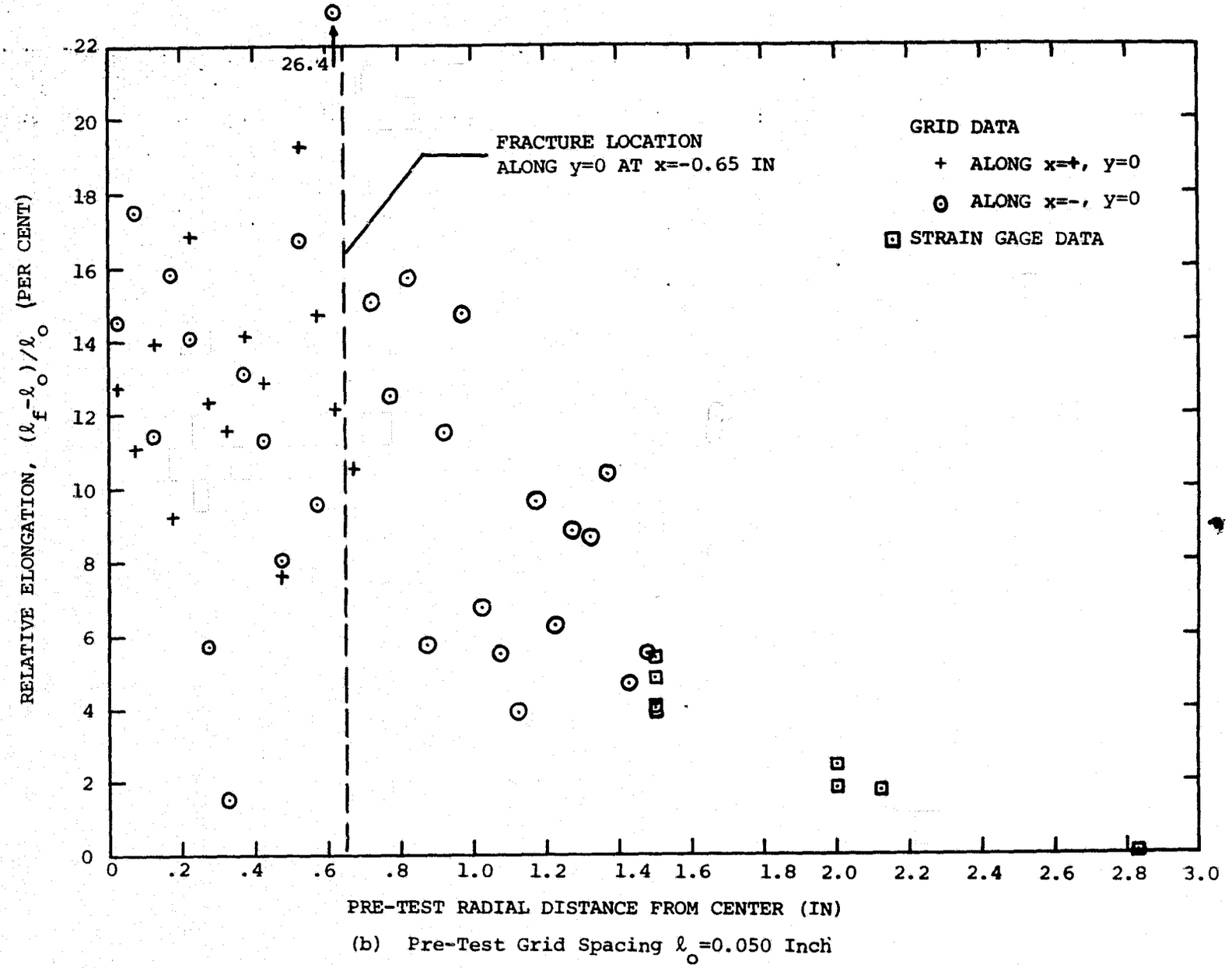

(b) Pre-Test Grid Spacing ℓ_o=0.050 Inch

FIG. 7 CONCLUDED (CP-2)

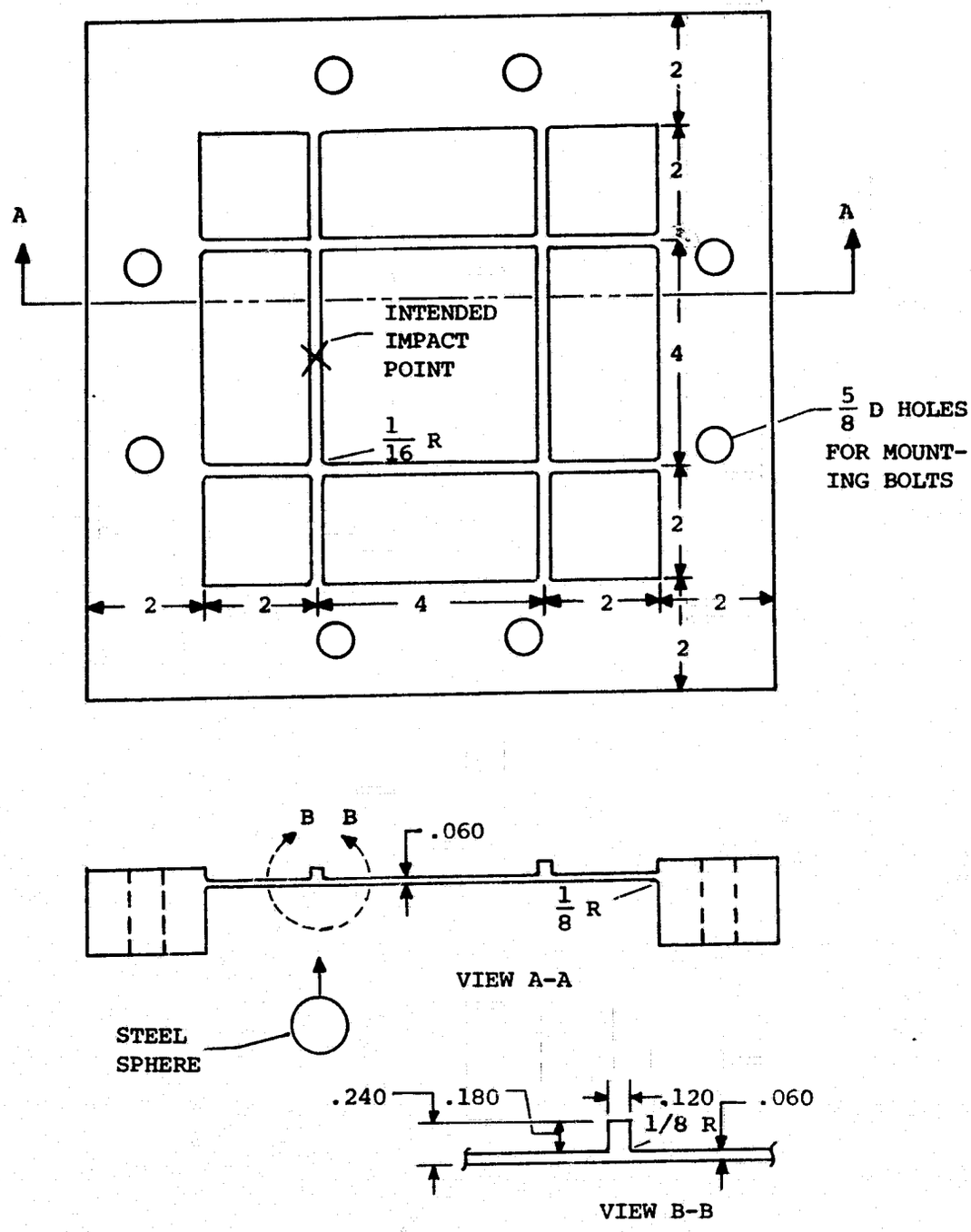

FIG. 8 GEOMETRY AND NOMINAL DIMENSIONS OF THE INTEGRALLY-STIFFENED 6061-T651 ALUMINUM PANEL MODELS

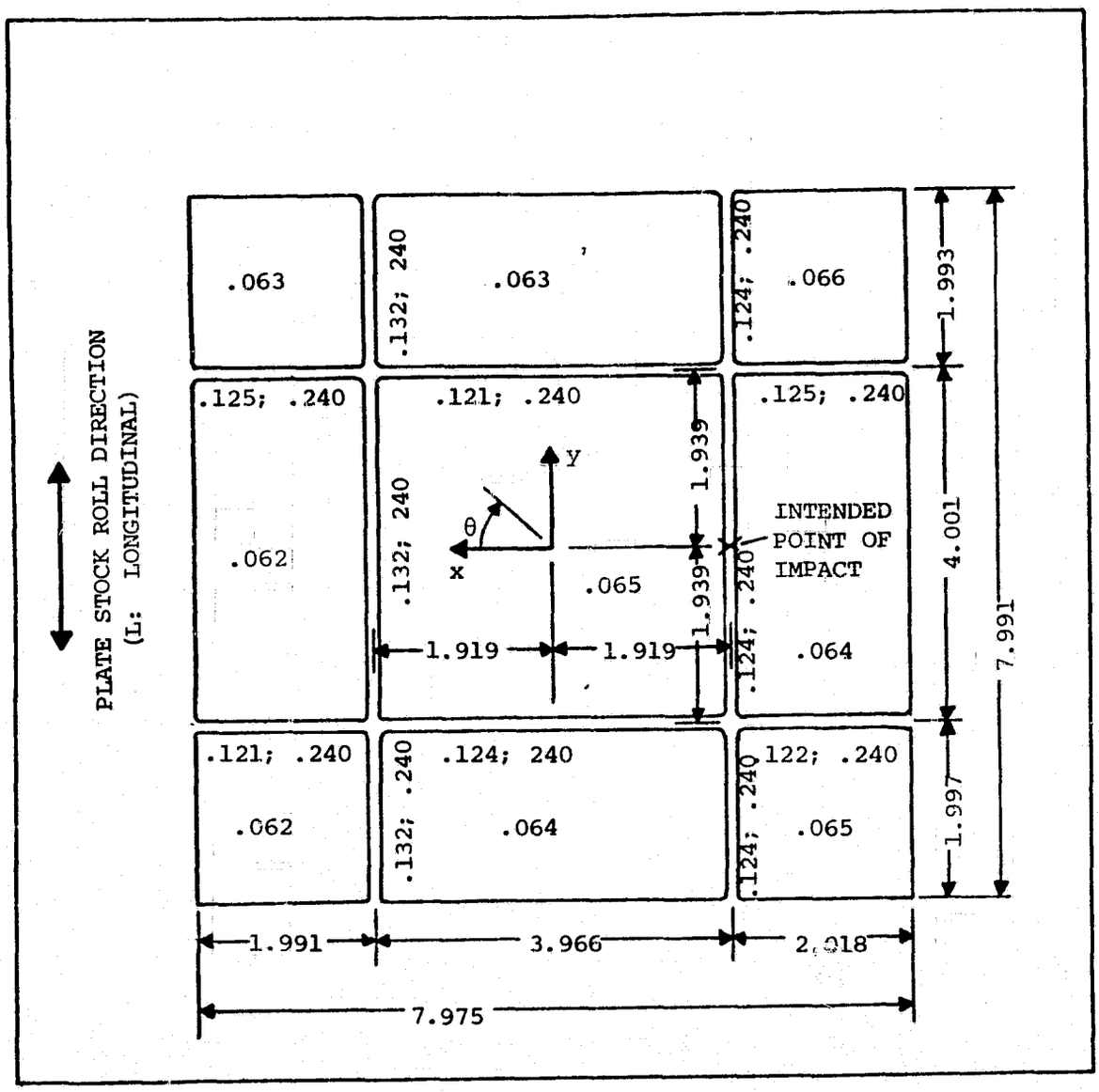

FIG. 9 DIMENSIONS AND NOMENCLATURE OF INTEGRALLY-STIFFENED 6061-T651 PANEL MODEL SCP-1

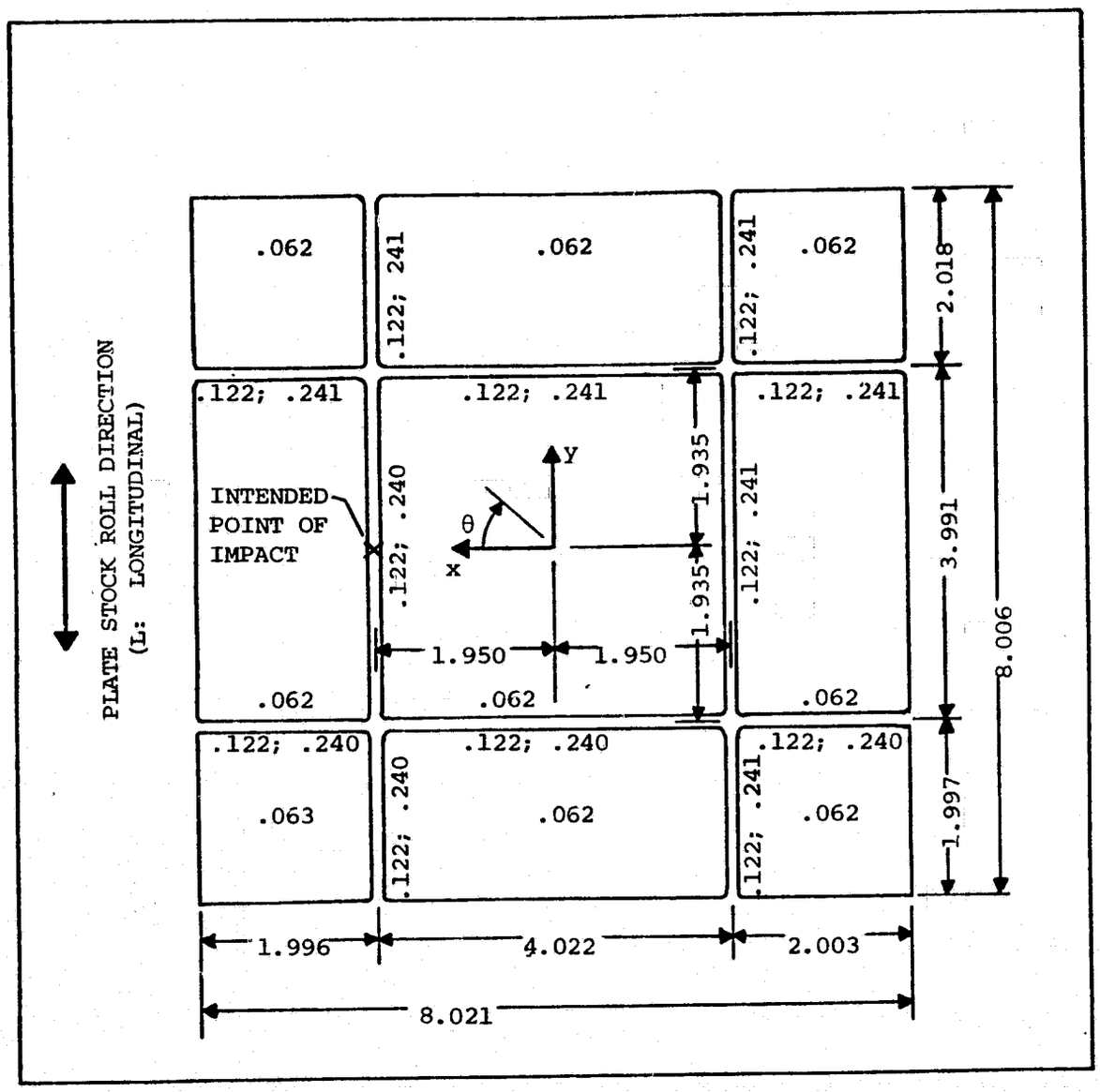

FIG. 10 DIMENSIONS AND NOMENCLATURE OF INTEGRALLY-STIFFENED 6061-T651 PANEL MODEL SCP-2

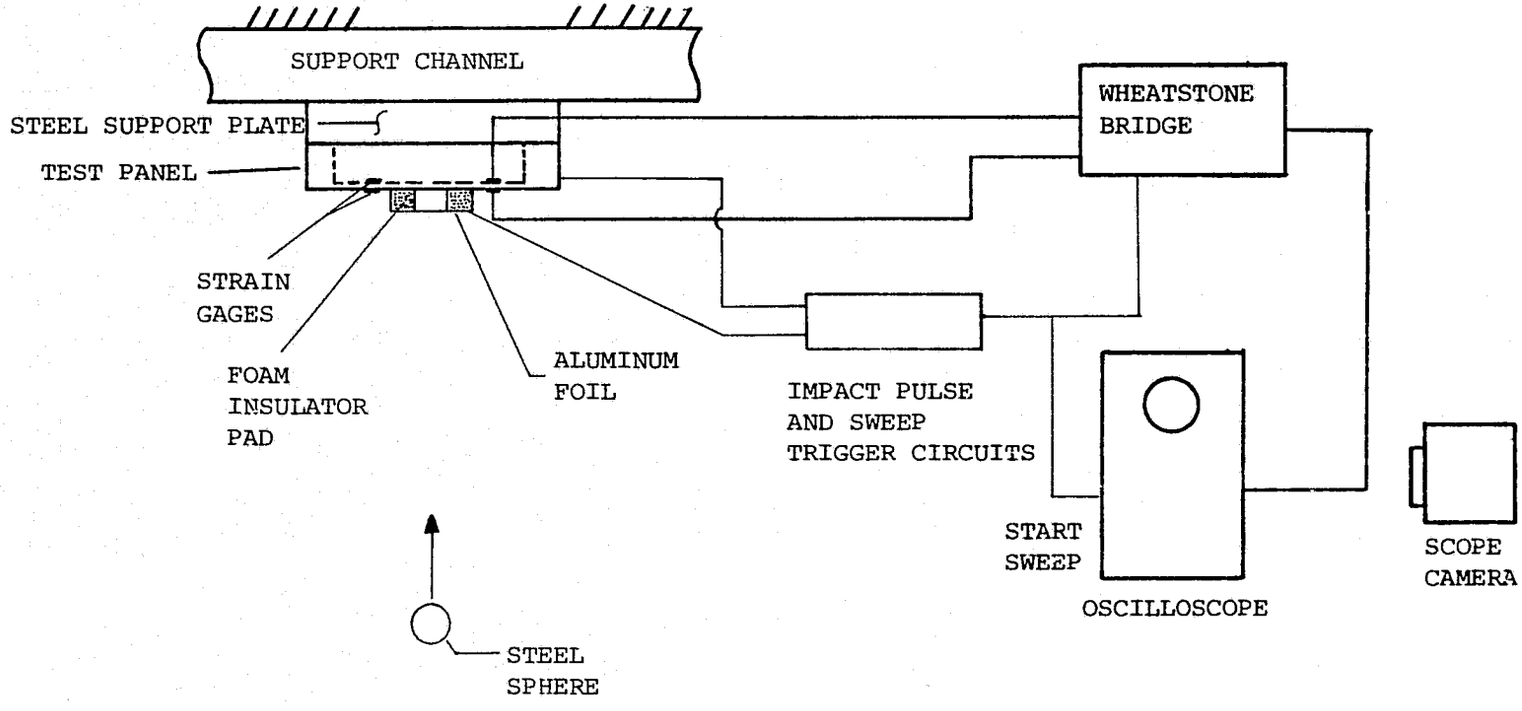

FIG. 11 TEST SCHEMATIC FOR STEEL-SPHERE-IMPACTED 6061-T651 ALUMINUM PANELS WITH CLAMPED EDGES

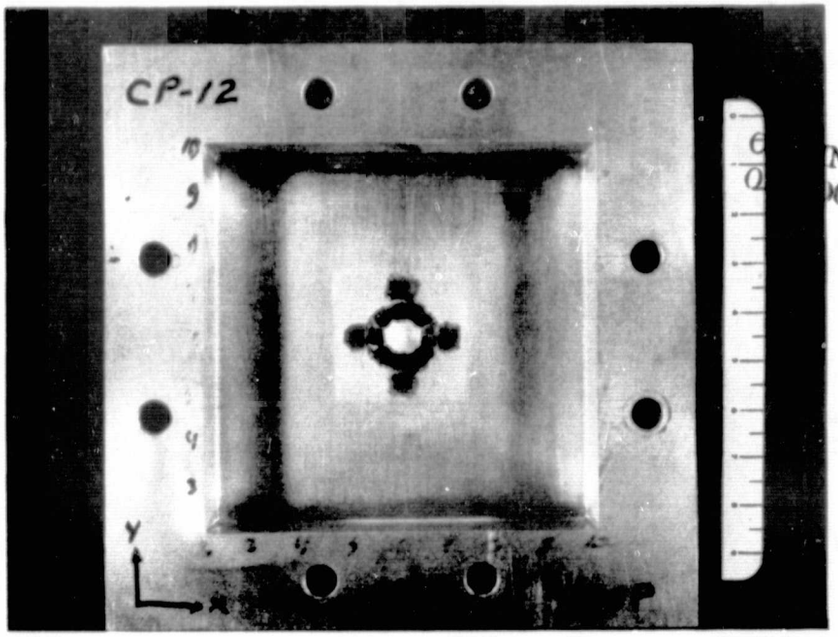

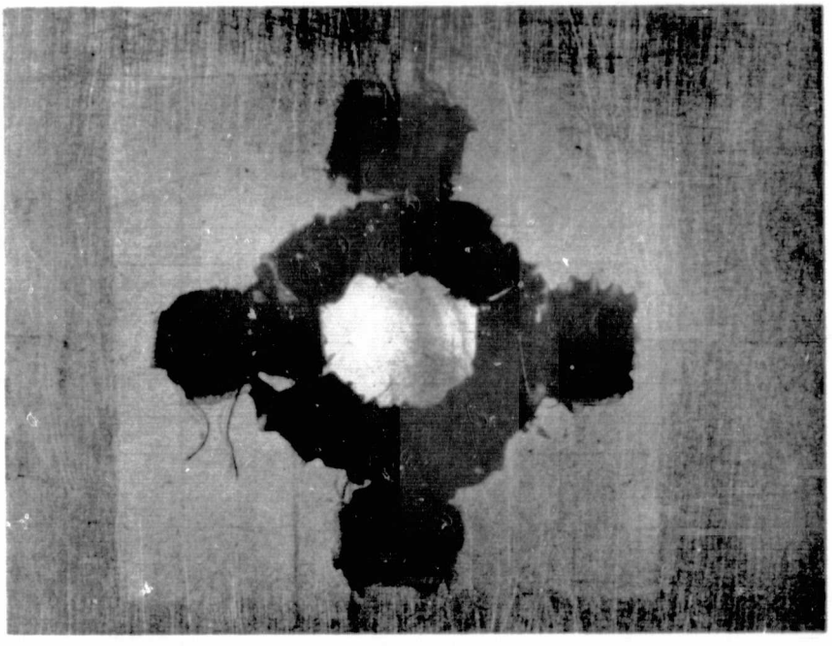

TOP
CLOSEUP

FIG. 12 POST-TEST PHOTOGRAPHS OF STEEL-SPHERE-IMPACTED PANEL SPECIMEN CP-12 (2395 IN/SEC)

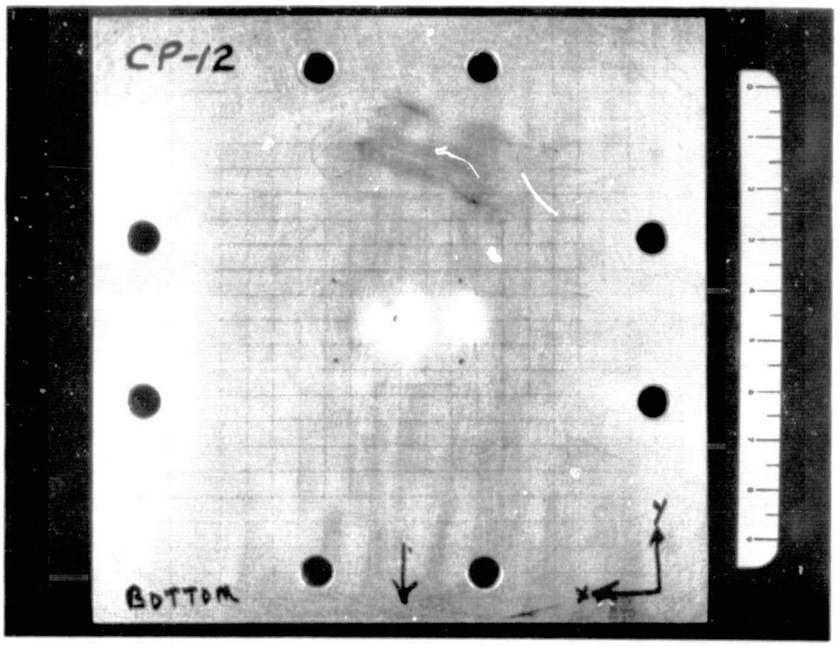

FIG. 12 CONCLUDED

C-2

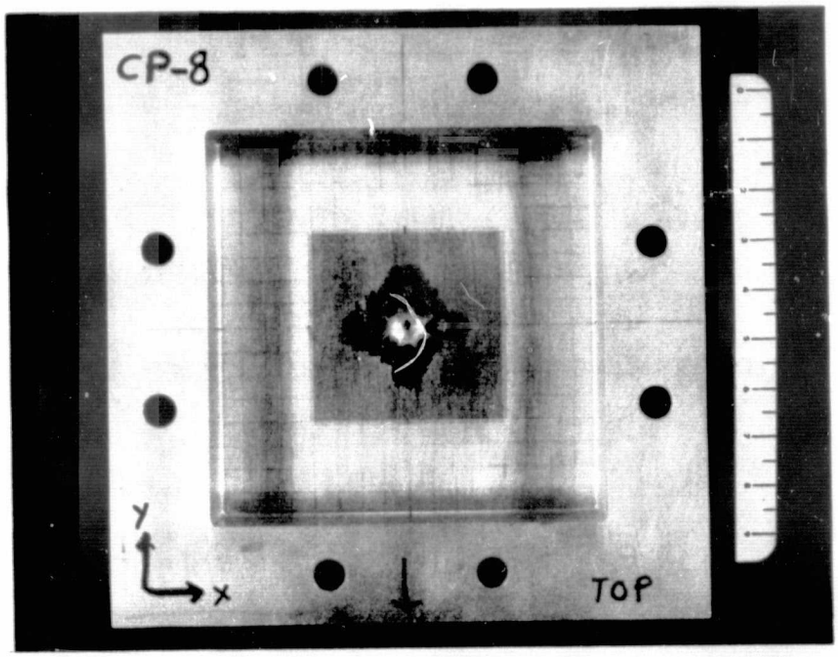

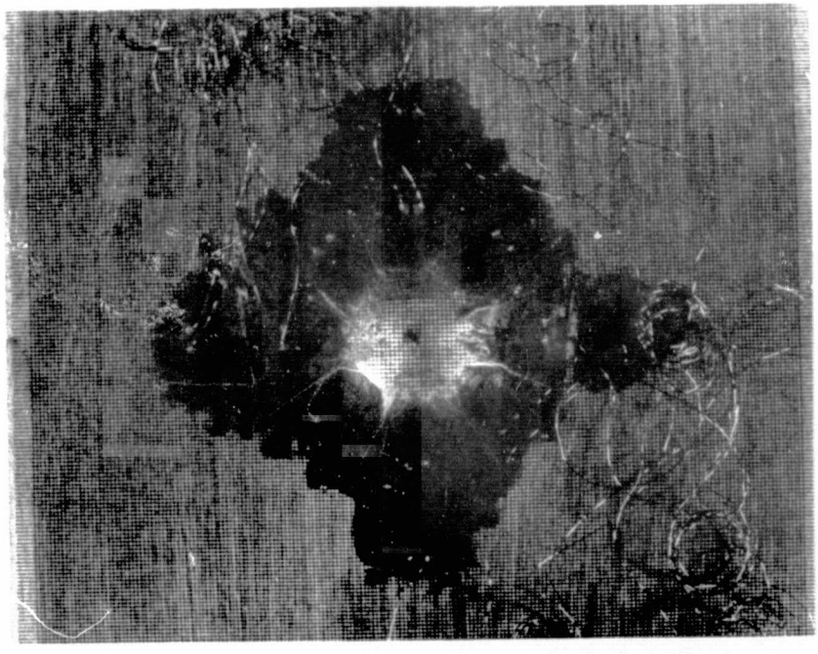

TOP
CLOSEUP

FIG. 13 POST-TEST PHOTOGRAPHS OF STEEL-SPHERE-IMPACTED PANEL SPECIMEN CP-8 (2435 IN/SEC)

ORIGINAL PAGE IS
OF POOR QUALITY

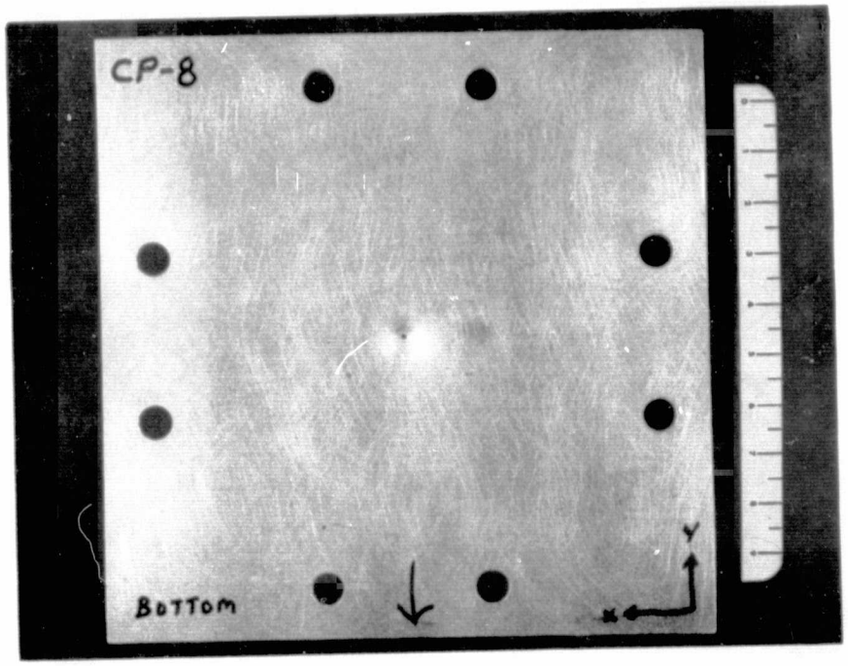

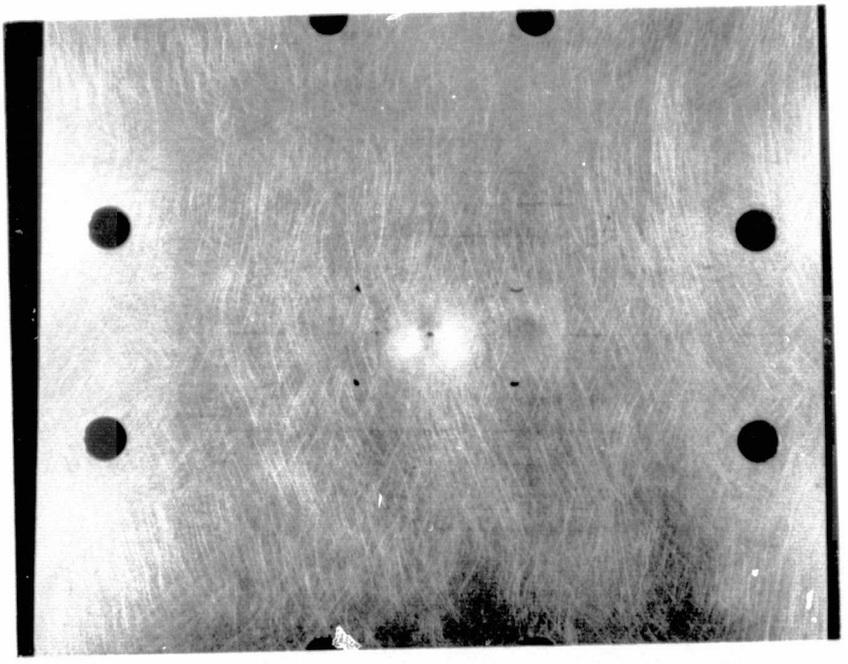

BOTTOM
CLOSEUP

FIG. 13 CONCLUDED

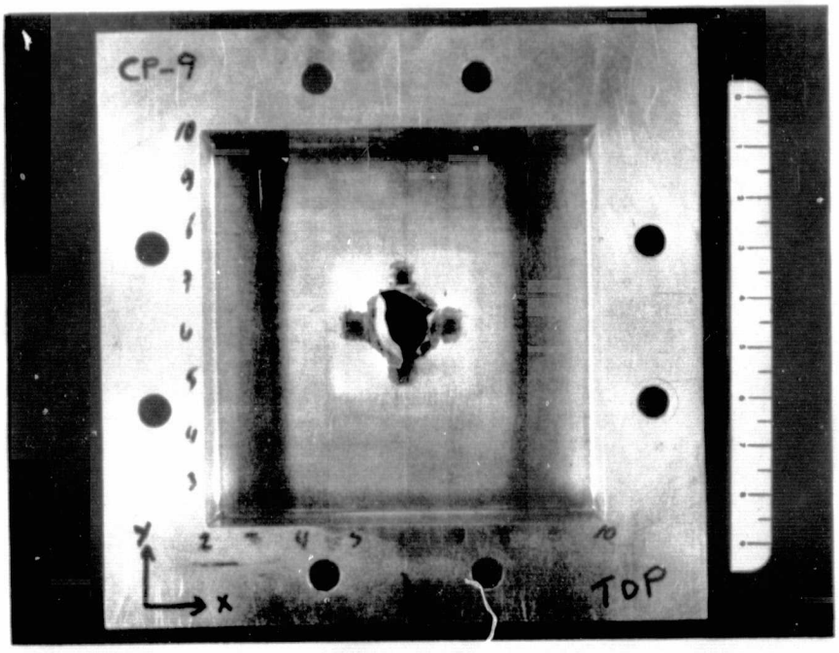

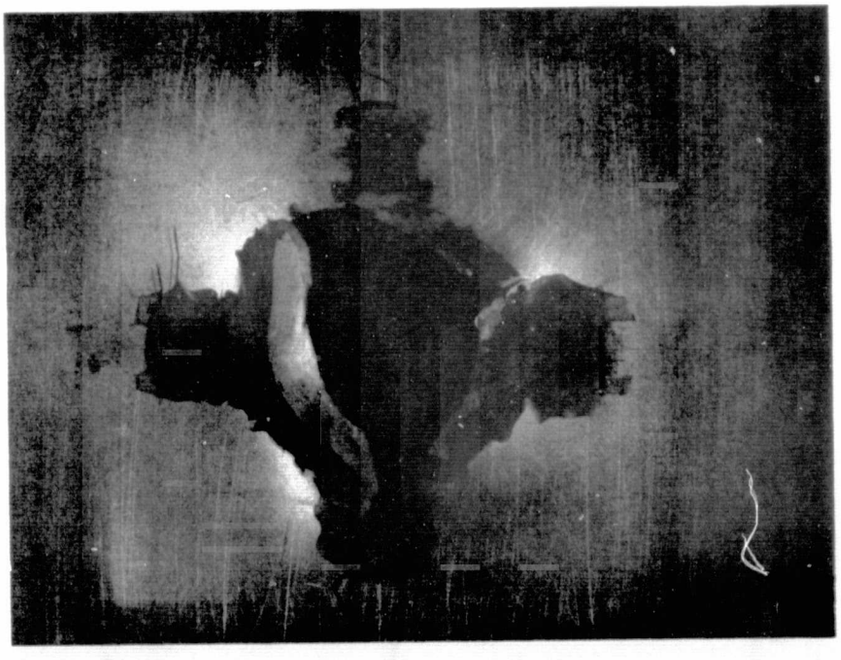

TOP
CLOSEUP

FIG. 14 POST-TEST PHOTOGRAPHS OF STEEL-SPHERE-IMPACTED PANEL SPECIMEN CP-9 (2755 IN/SEC)

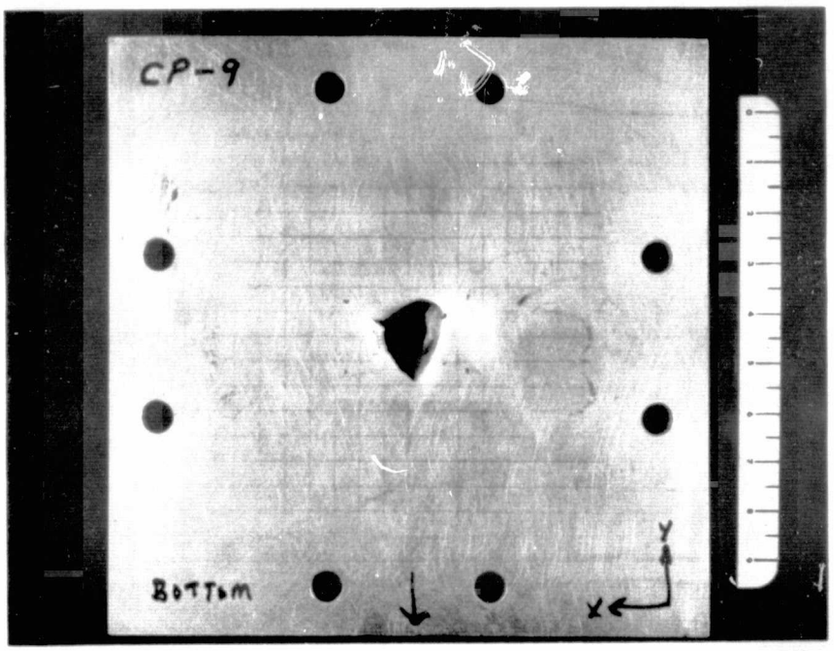

FIG. 14 CONCLUDED

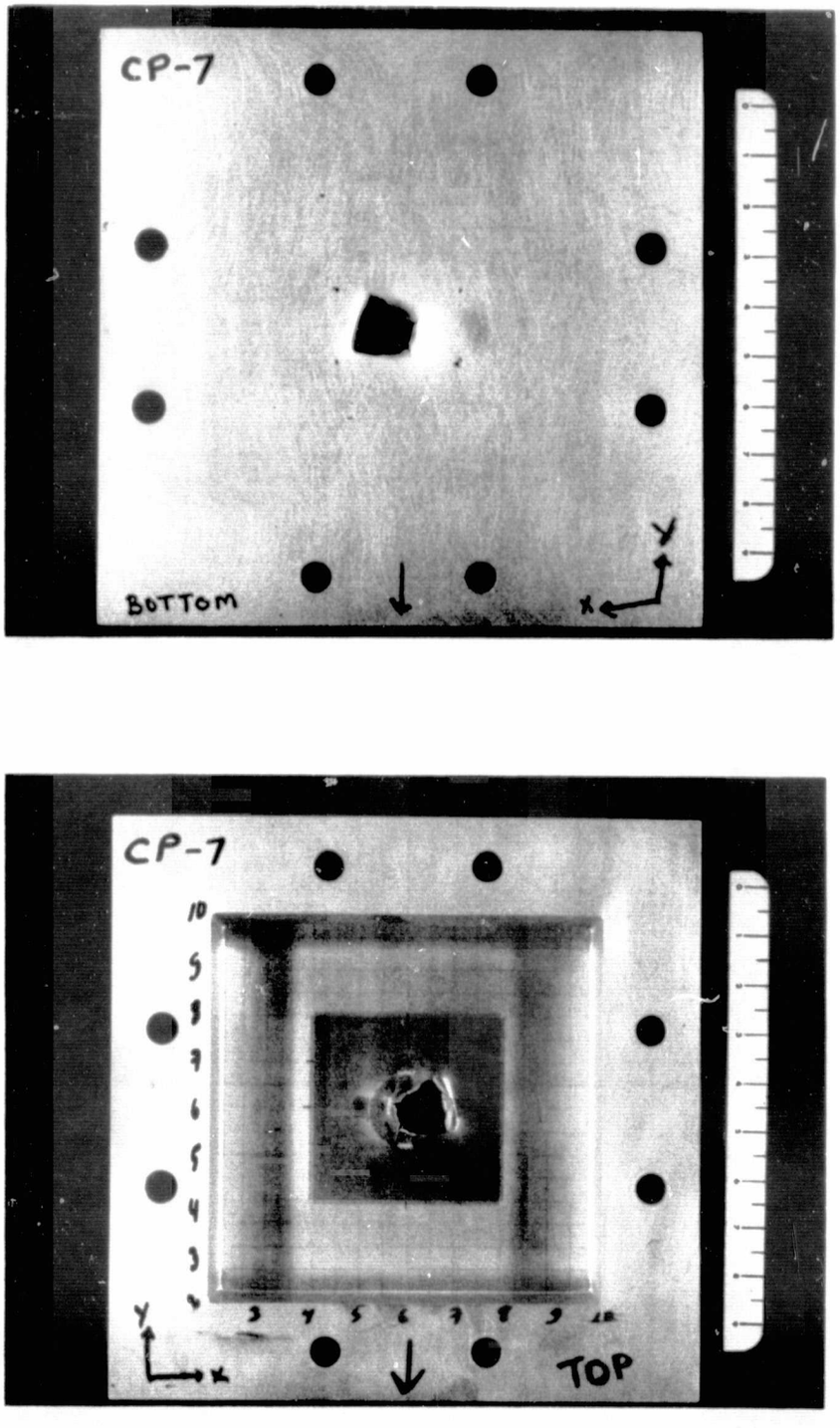

FIG. 15 POST-TEST PHOTOGRAPHS OF STEEL-SPHERE-IMPACTED PANEL SPECIMEN CP-7 (2850 IN/SEC)

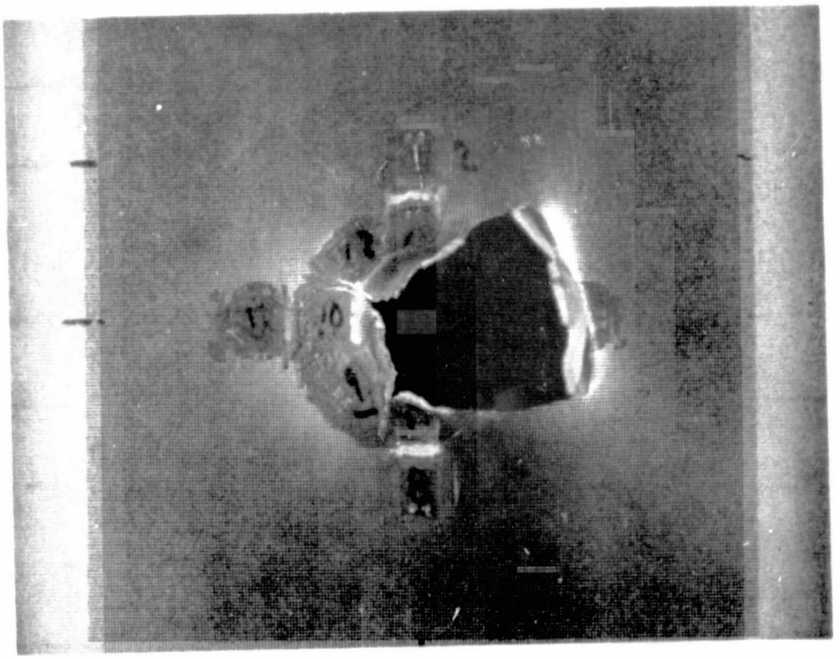

TOP
CLOSEUP

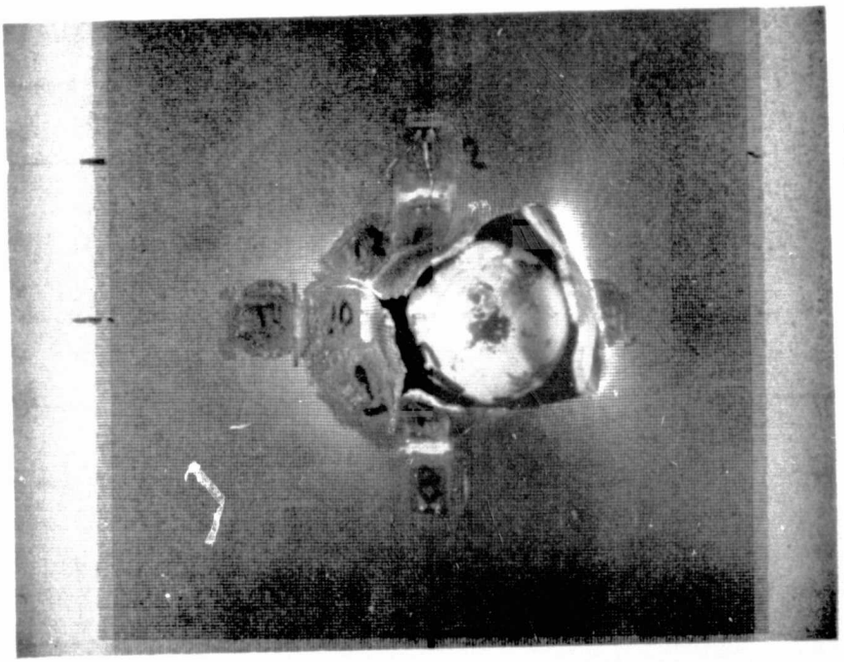

TOP
CLOSEUP

FIG. 15 CONCLUDED

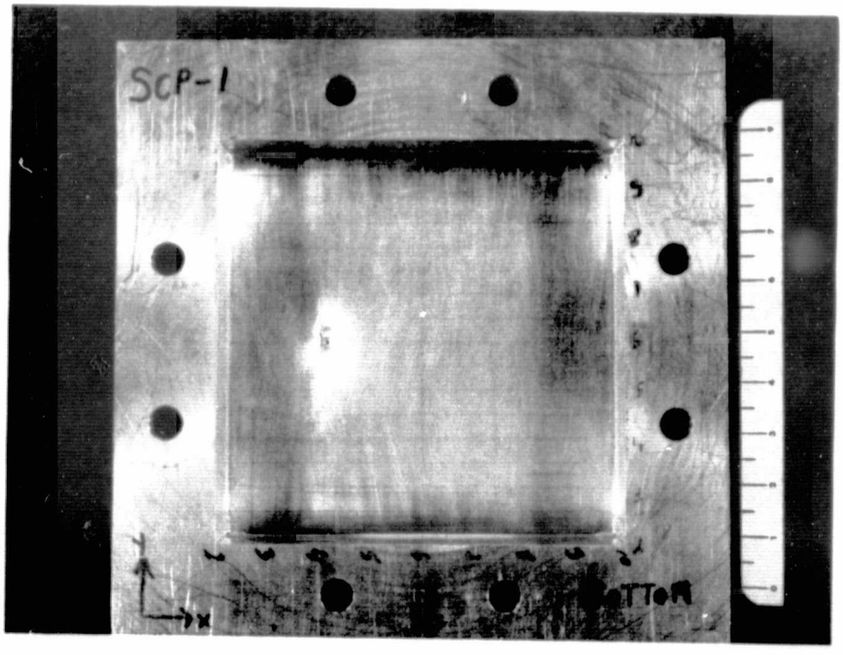

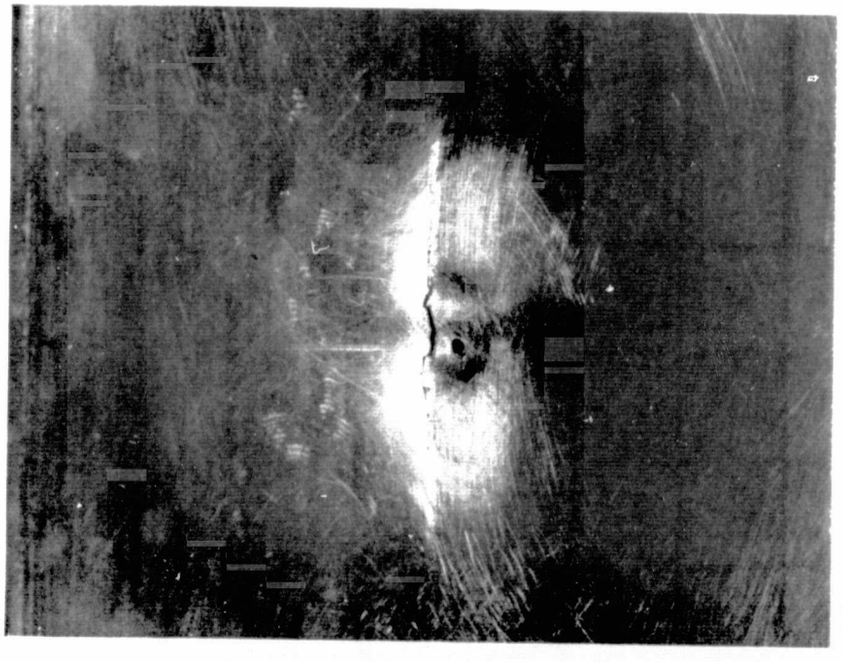

BOTTOM
CLOSEUP

FIG. 16 POST-TEST PHOTOGRAPHS OF STEEL-SPHERE-IMPACTED INTEGRALLY-STIFFENED PANEL SPECIMEN SCP-1 (2400 IN/SEC)

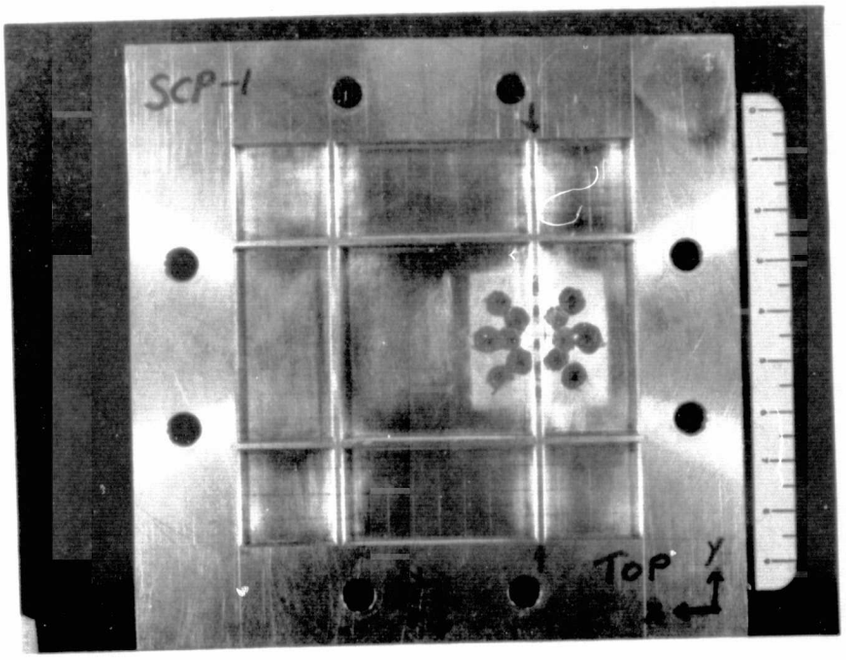

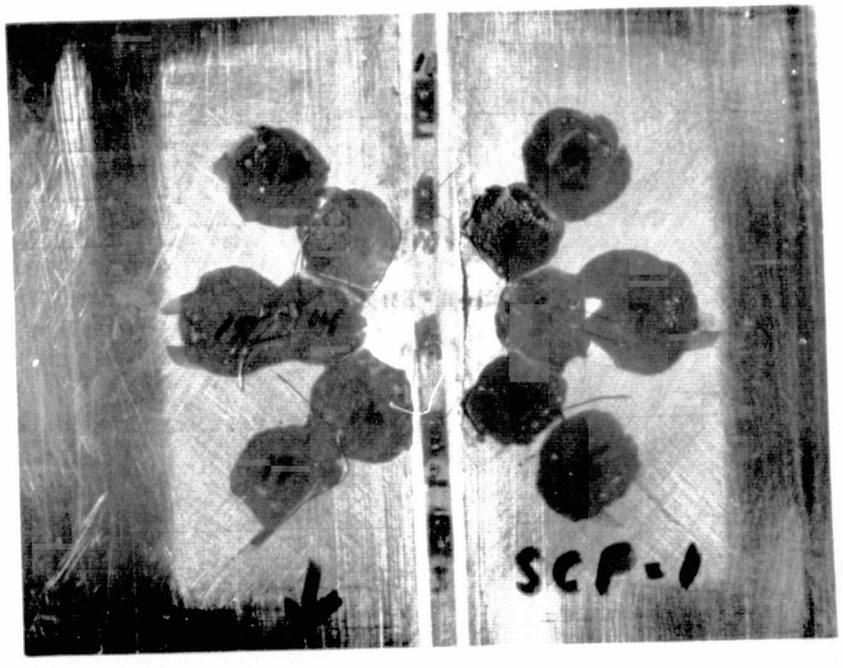

TOP
CLOSEUP

FIG. 16 CONCLUDED

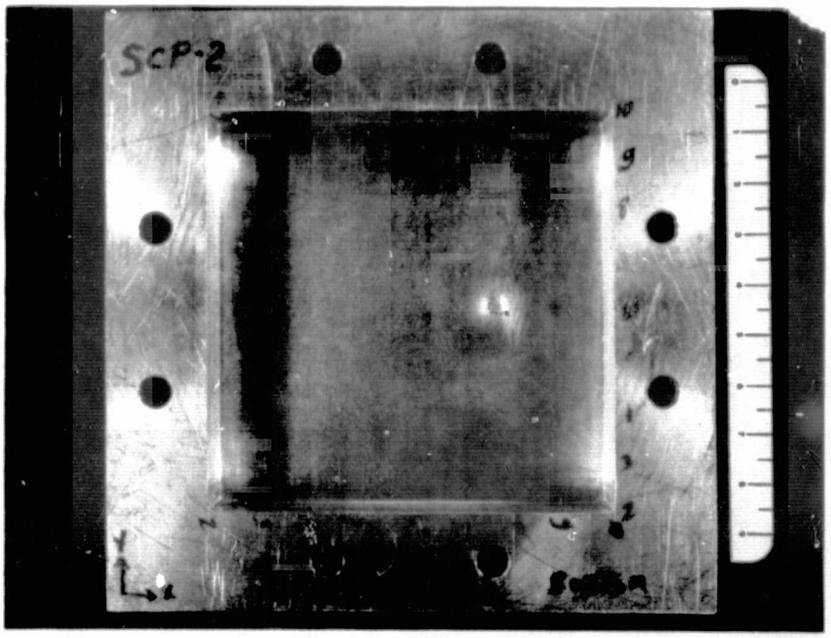

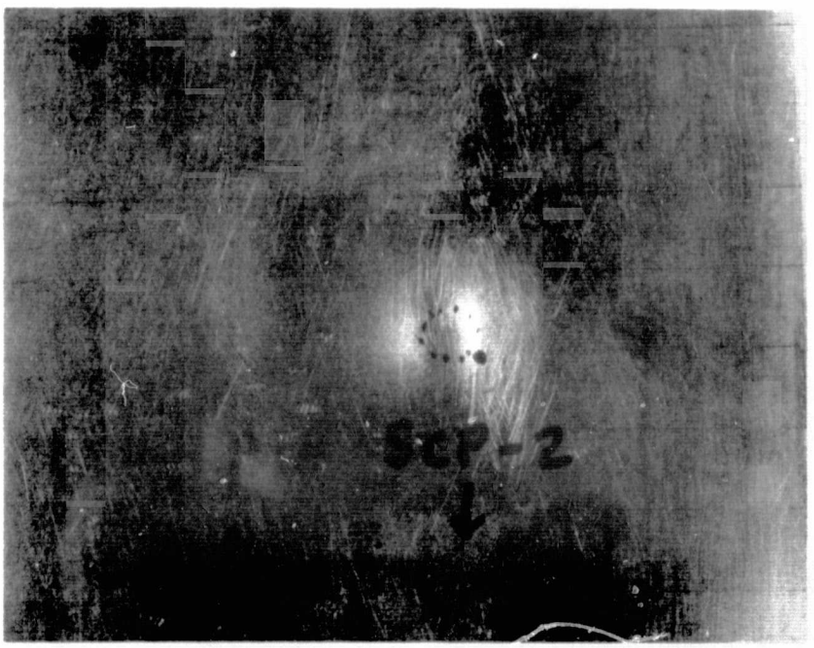

BOTTOM
CLOSEUP

FIG. 17 POST-TEST PHOTOGRAPHS OF STEEL-SPHERE-IMPACTED INTEGRALLY-STIFFENED PANEL SPECIMEN SCP-2 (2125 IN/SEC)

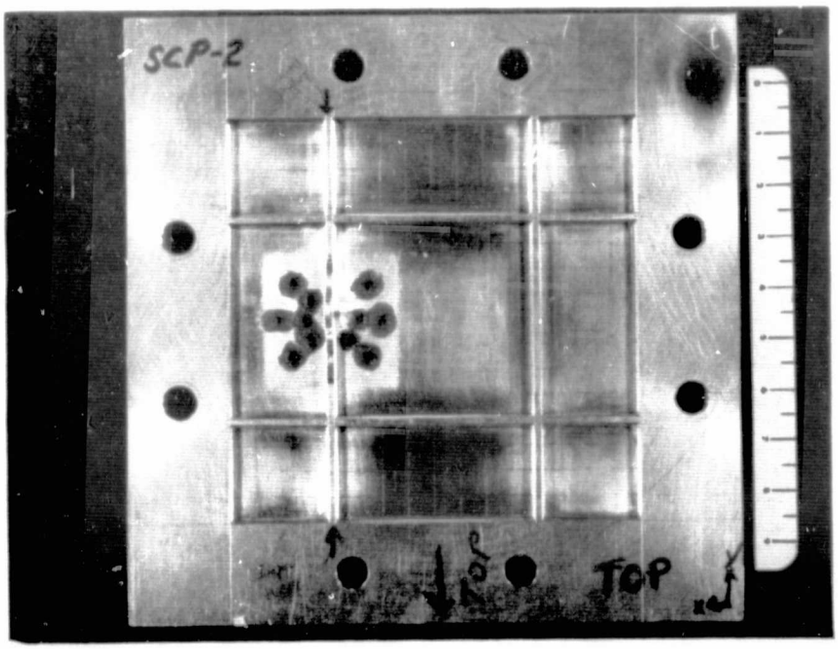

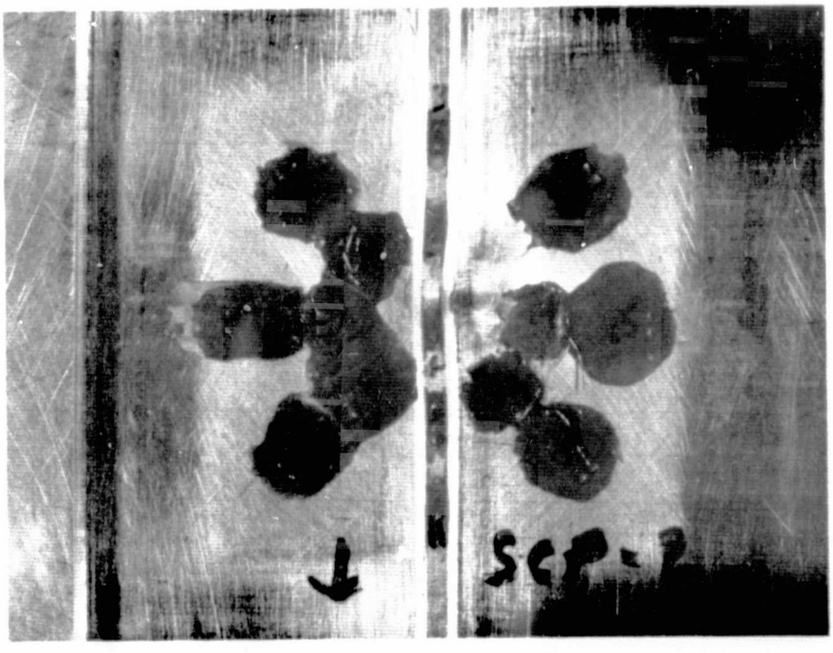

TOP
CLOSEUP

FIG. 17 CONCLUDED

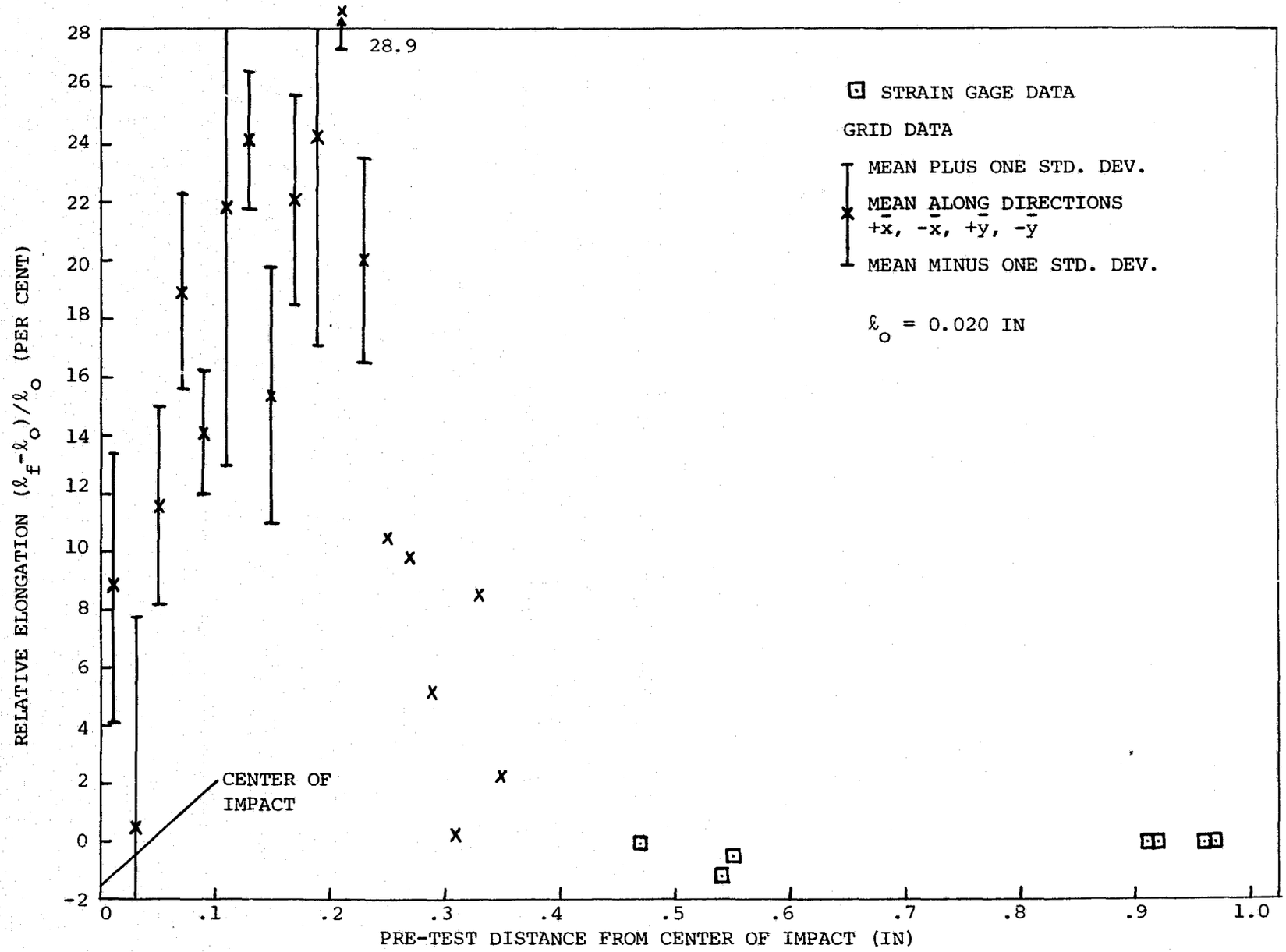

Fig. 18 UPPER SURFACE PERMANENT RELATIVE ELONGATION DATA FOR THE STEEL-SPHERE-IMPACTED PANEL SPECIMEN CP-8

ABSCISSA: TIME, 50 μSEC/DIV
ORDINATE: UNCORRECTED RELATIVE
ELONGATION IN PER CENT
+ = TENSION (UP)
− = COMPRESSION (DOWN)
▽: TIME = 0

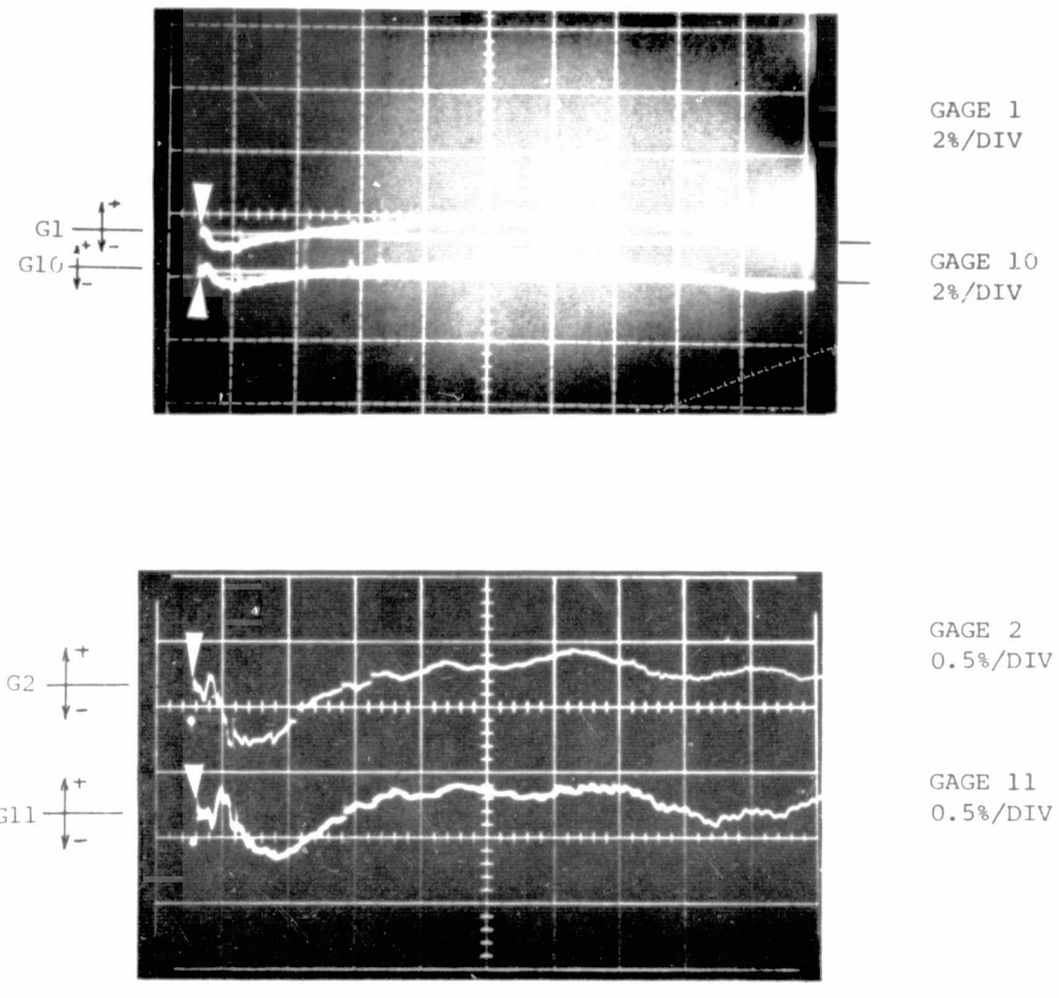

FIG. 19 UNCORRECTED TRANSIENT RELATIVE ELONGATION RECORDS FOR STEEL-SPHERE IMPACTED 6061-T651 PANEL MODEL CP-12 WITH CLAMPED EDGES

ABSCISSA: TIME, 50 μSEC/DIV
ORDINATE: UNCORRECTED RELATIVE
ELONGATION IN PER CENT
+ = TENSION (UP)
- = COMPRESSION (DOWN)
▽: TIME = 0

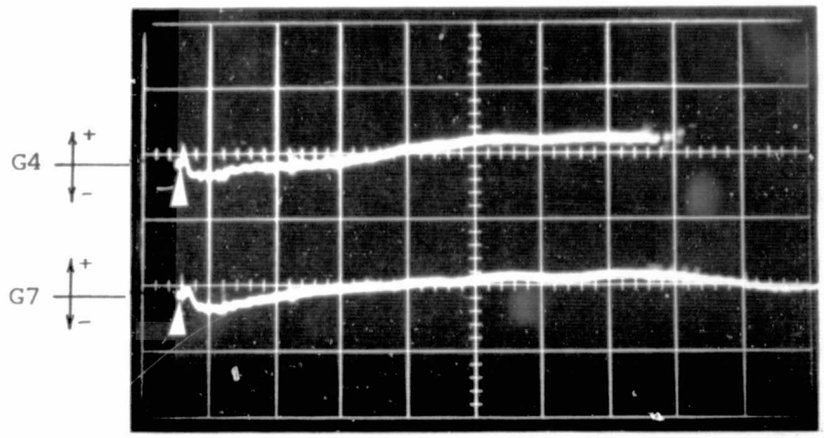

GAGE 4
2%/DIV

GAGE 7
2%/DIV

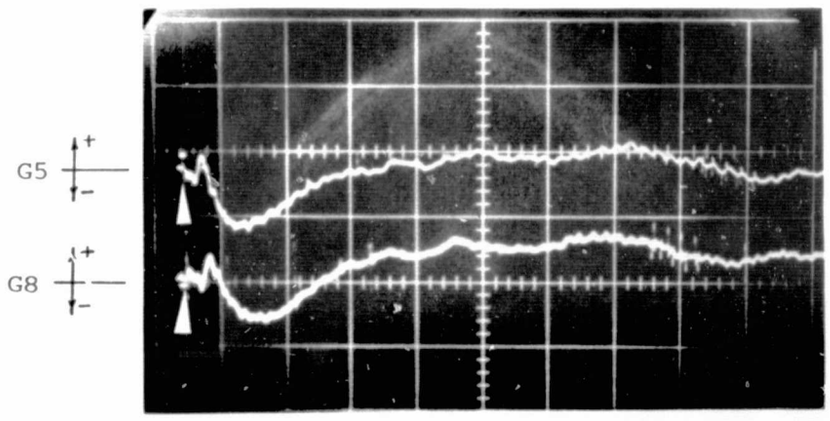

GAGE 5
0.5%/DIV

GAGE 8
0.5%/DIV

FIG. 19 CONCLUDED (CP-12; 2395 IN/SEC)

ABSCISSA: TIME, 50 μSEC/DIV
ORDINATE: UNCORRECTED RELATIVE
ELONGATION IN PER CENT
+ = TENSION (UP)
- = COMPRESSION (DOWN)
∇: TIME = 0

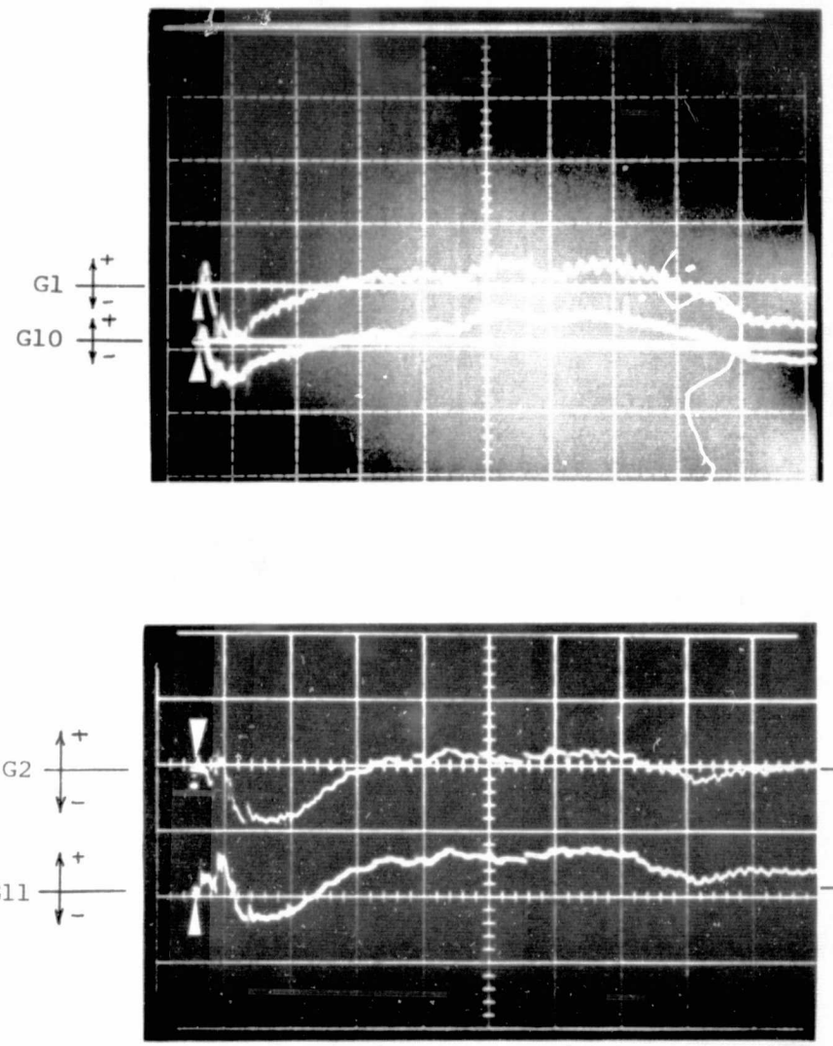

FIG. 20 UNCORRECTED TRANSIENT RELATIVE ELONGATION RECORDS FOR STEEL-SPHERE IMPACTED 6061-T651 PANEL MODEL CP-8 WITH CLAMPED EDGES

ABSCISSA: TIME, 50 μSEC/DIV
ORDINATE: UNCORRECTED RELATIVE
ELONGATION IN PER CENT
+ = TENSION (UP)
- = COMPRESSION (DOWN)
∇: TIME = 0

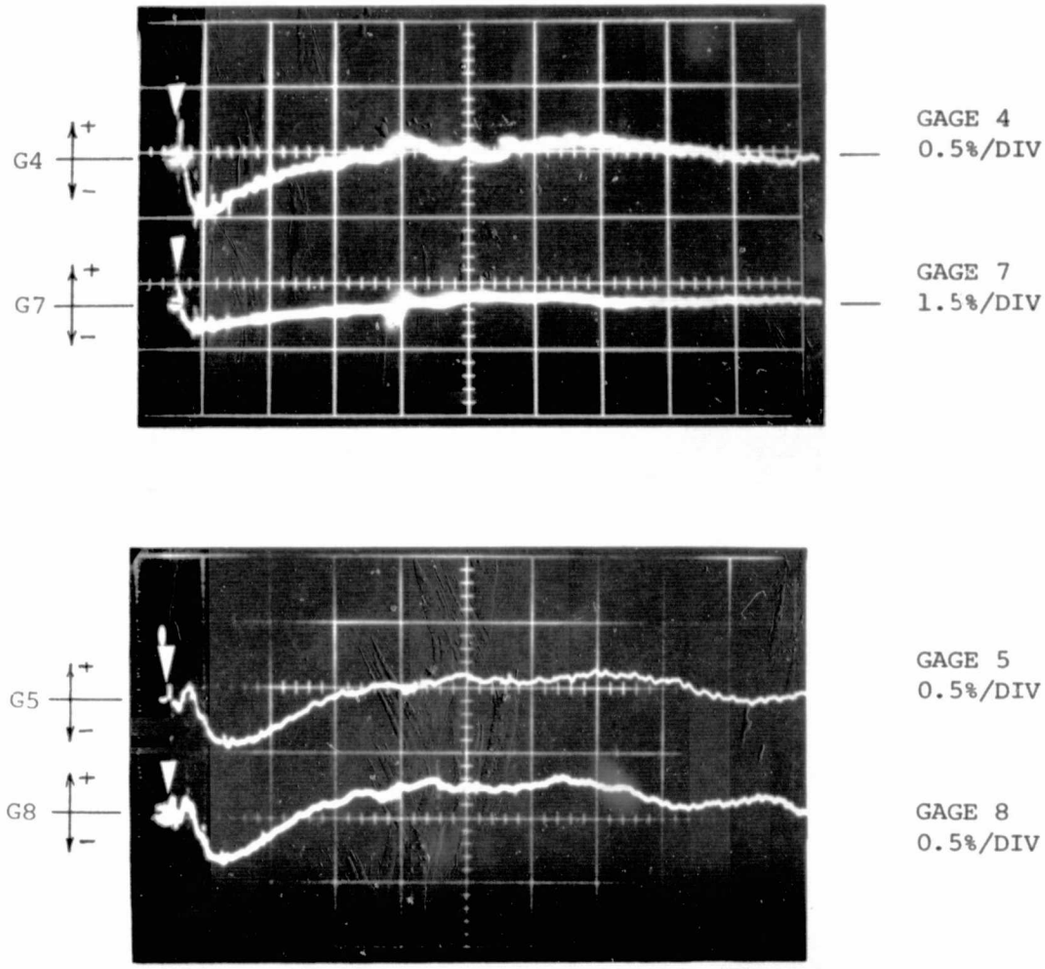

FIG. 20 CONCLUDED (CP-8; 2435 IN/SEC)

ABSCISSA: TIME, 50 μSEC/DIV
ORDINATE: UNCORRECTED RELATIVE ELONGATION IN PER CENT
+ = TENSION (UP)
- = COMPRESSION (DOWN)
∇: TIME = 0

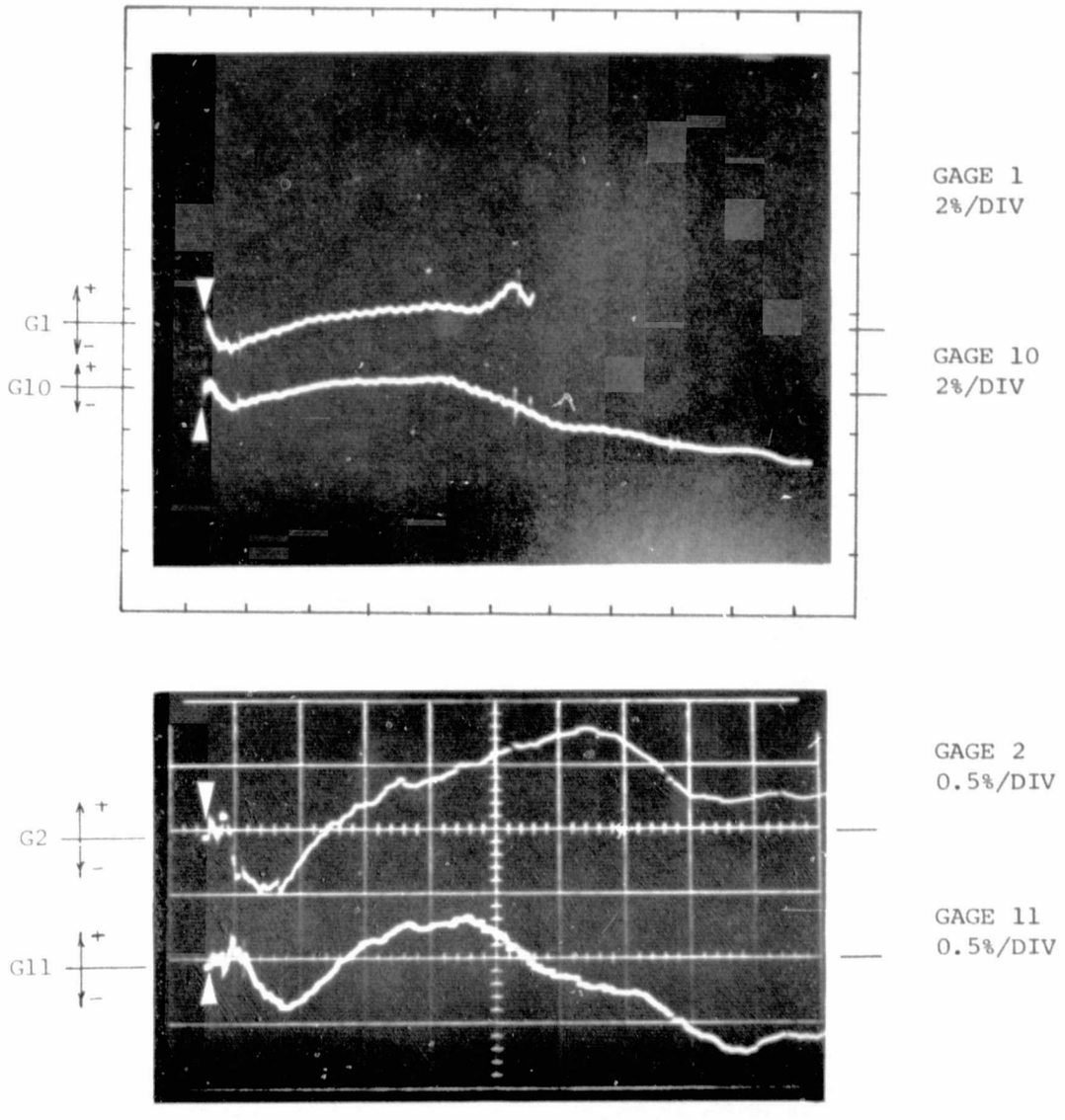

FIG. 21 UNCORRECTED TRANSIENT RELATIVE ELONGATION RECORDS FOR STEEL-SPHERE-IMPACTED 6061-T651 PANEL MODEL CP-9 WITH CLAMPED EDGES

ABSCISSA: TIME, 50 μSEC/DIV
ORDINATE: UNCORRECTED RELATIVE
ELONGATION IN PER CENT
+ = TENSION (UP)
- = COMPRESSION (DOWN)
∇: TIME = 0

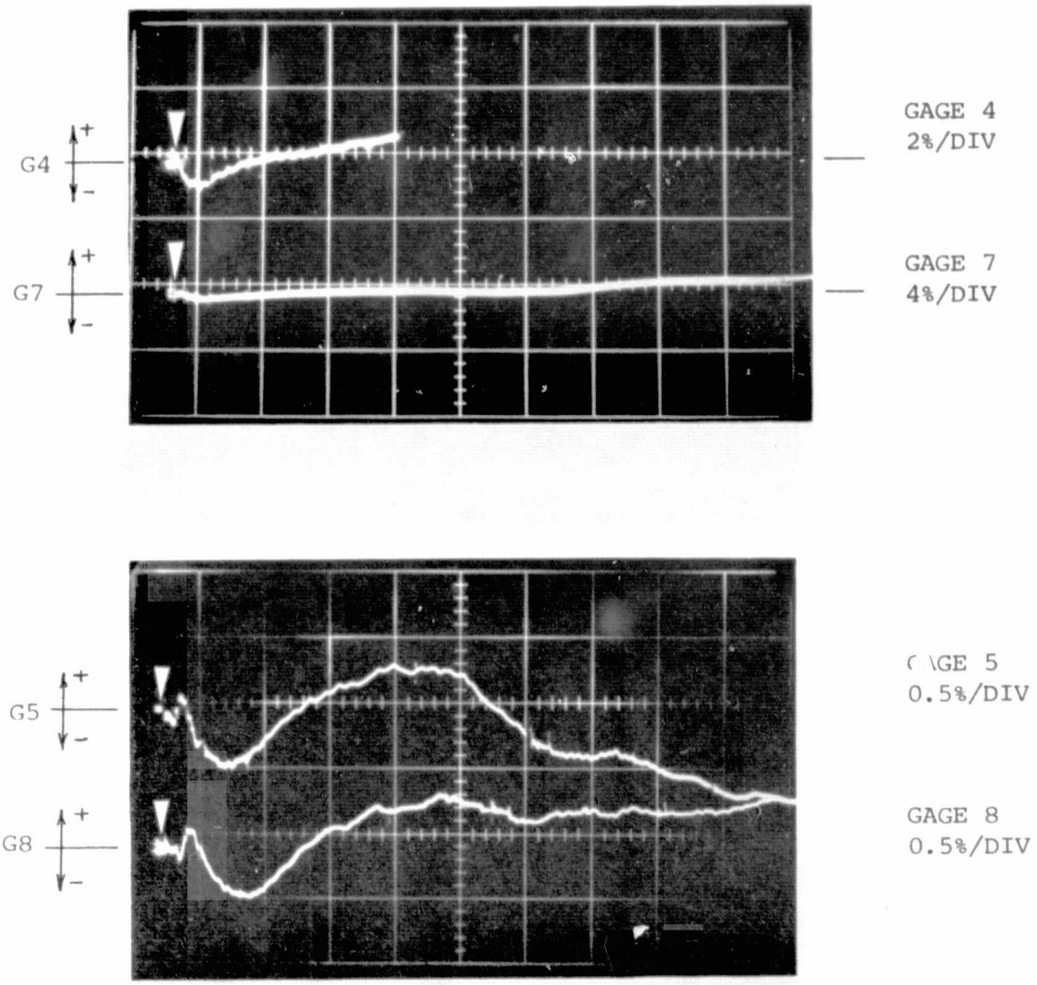

FIG. 21 CONCLUDED (CP-9; 2755 IN/SEC)

ABSCISSA: TIME, 50 μSEC/DIV
ORDINATE: UNCORRECTED RELATIVE
ELONGATION IN PER CENT
+ = TENSION (UP)
- = COMPRESSION (DOWN)
∇: TIME = 0

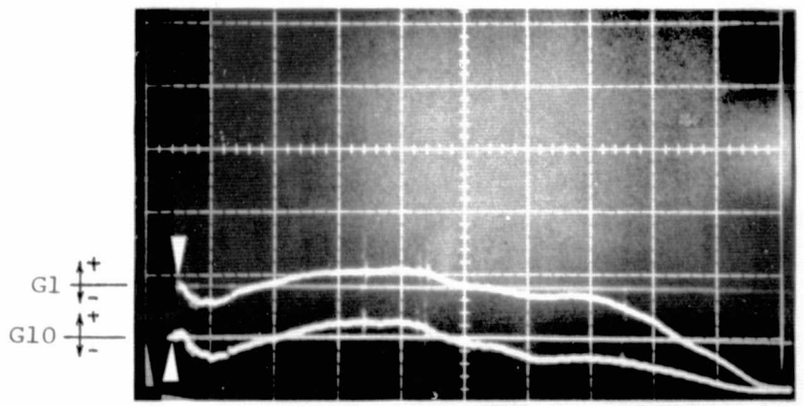

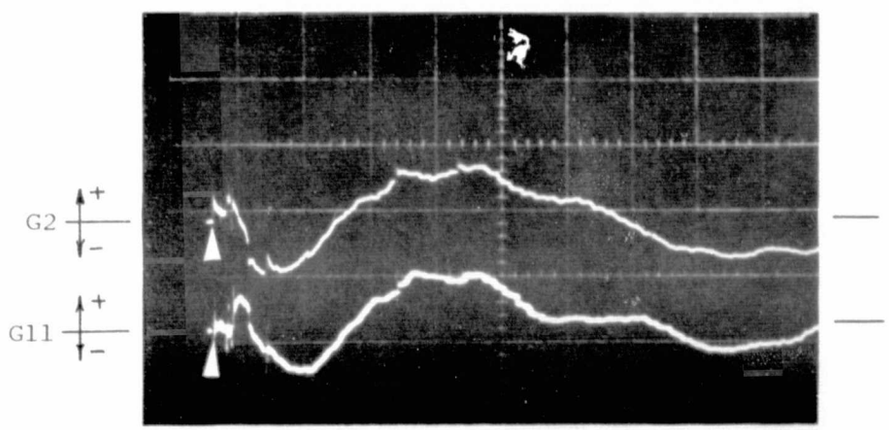

22 UNCORRECTED TRANSIENT RELATIVE ELONGATION RECORDS FOR STEEL-SPHERE-IMPACTED 6061-T651 PANEL MODEL CP-7 WITH CLAMPED EDGES

ABSCISSA: TIME, 50 μSEC/DIV
ORDINATE: UNCORRECTED RELATIVE
ELONGATION IN PER CENT
+ = TENSION (UP)
- = COMPRESSION (DOWN)
∇: TIME = 0

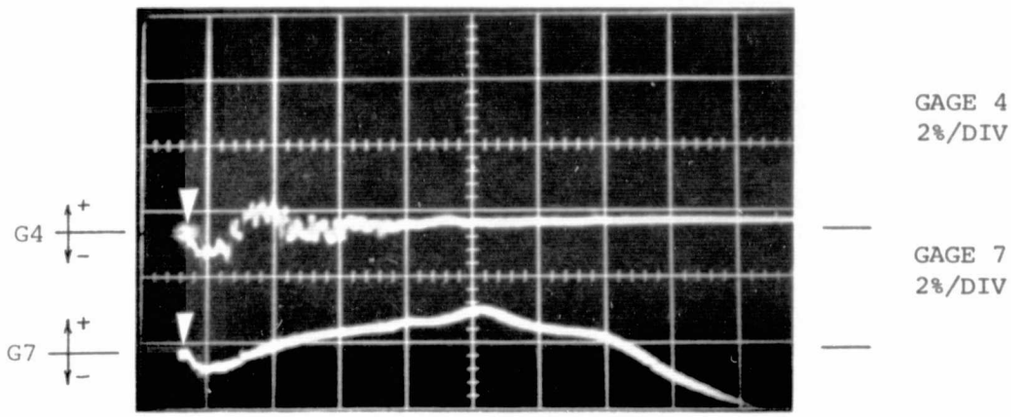

FIG. 22 CONCLUDED (CP-7; 2850 IN/SEC)

ABSCISSA: TIME, 50 μSEC/DIV
ORDINATE: UNCORRECTED RELATIVE ELONGATION IN PER CENT
+ = TENSION (UP)
- = COMPRESSION (DOWN)
∇: TIME = 0

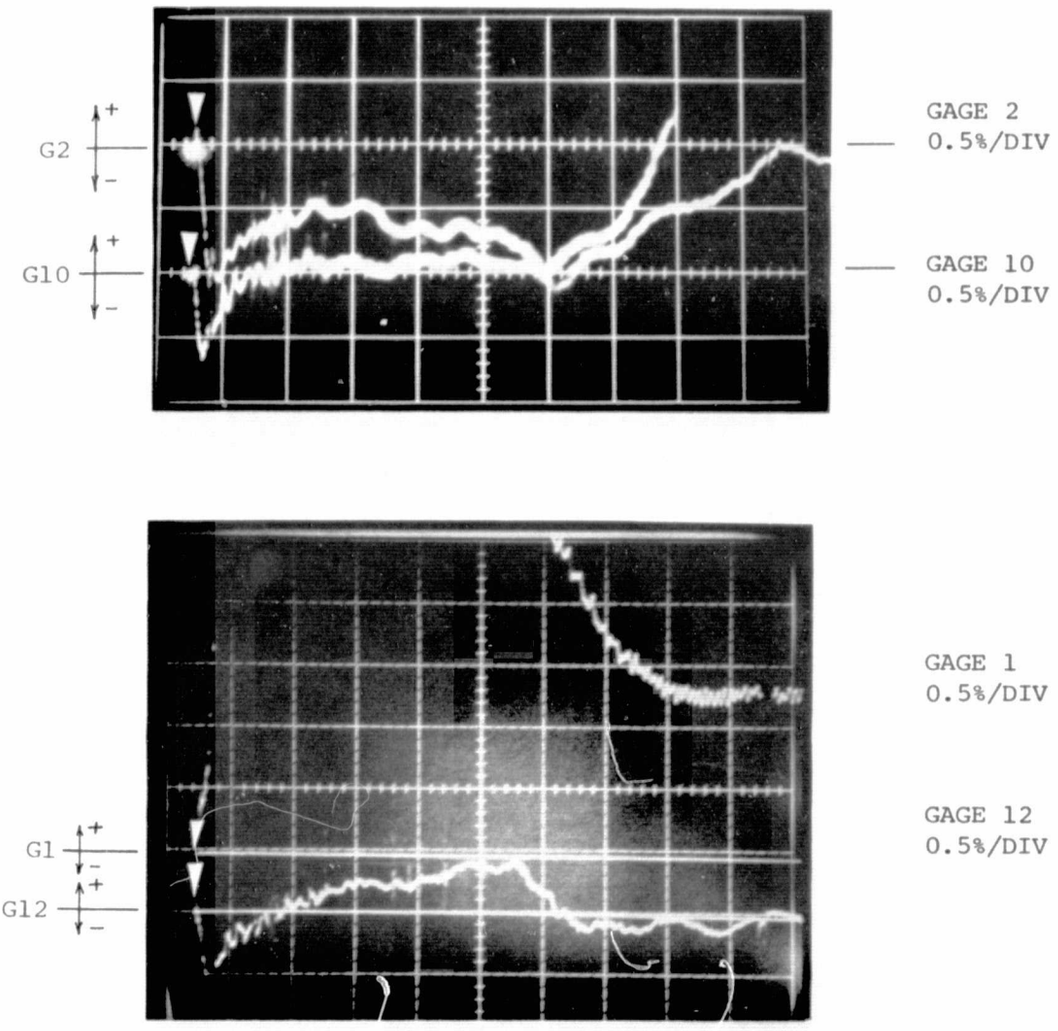

FIG. 23 UNCORRECTED TRANSIENT RELATIVE ELONGATION RECORDS FOR STEEL-SPHERE-IMPACTED INTEGRALLY-STIFFENED 6061-T651 PANEL MODEL SCP-1 WITH CLAMPED EDGES

ABSCISSA: TIME, 50 μSEC/DIV
ORDINATE: UNCORRECTED RELATIVE ELONGATION IN PER CENT
+ = TENSION (UP)
- = COMPRESSION (DOWN)
∇: TIME = 0

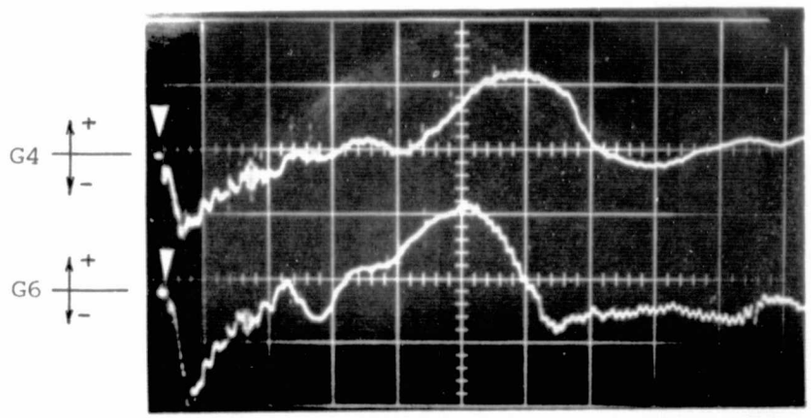

GAGE 4
0.5%/DIV

GAGE 6
0.5%/DIV

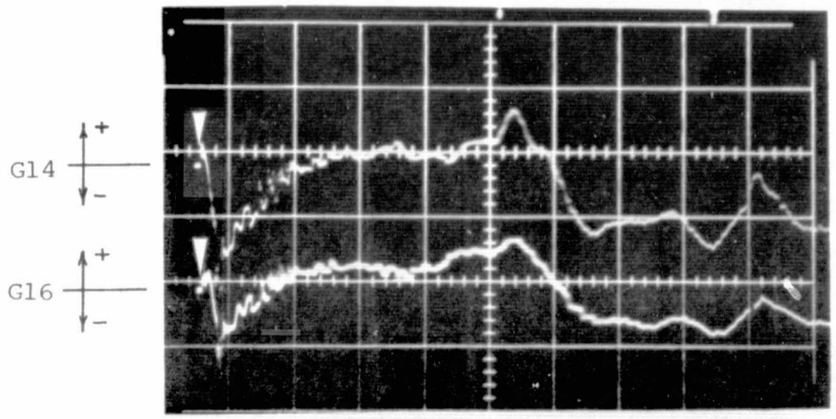

GAGE 14
0.5%/DIV

GAGE 16
0.5%/DIV

FIG. 23 CONCLUDED (SCP-1; 2400 IN/SEC)

ABSCISSA: TIME, 50 μSEC/DIV
ORDINATE: UNCORRECTED RELATIVE ELONGATION IN PER CENT
+ = TENSION (UP)
- = COMPRESSION (DOWN)
▽: TIME = 0

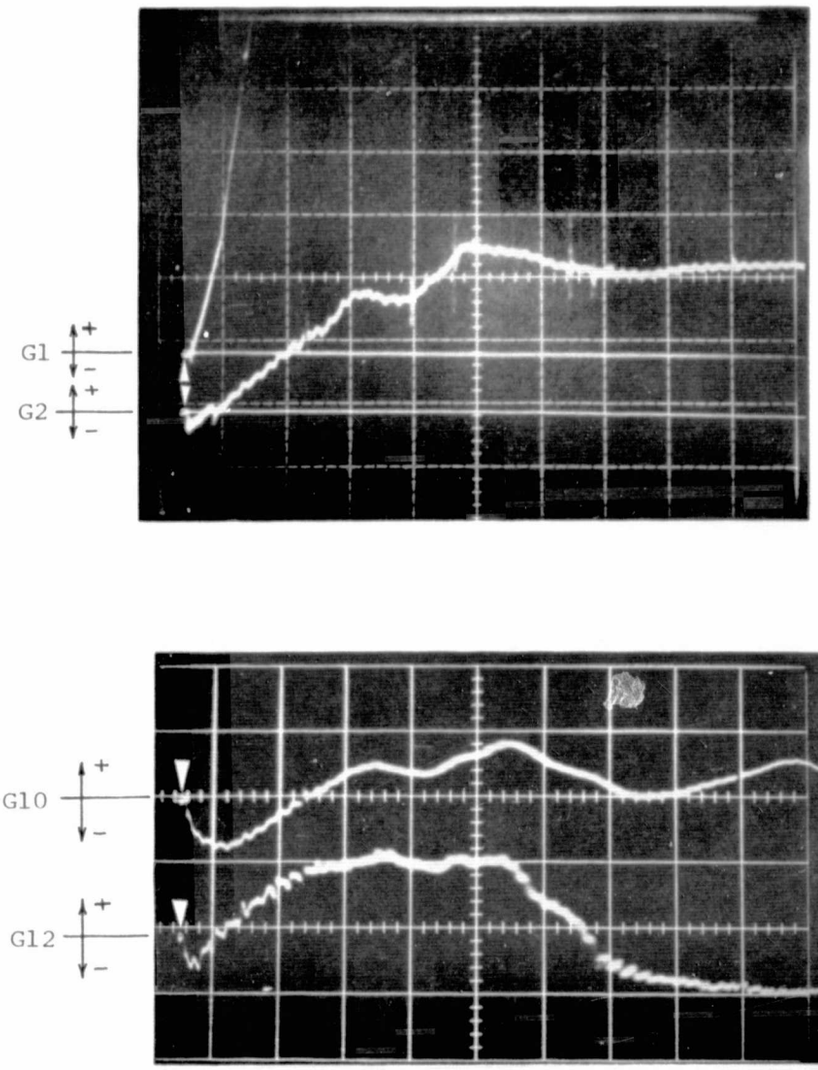

FIG. 24 UNCORRECTED TRANSIENT RELATIVE ELONGATION RECORDS FOR STEEL-SPHERE-IMPACTED INTEGRALLY-STIFFENED 6061-T651 PANEL MODEL SCP-2 WITH CLAMPED EDGES

ABSCISSA: TIME, 50 μSEC/DIV
ORDINATE: UNCORRECTED RELATIVE
ELONGATION IN PER CENT
+ = TENSION
- = COMPRESSION (DOWN)
∇: TIME = 0

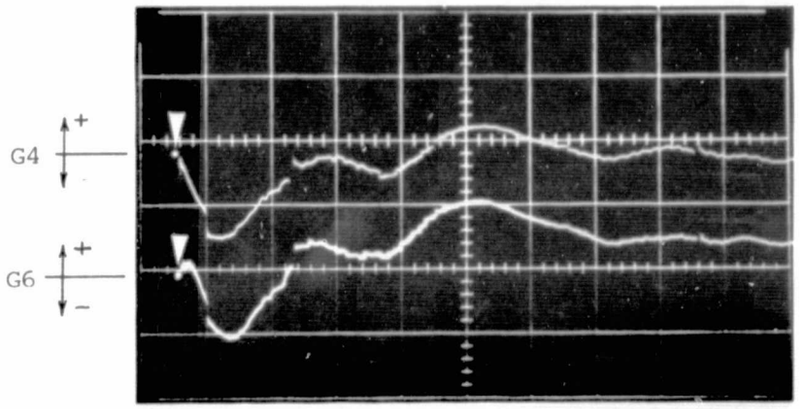

GAGE 4
0.5%/DIV

GAGE 6
0.5%/DIV

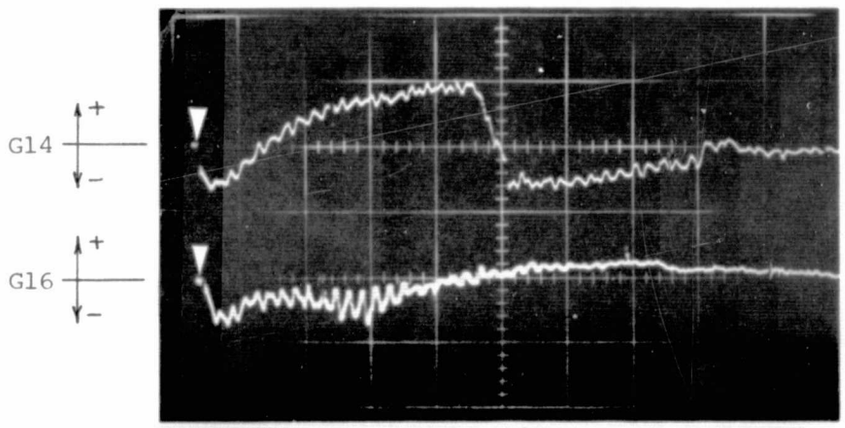

GAGE 14
0.5%/DIV

GAGE 16
0.5%/DIV

FIG. 24 CONCLUDED (SCP-2; 2125 IN/SEC)

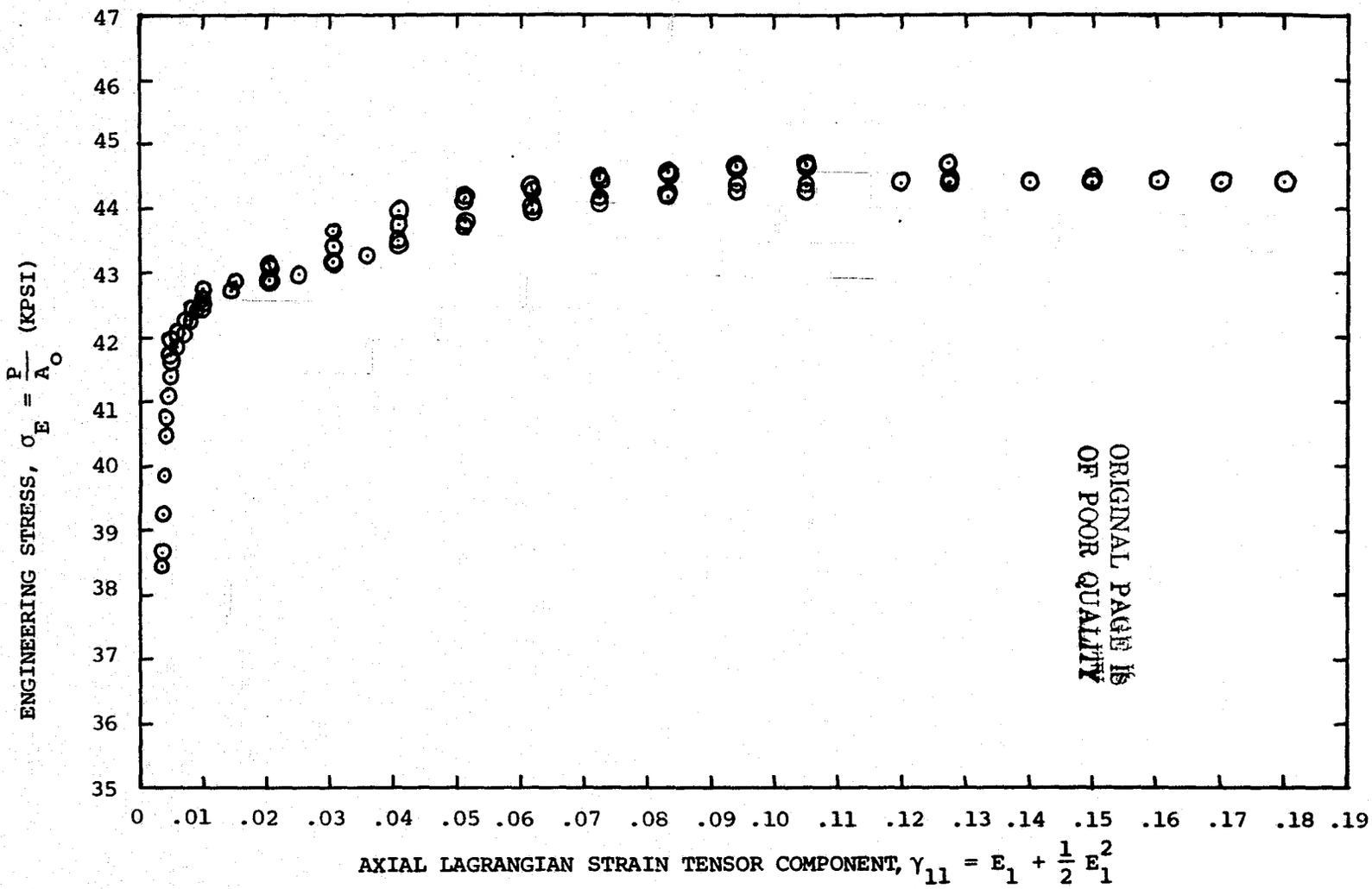

(a) Longitudinal Direction Specimens

FIG. 25 TENSILE UNIAXIAL STATIC STRESS-STRAIN DATA FOR RECTANGULAR CROSS-SECTION SPECIMENS OF 6061-T651 ALUMINUM PLATE STOCK: σ_E VS. γ_{11}

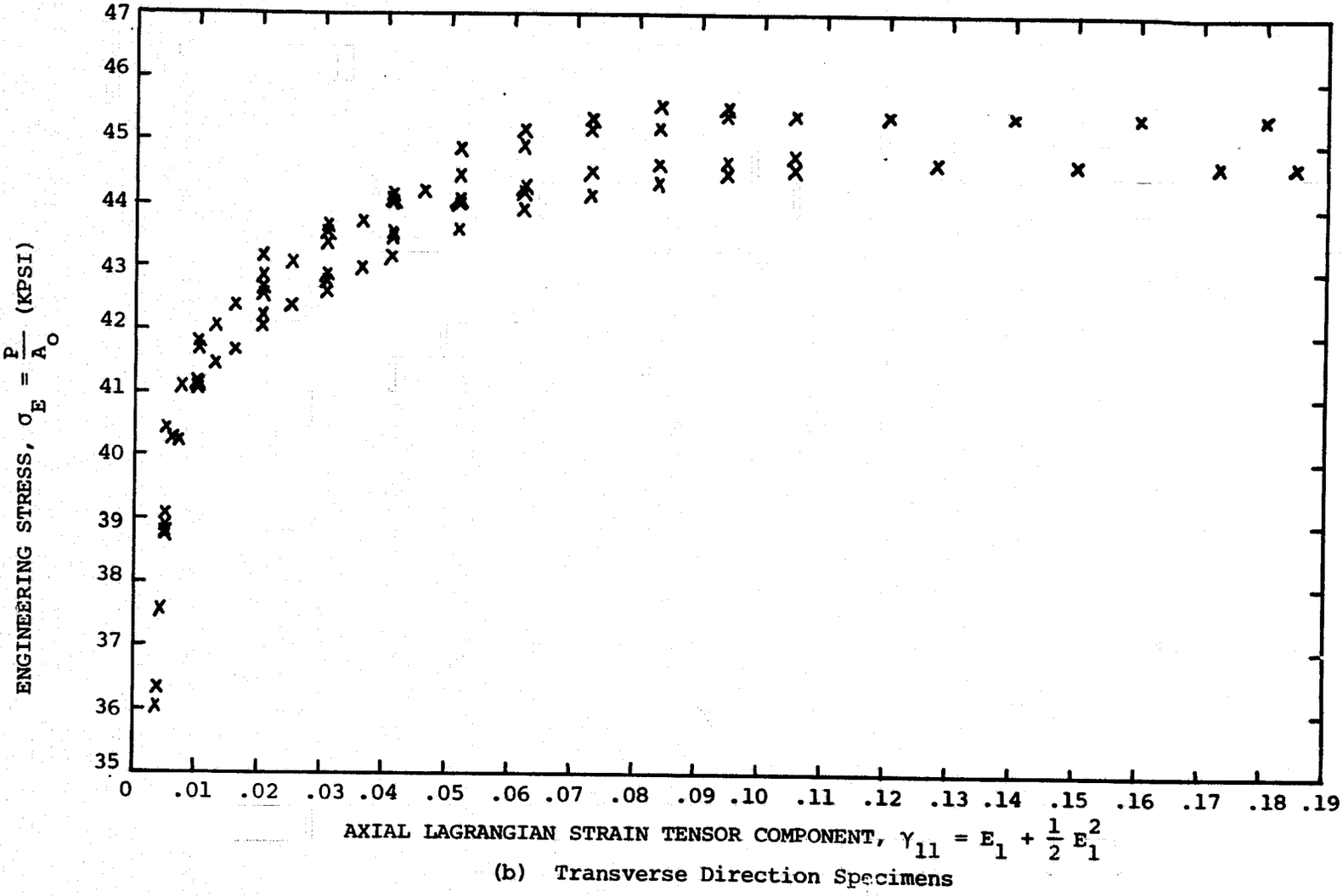

(b) Transverse Direction Specimens

FIG. 25 CONCLUDED (6061-T651)

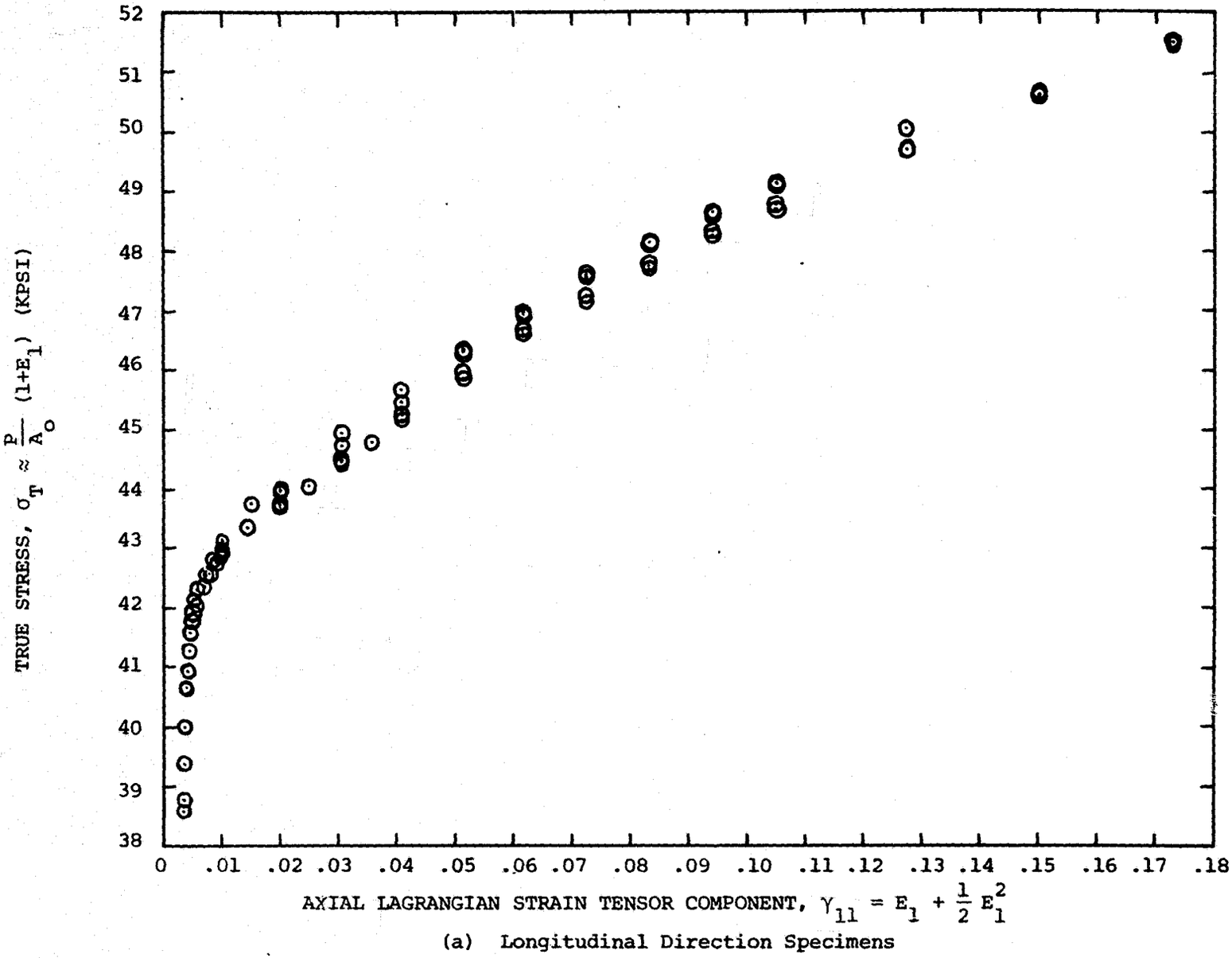

(a) Longitudinal Direction Specimens

FIG. 26 TENSILE UNIAXIAL STATIC STRESS-STRAIN DATA FOR RECTANGULAR CROSS-SECTION SPECIMENS OF 6061-T651 ALUMINUM PLATE STOCK: σ_T VS. γ_{11}

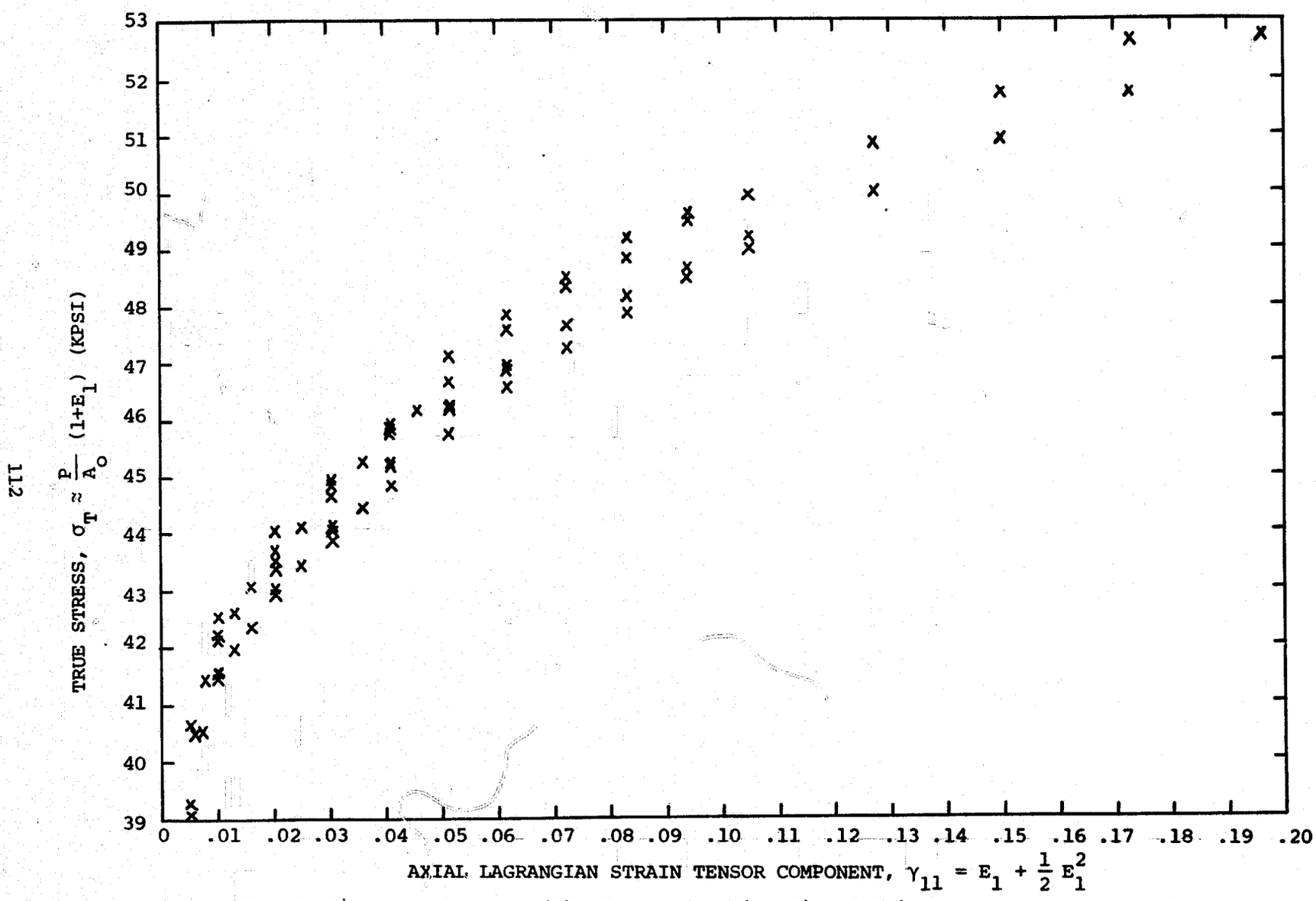

(b) Transverse Direction Specimens

FIG. 26 CONCLUDED (6061-T651)

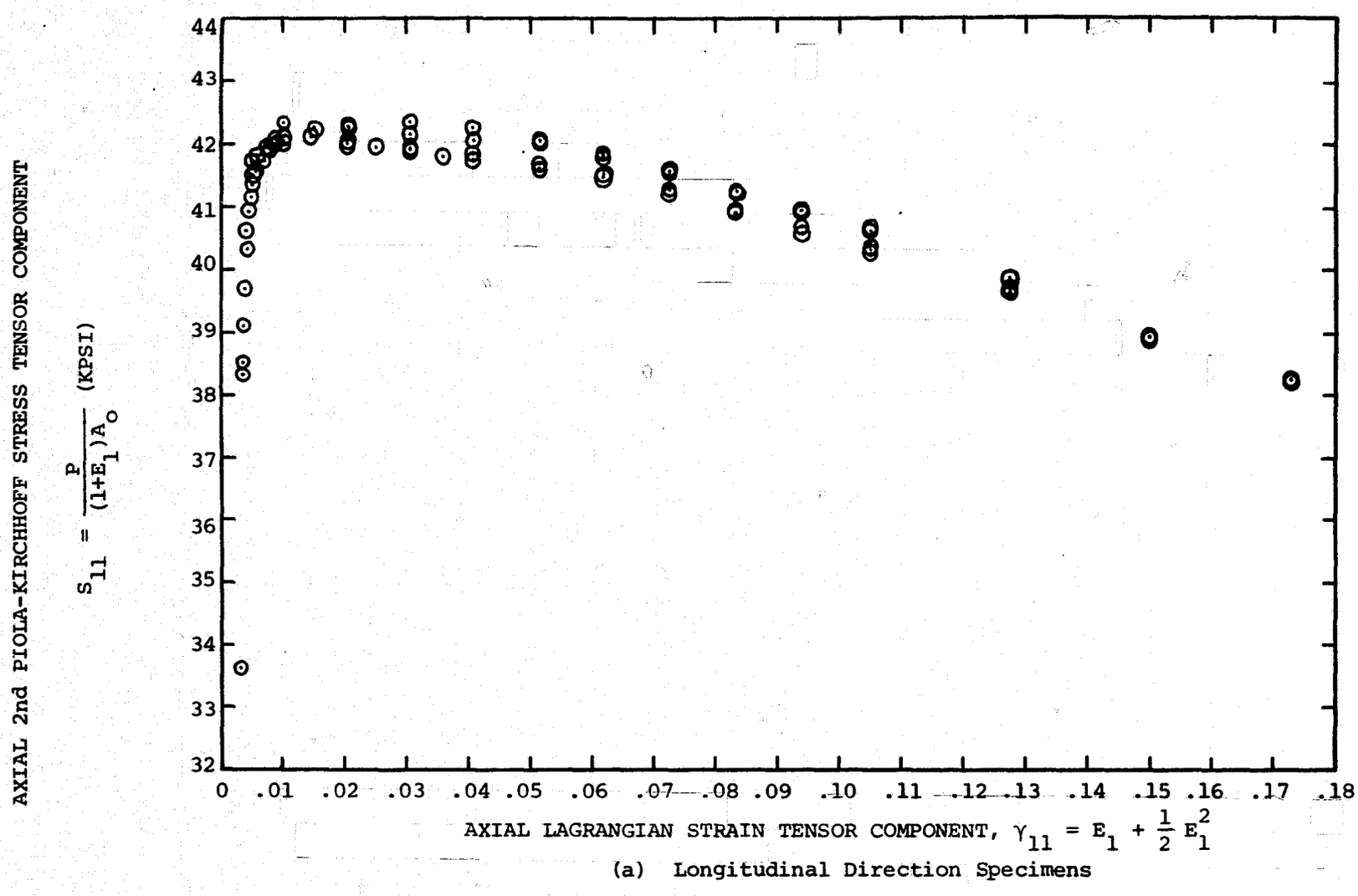

(a) Longitudinal Direction Specimens

FIG. 27 TENSILE UNIAXIAL STATIC STRESS-STRAIN DATA FOR RECTANGULAR CROSS-SECTION SPECIMENS OF 6061-T651 ALUMINUM PLATE STOCK: S_{11} VS. γ_{11}

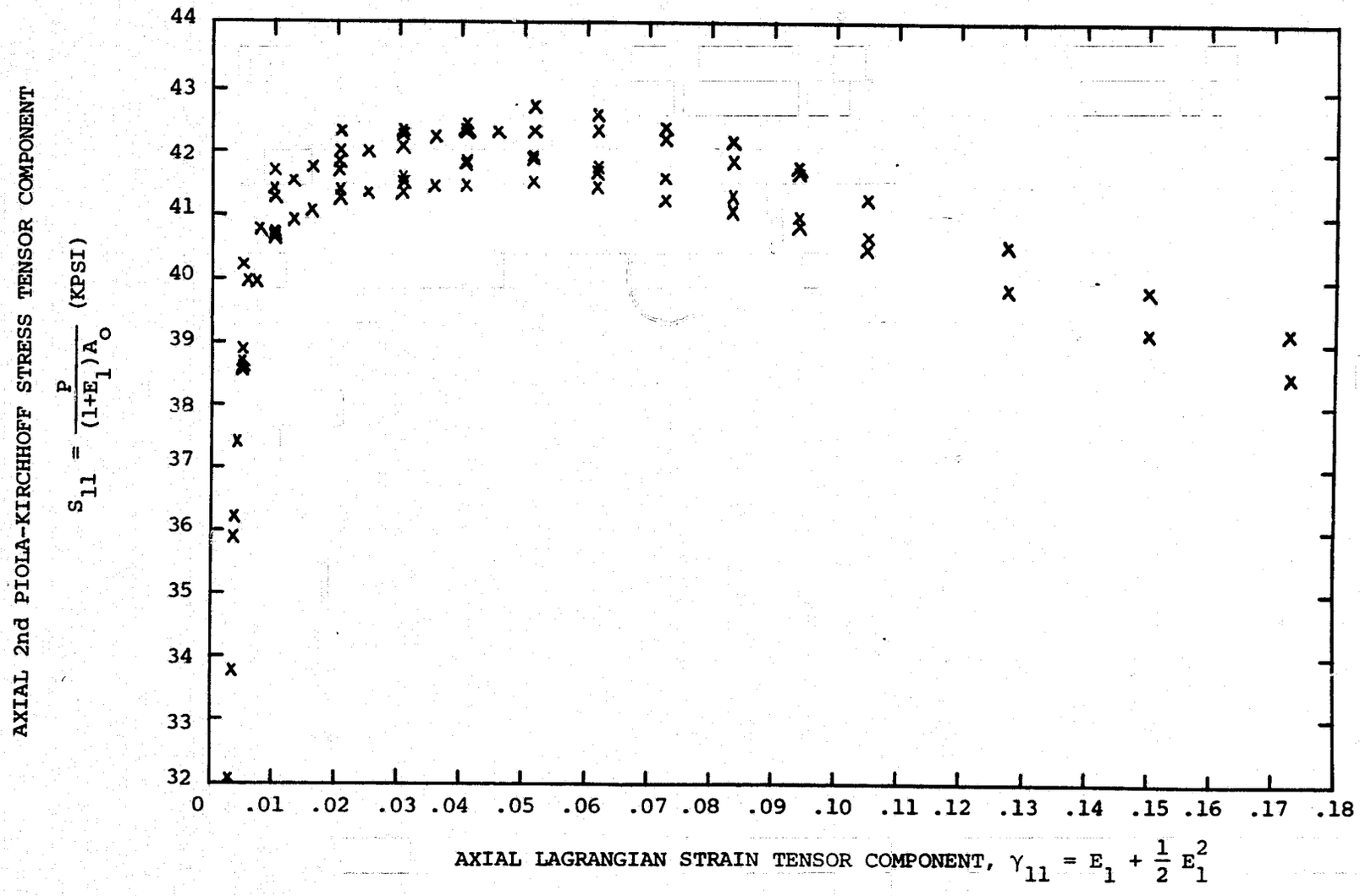

(b) Transverse Direction Specimens

FIG. 27 CONCLUDED (6061-T651)

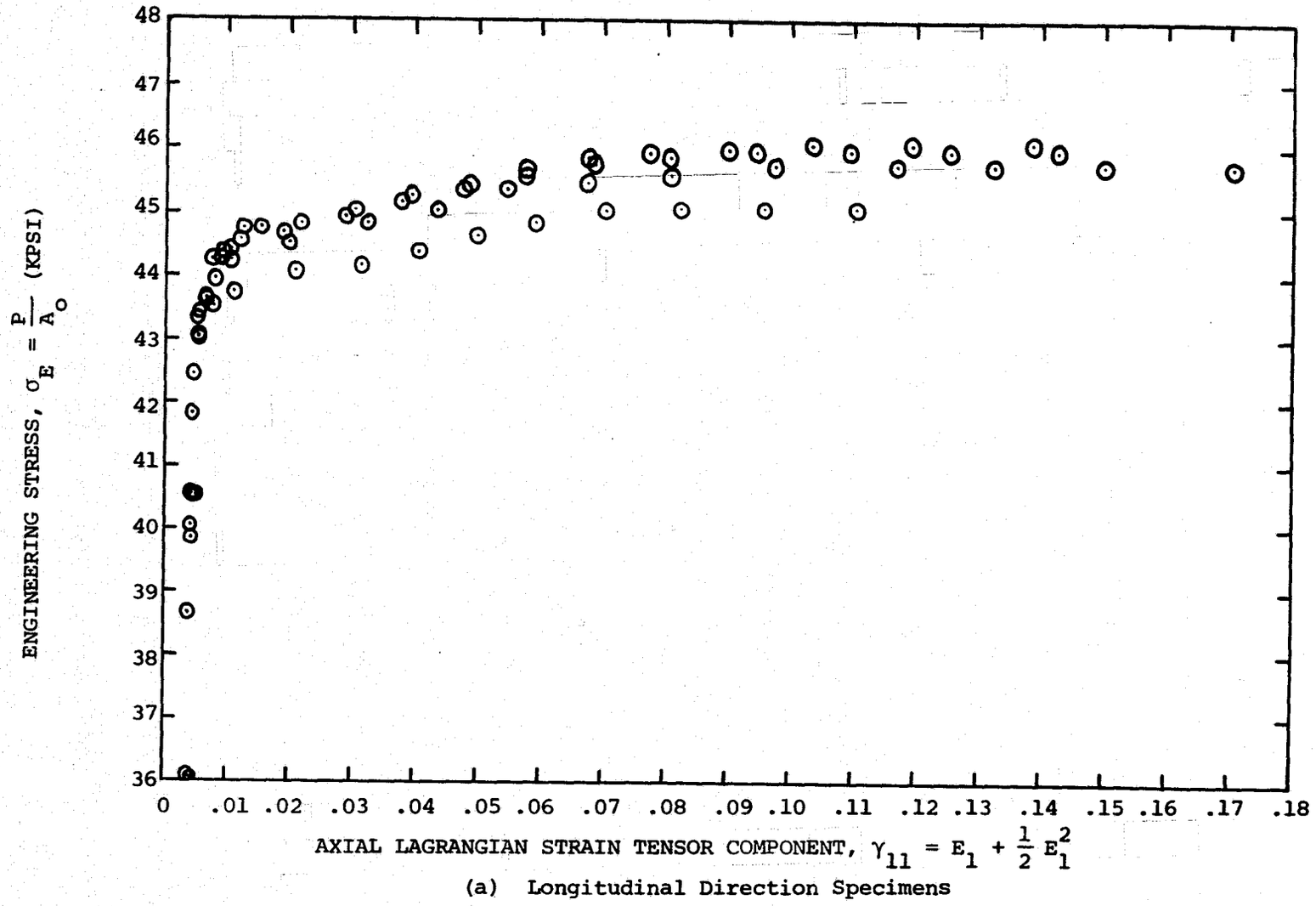

(a) Longitudinal Direction Specimens

FIG. 28 TENSILE UNIAXIAL STATIC STRESS-STRAIN DATA FOR CIRCULAR CROSS-SECTION SPECIMENS OF 6061-T651 ALUMINUM PLATE STOCK: σ_E VS. γ_{11}

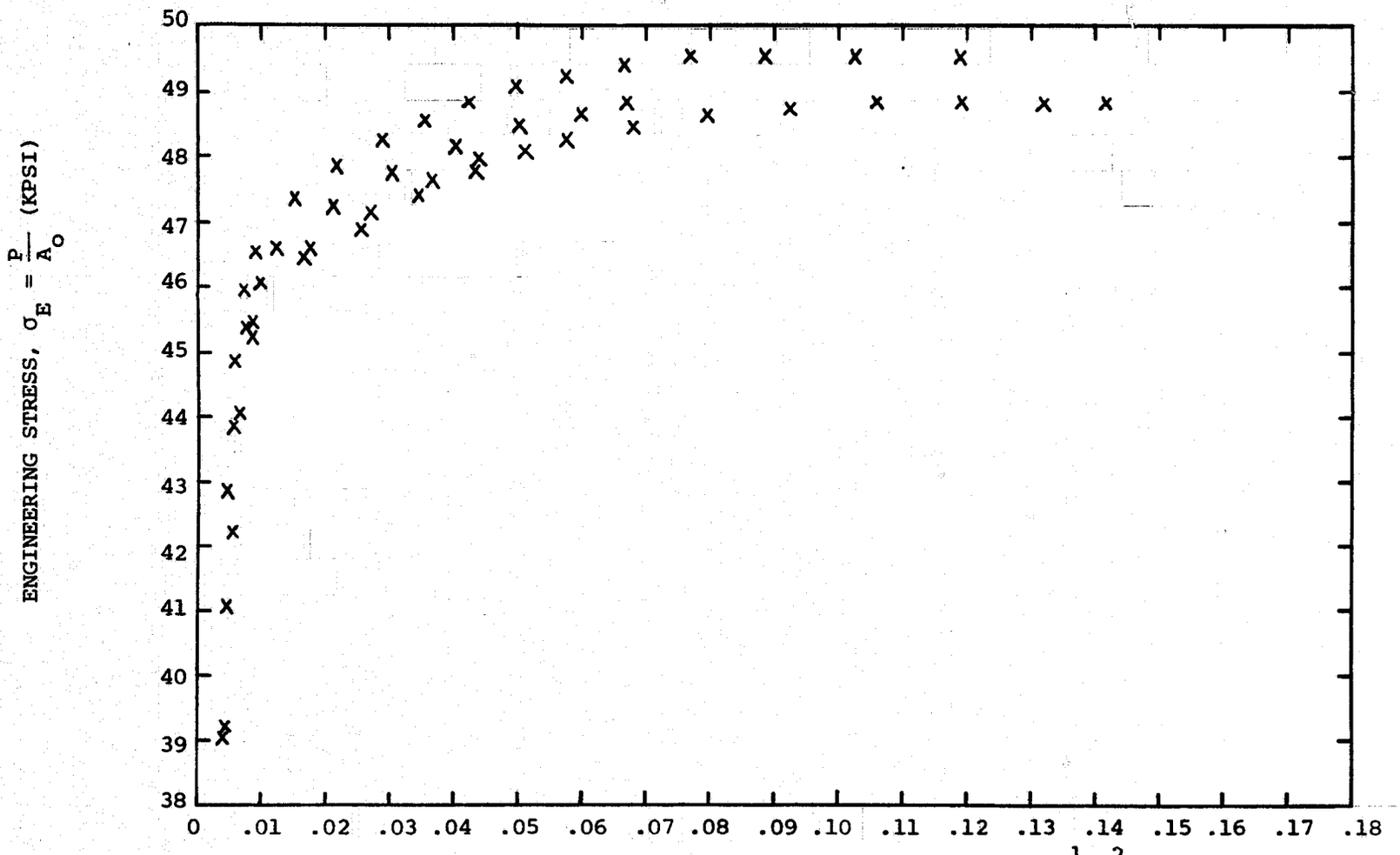

(b) Transverse Direction Specimens

FIG. 28 CONCLUDED (6061-T651)

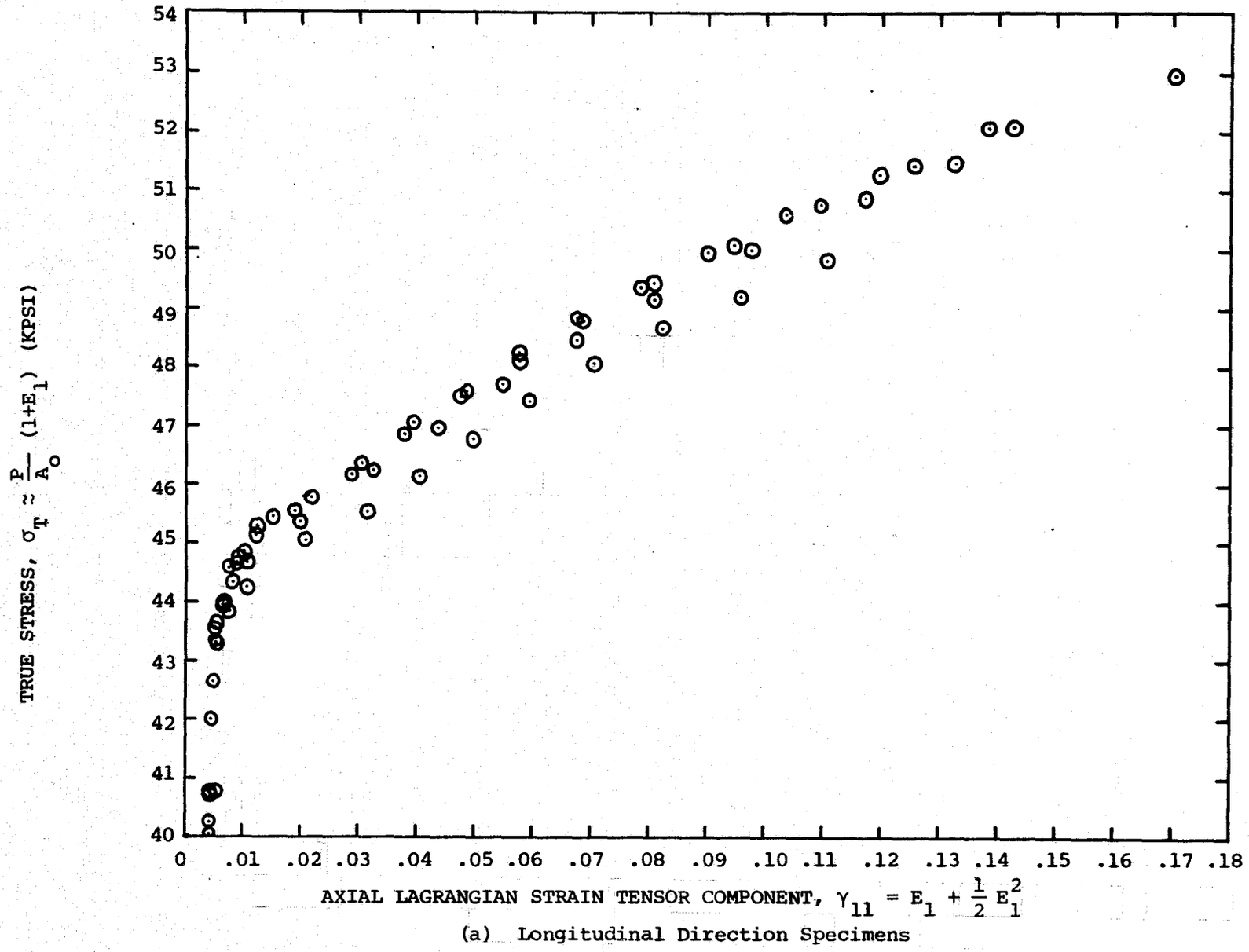

(a) Longitudinal Direction Specimens

FIG. 29 TENSILE UNIAXIAL STATIC STRESS-STRAIN DATA FOR CIRCULAR CROSS-SECTION SPECIMENS OF 6061-T651 ALUMINUM PLATE STOCK: σ_T VS. γ_{11}

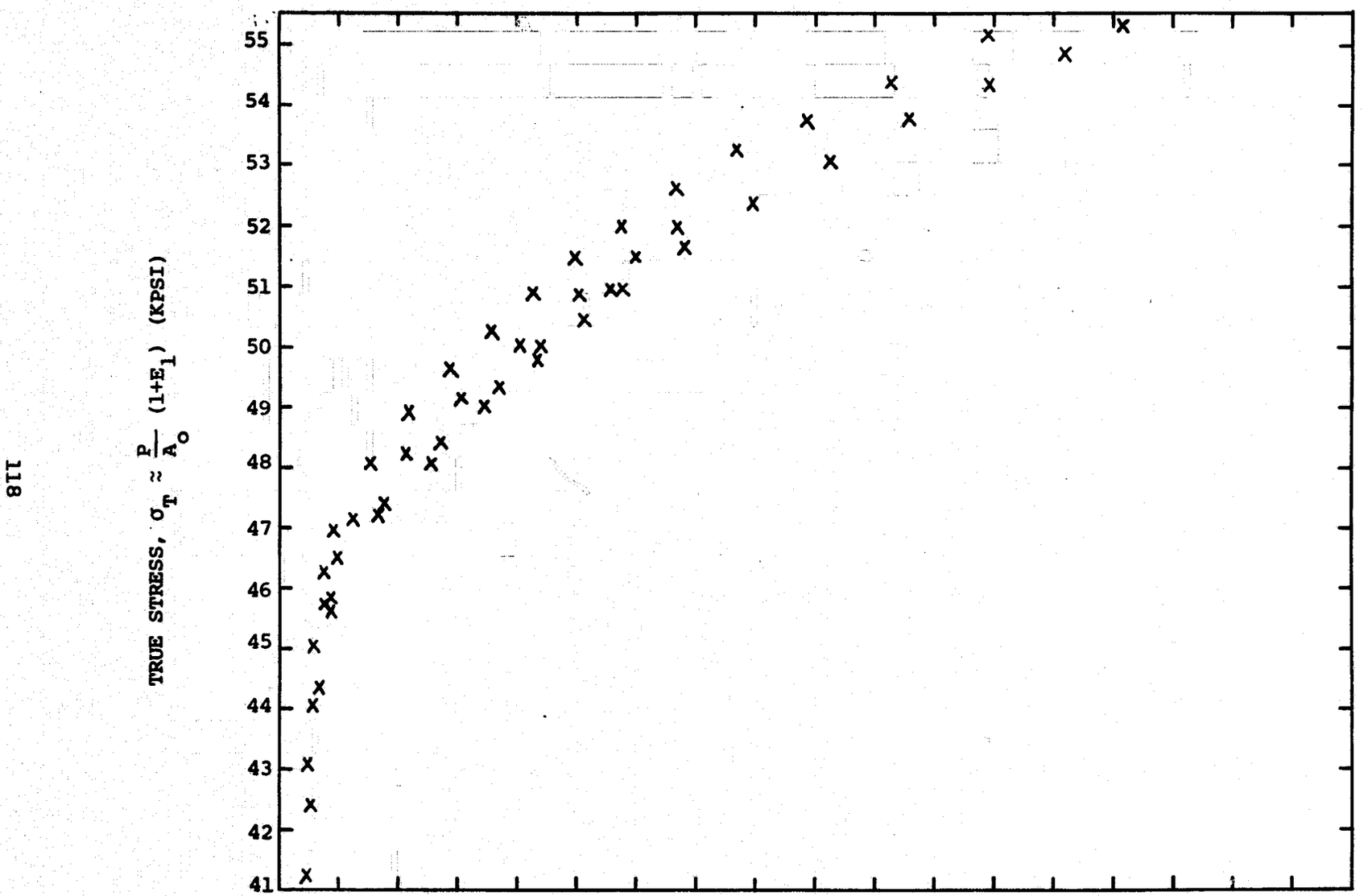

(b) Transverse Direction Specimens

FIG. 29 CONCLUDED (6061-T651)

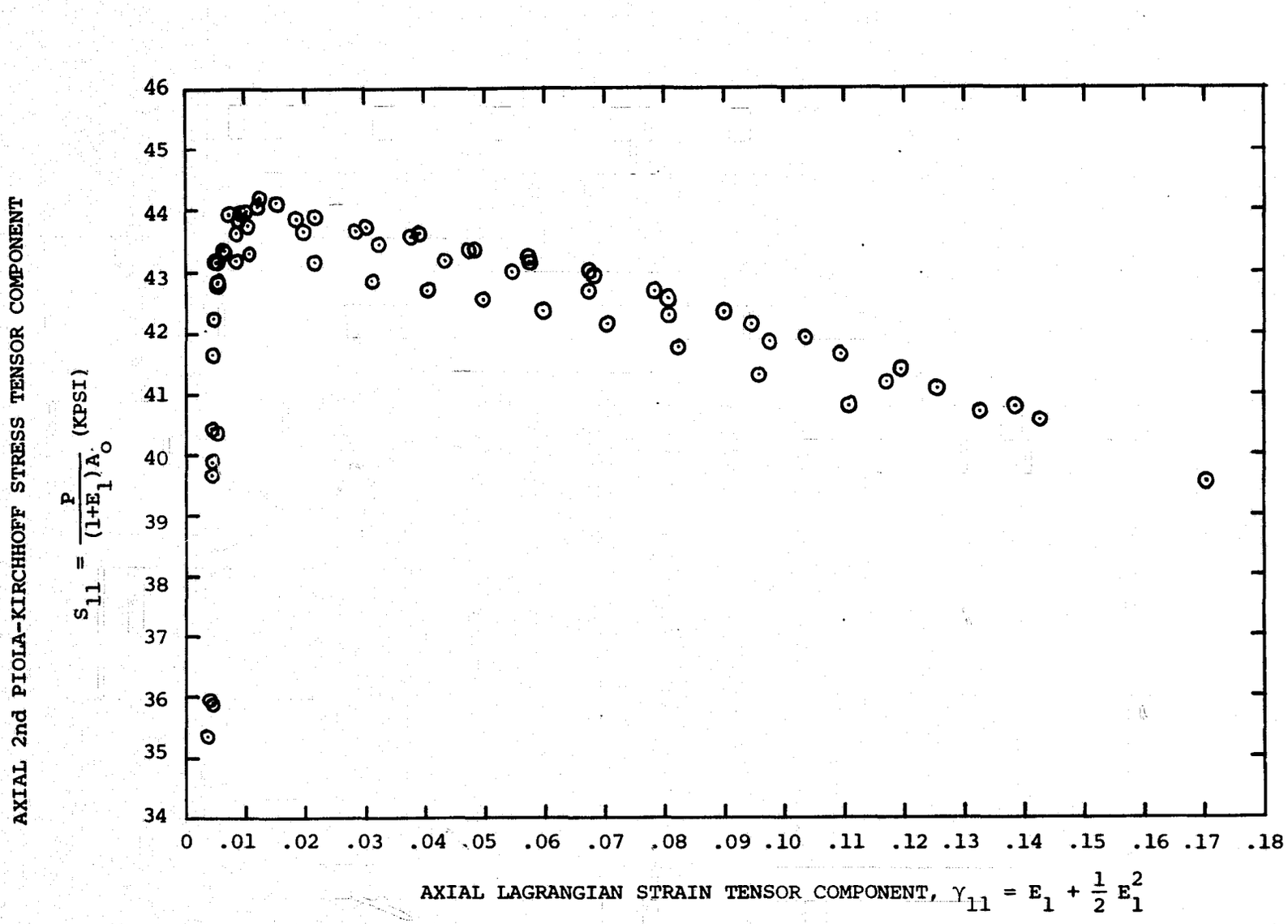

(a) Longitudinal Direction Specimens

FIG. 30 TENSILE UNIAXIAL STATIC STRESS-STRAIN DATA FOR CIRCULAR CROSS-SECTION SPECIMENS OF 6061-T651 ALUMINUM PLATE STOCK: S_{11} VS. γ_{11}

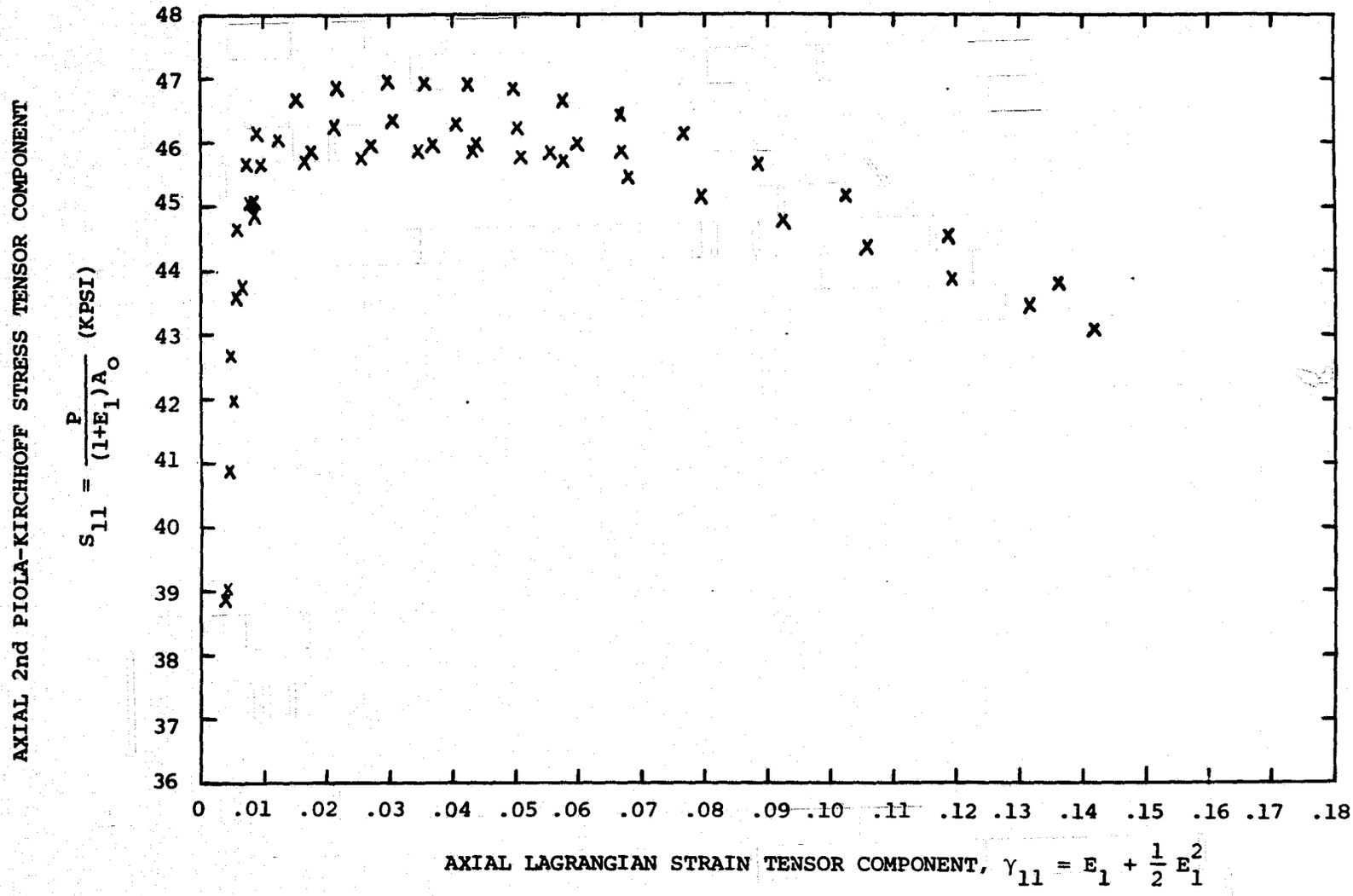

(b) Transverse Direction Specimens

FIG. 30 CONCLUDED (6061-T651)

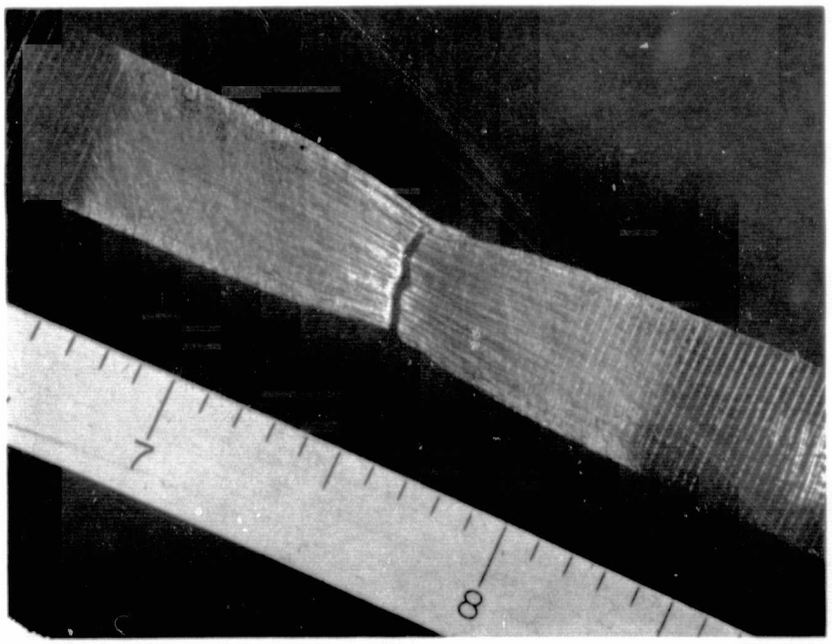

SPECIMEN 76-L4, UPPER SURFACE

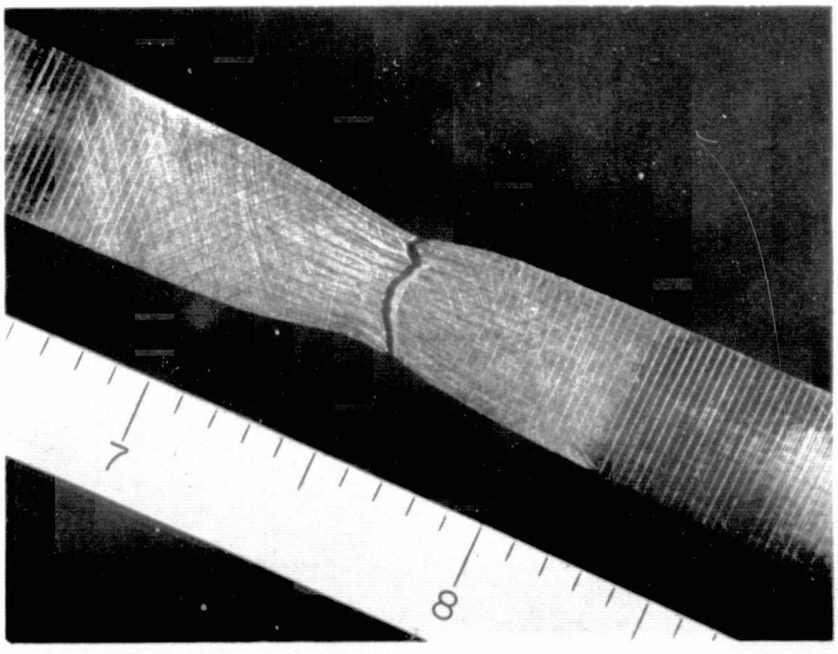

SPECIMEN 76-L4, LOWER SURFACE

FIG. 31 PHOTOGRAPHS OF MECHANICALLY-GRIDDED UNIAXIAL TENSILE SPECIMENS 76-L4 AND 76-T6 OF 6061-T651 ALUMINUM PLATE STOCK TESTED TO FRACTURE

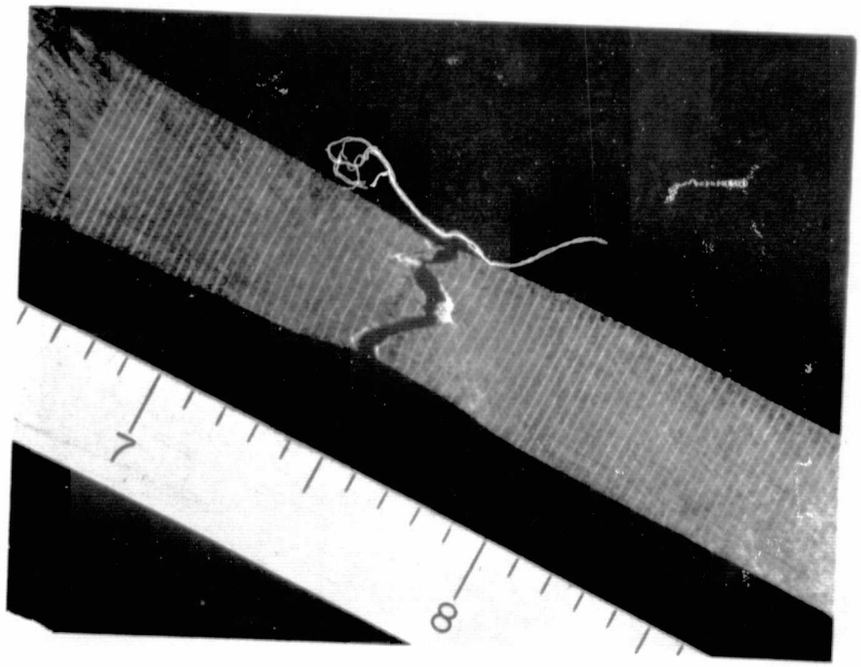

SPECIMEN 76-T6, UPPER SURFACE

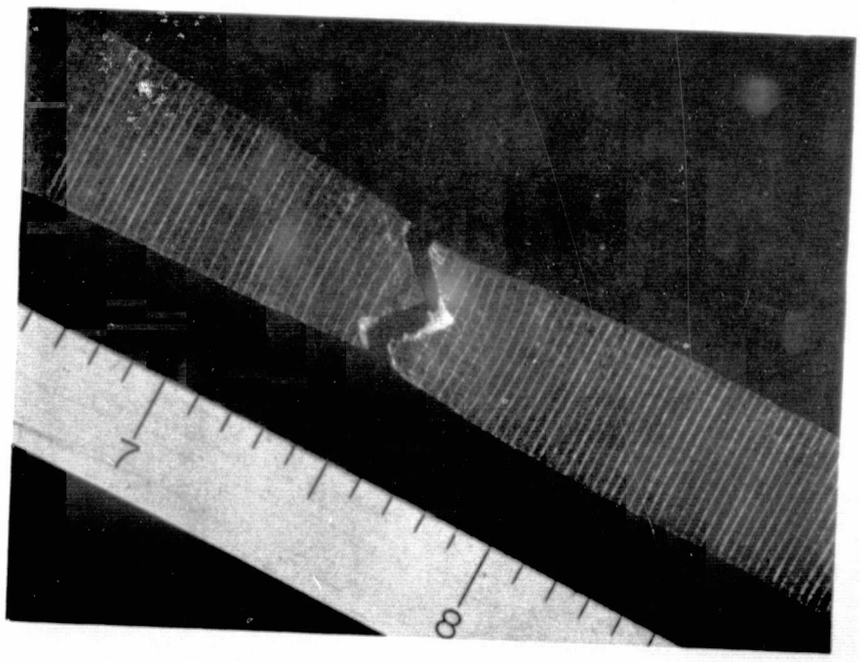

SPECIMEN 76-T6, LOWER SURFACE

FIG. 31 CONCLUDED

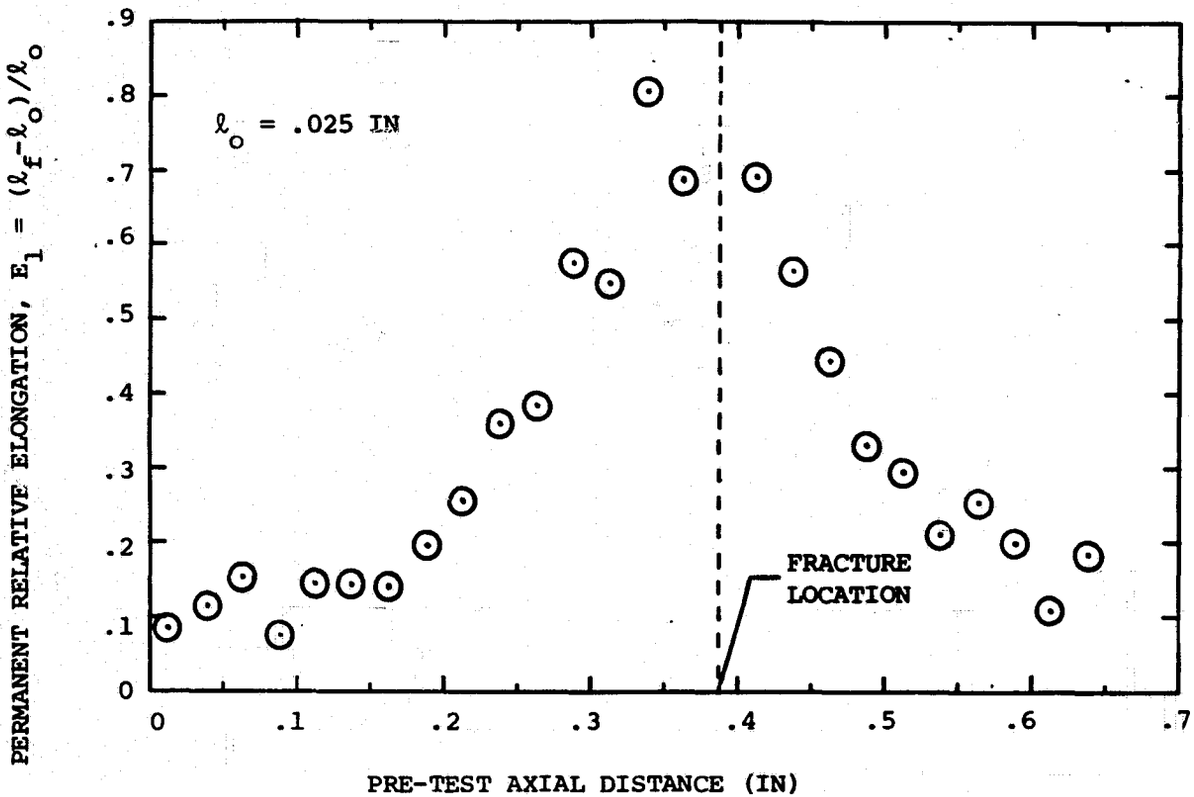

(a) Longitudinal Direction Specimen 76-L4, Upper Surface

FIG. 32 PERMANENT RELATIVE ELONGATION DATA IN THE NECKED REGION FOR MECHANICALLY-GRIDDED AND FRACTURED RECTANGULAR CROSS-SECTION SPECIMENS OF 6061-T651 ALUMINUM PLATE STOCK

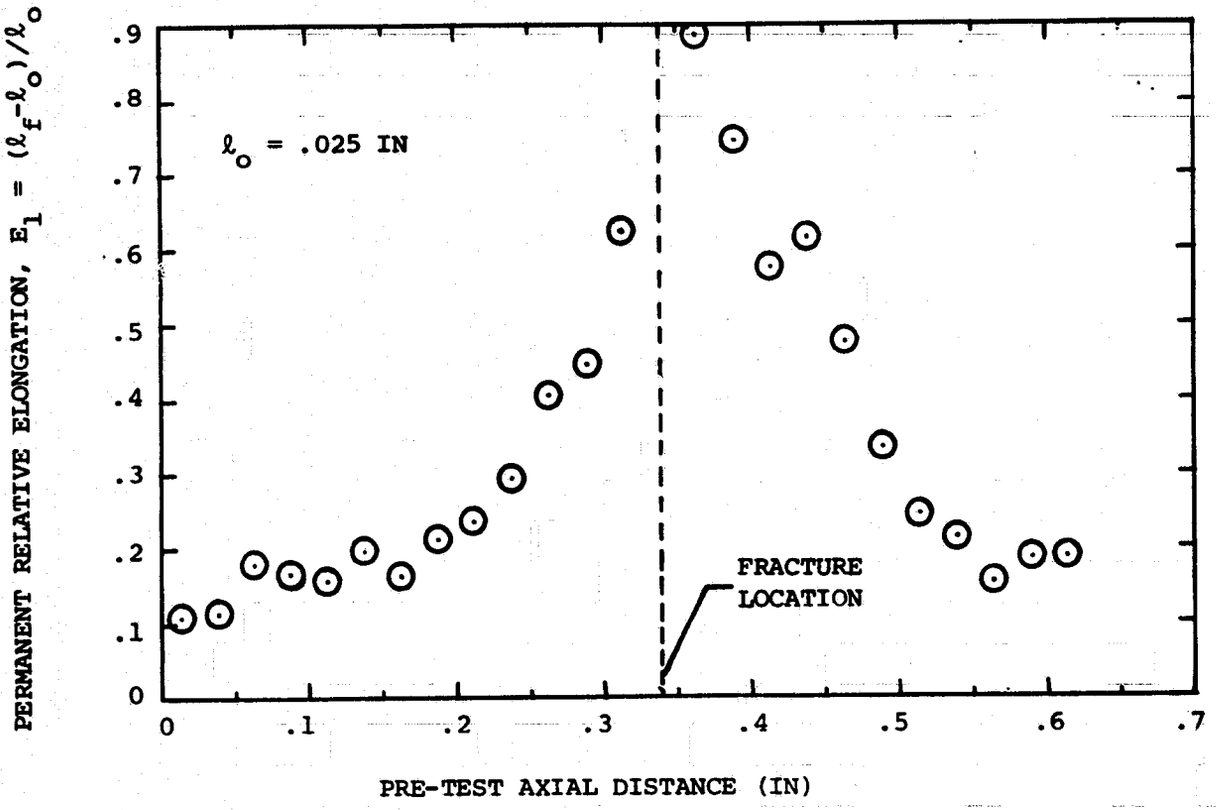

(b) Longitudinal Direction Specimen 76-L4, Lower Surface

FIG. 32 CONTINUED (6061-T651)

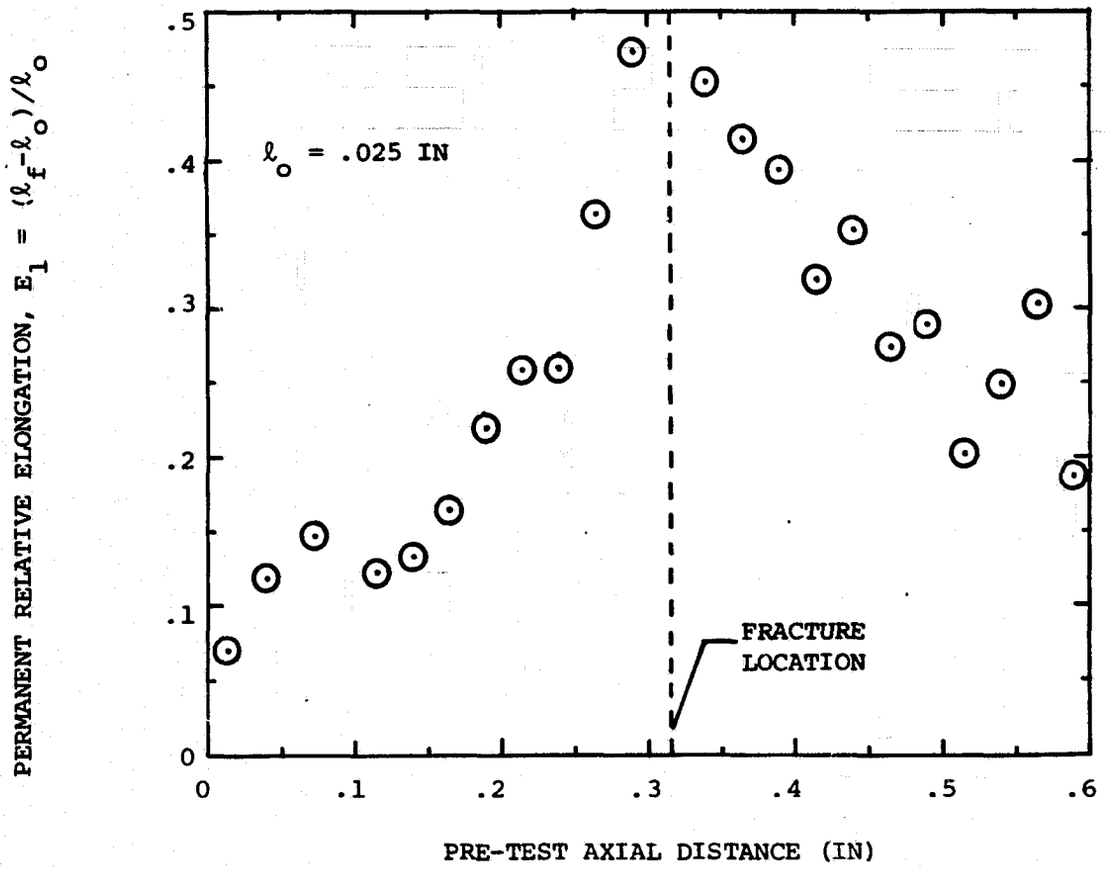

(c) Transverse Direction Specimen 76-T6, Upper Surface

FIG. 32 CONTINUED (6061-T651)

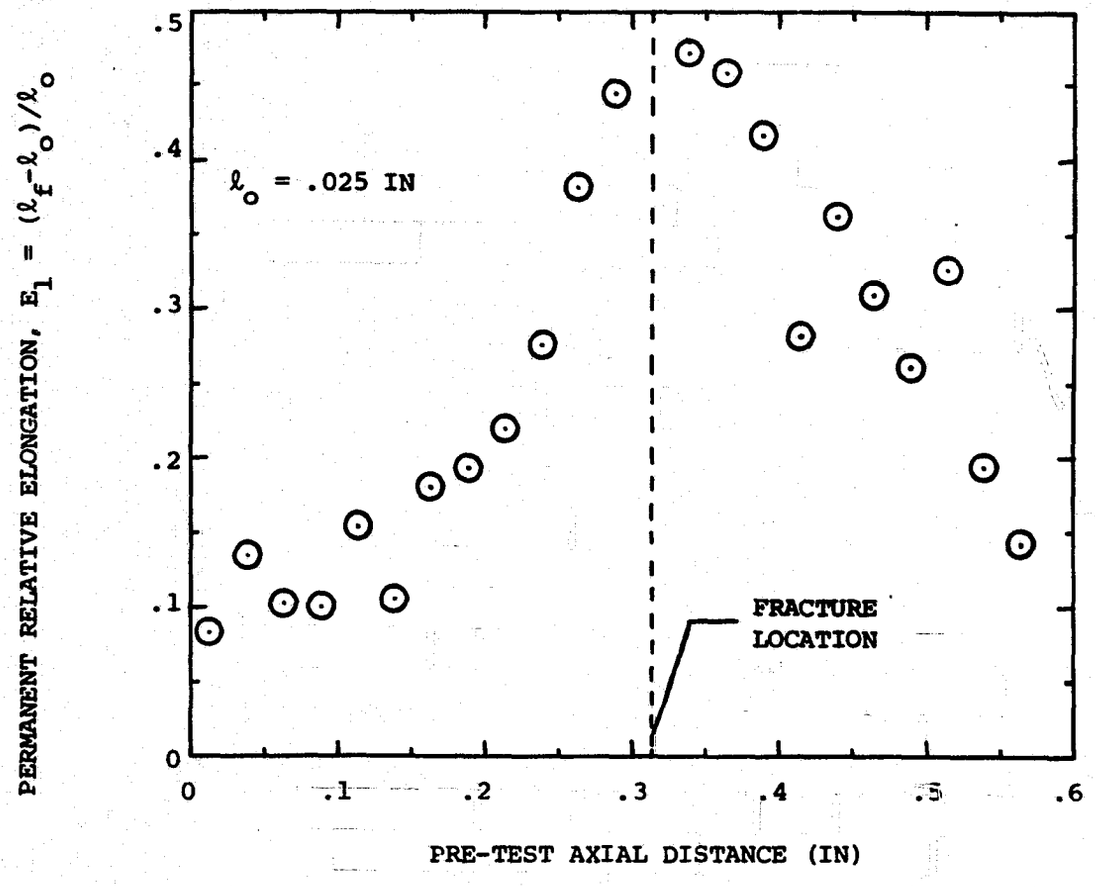

(d) Transverse Direction Specimen 76-T6, Lower Surface

FIG. 32 CONCLUDED (6061-T651)

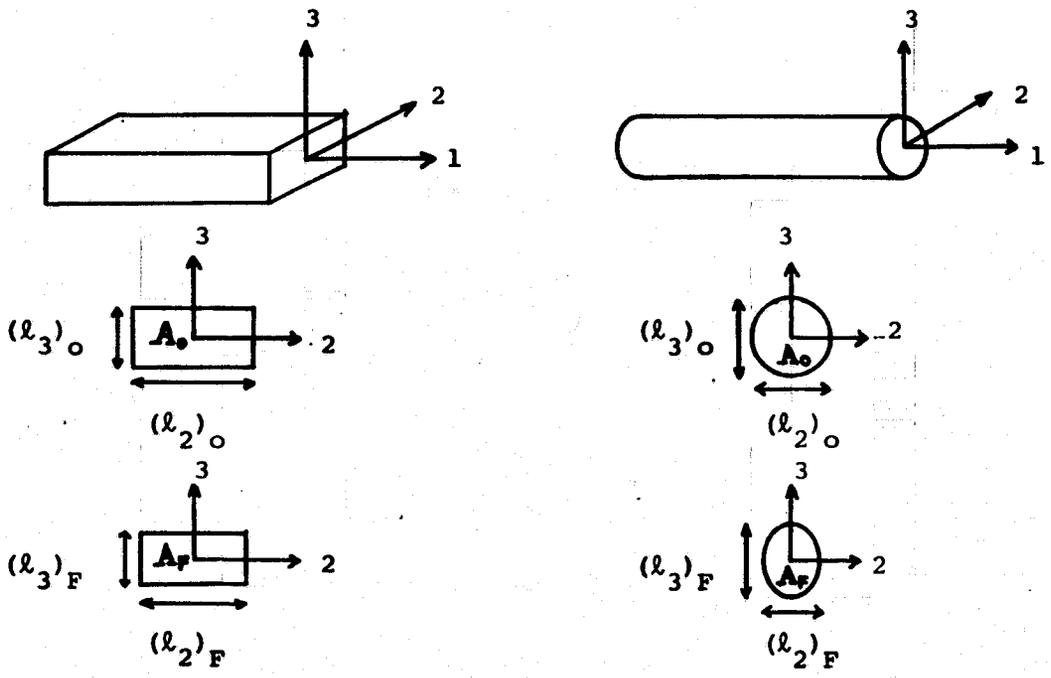

RECTANGULAR CROSS-SECTION SPECIMENS

$(\ell_2)_o > (\ell_3)_o$

$(\ell_2)_F > (\ell_3)_F$

$[-E_2]_F > [-E_3]_F$

ORIGINALLY-CIRCULAR CROSS-SECTION SPECIMENS

$(\ell_2)_o = (\ell_3)_o$

$(\ell_2)_F < (\ell_3)_F$

$[-E_2]_F > [-E_3]_F$

⊙ PERMANENT RELATIVE AXIAL ELONGATION AT FRACTURE: $[E_1]_F \approx \frac{A_o}{A_F} - 1$

X PERMANENT UNIT CONTRACTION IN DIRECTION 2
AT FRACTURE: $[-E_2]_F = 1 - \frac{(\ell_2)_F}{(\ell_2)_o}$

\+ PERMANENT UNIT CONTRACTION IN DIRECTION 3
AT FRACTURE: $[-E_3]_F = 1 - \frac{(\ell_3)_F}{(\ell_3)_o}$

FIG. 33 NOMENCLATURE AND DEFINITIONS OF RELATIVE ELONGATION MEASURES $[E_1]_F$, $[-E_2]_F$, AND $[-E_3]_F$ AT FRACTURE PERTAINING TO FIG. 34

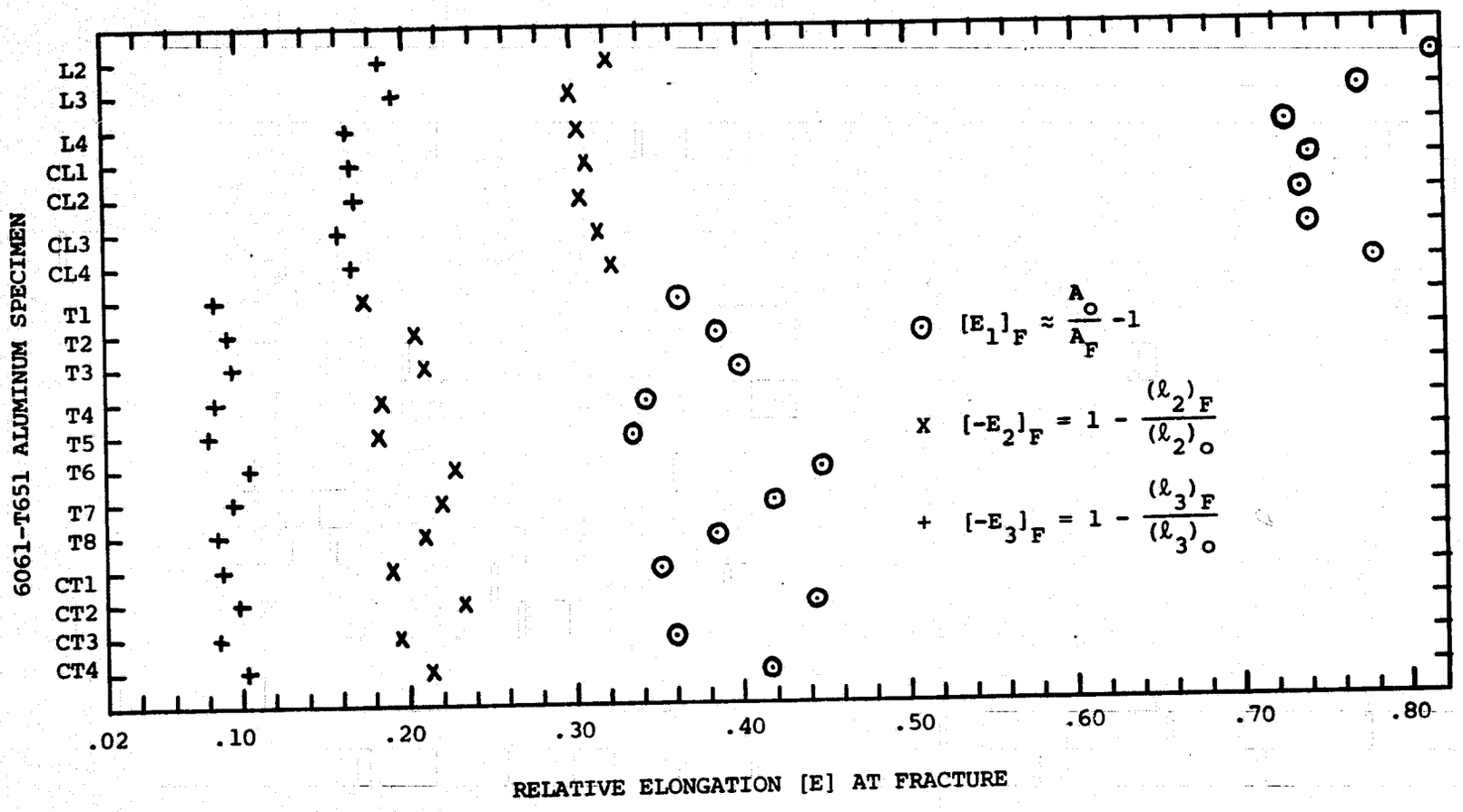

FIG. 34 PERMANENT RELATIVE ELONGATION DATA FOR FRACTURED SPECIMENS OF 6061-T651 ALUMINUM PLATE STOCK AT THE FRACTURE LOCATION

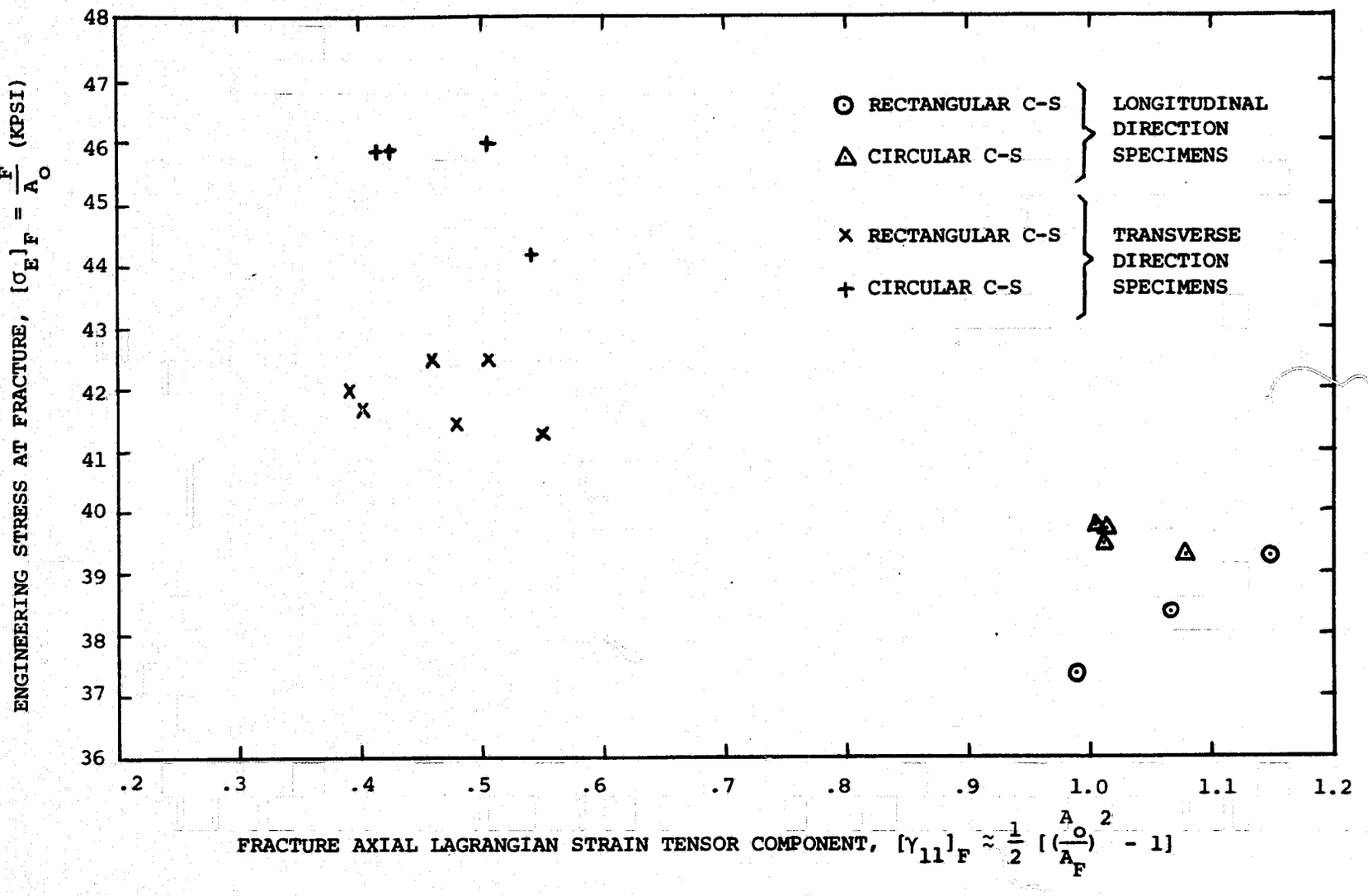

FIG. 35 TENSILE STATIC FRACTURE STRESS VERSUS PERMANENT STRAIN DATA FOR SPECIMENS OF 6061-T651 ALUMINUM PLATE STOCK: $[\sigma_E]_F$ VS. $[\gamma_{11}]_F$

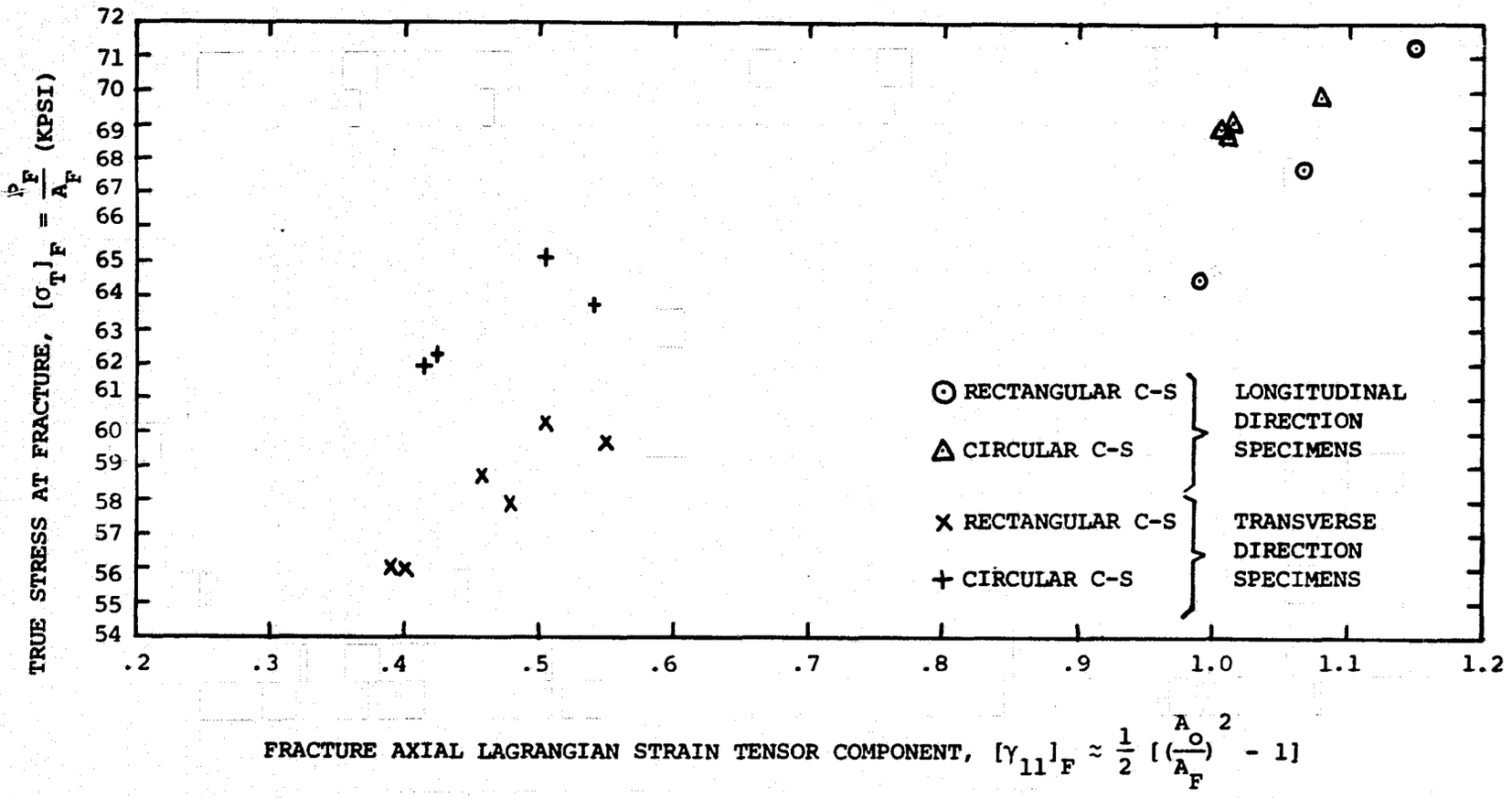

FIG. 36 TENSILE STATIC FRACTURE STRESS VERSUS PERMANENT STRAIN DATA FOR SPECIMENS OF 6061-T651 ALUMINUM PLATE STOCK: $[\sigma_T]_F$ VS. $[\gamma_{11}]_F$

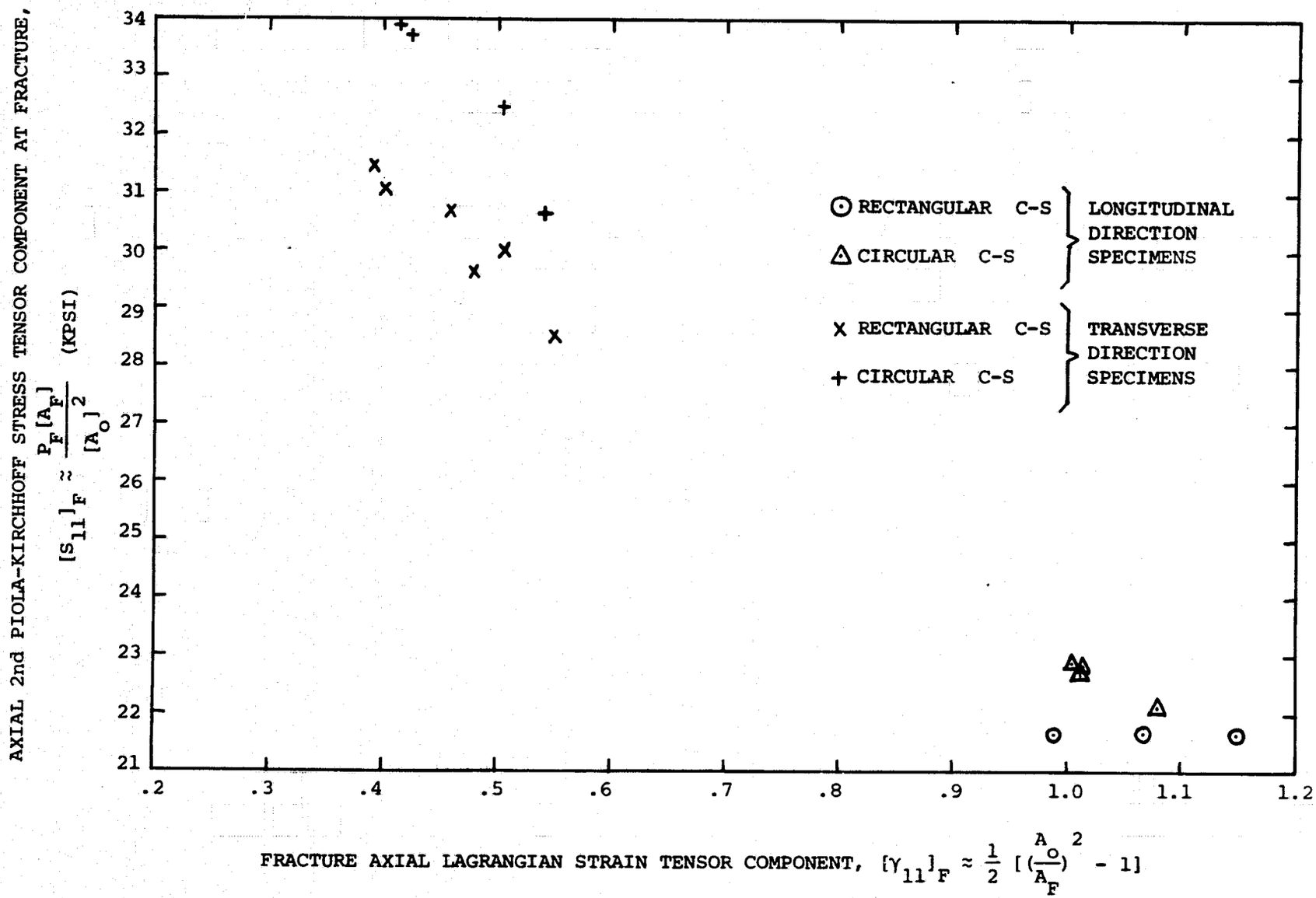

FIG. 37 TENSILE STATIC FRACTURE STRESS VERSUS PERMANENT STRAIN DATA FOR SPECIMENS OF 6061-T651 ALUMINUM PLATE STOCK: $[S_{11}]_F$ VS. $[\gamma_{11}]_F$